Hartree-Fock-Slater Studies of Bonding to Transition Metals: Surfaces and Complexes, Chemisorption of Acetylene

Petro Geurts

Hartree-Fock-Slater Studies of Bonding to Transition Metals: Surfaces and Complexes, Chemisorption of Acetylene

Promotor

prof dr ir A van der Avoird

Hartree-Fock-Slater Studies of Bonding to Transition Metals: Surfaces and Complexes, Chemisorption of Acetylene

Proefschrift

ter verkrijging van de graad van doctor in de wiskunde en natuurwetenschappen aan de Katholieke Universiteit te Nijmegen, op gezag van de rector magnificus prof dr P G A B Wijdeveld, volgens besluit van het college van decanen in het openbaar te verdedigen op donderdag 25 september 1980, des namiddags te 2 00 uur precies

door

Peter Jozef Mathilde Geurts
geboren te Kerkrade

1980

krips repro meppel

Graag bedank ik iedereen die heeft bijgedragen aan de totstandkoming van dit proefschrift.

Behalve naar de co-auteurs van de verschillende hoofdstukken en degenen genoemd in de "acknowledgements" van die hoofdstukken, gaat mijn dank in het bijzonder uit naar:

--De (ex-)medewerkers en (ex-)studenten van de afdeling Theoretische Chemie voor de vruchtbare en prettige samenwerking.
--Monique Bongers-de Bie voor het nauwgezet en kundig verzorgen van het complete typewerk.
--De medewerkers van het Universitair Rekencentrum.
--De medewerkers van de dienstverlenende afdelingen van de faculteit der wiskunde en natuurwetenschappen, vooral van de afdeling Illustratie (met name de heer Th.C. Oor) voor de fraaie figuren en van de afdelingen Fotografie en Reproductie.
--De medewerkers van de Mathematisch-Statistische Adviesafdeling voor het ter beschikking stellen van de typemachine.

Aan mijn ouders,

Gaby,

Ygor.

CONTENTS

CHAPTER I

Introduction

Especially nowadays, in view of the complex environmental and energy problems, it is important to improve existing and to develop new useful catalytic processes in chemistry. A thorough understanding of these, often complicated, chemical processes can be of great help. Unravelling these processes in the more elementary steps and studying the latter under well-defined conditions can be an approach to this understanding. An elementary and often first step in many catalytic reactions is the (possibly dissociative) adsorption of the reagent(s) on the catalyst surface, which mostly is a transition metal. Much attention has been paid to the adsorption of small organic molecules (e.g. hydrocarbons) on supported transition metal particles, on films, and, especially the last few years on well-characterized single crystal surfaces of transition metals. These studies involve experimental as well as theoretical work; theoretical models and calculations are often needed to interpret the experimental data and they can provide valuable extra information.

Part of this thesis presents a systematic theoretical study of the adsorption of acetylene on different surfaces of iron, nickel and copper; these surfaces are modelled by small clusters of one to four metal atoms. We have investigated the geometrical and electronic structure of the adsorbed C_2H_2 and we have compared our results with experimental data for molecularly adsorbed C_2H_2 on the metals mentioned. The comparison is most direct with the ionization energies from ultraviolet photoelectron spectroscopy (UPS) and with the stretch frequencies from electron energy loss spectroscopy (ELS). Most experimental data are available for C_2H_2 on the Ni(111) face.

Of course, not only the adsorption of molecular acetylene, but also the formation and adsorption of dissociation products is interesting from the catalytic view-point. Again, most experimental data have been reported for nickel surfaces. Therefore, we have considered possible dissociation pathways for C_2H_2 on Ni and studied the interaction of some fragments, CH, CH_2 and C_2H with nickel clusters.

Another part of this thesis concerns a theoretical study of the electronic structure and properties of some transition metal complexes. We have chosen the nickel complexes, $[\pi\text{-}(C_2H_2)Ni(CO)_2]$, $[\pi\text{-}(C_2H_2)Ni(CNH)_2]$ and

$[\mu_2\text{-}(C_2H_2)\{Ni(CNH)_2\}_2]$, in order to compare the binding of C_2H_2 to complexes with the adsorption binding. The π and μ_2 binding sites occurring on these complexes are quite similar to some of the metal surface binding sites, but the effects of the ligands in the complex (carbonyl or isocyanide) may be different from the metal bulk effects. Such a comparison is interesting in view of the relations between heterogeneous and homogeneous catalysis. Moreover, we can use the results calculated for these C_2H_2-nickel complexes, for which the C≡C stretch frequencies have been measured (for substituted alkynes, actually), to calibrate the relation between these frequencies and the calculated C≡C overlap populations. This relation can then be used, in combination with the C≡C stretch frequency measured for C_2H_2 on the Ni(111) surface (by ELS) and the C≡C overlap populations, which we have calculated in our models for the different binding sites (π, di-σ, μ_2, μ_3) of C_2H_2 on this surface (see above), to determine which sites are actually occupied and to characterize the binding.

Calculations on $[Fe_4S_4(SH)_4]^{n-}$ and on Cu(II) bis(dithiocarbamate), $[Cu(dtc)_2]$, have been performed both to obtain information about the electronic properties of these complexes and to make further tests of the Hartree-Fock-Slater (HFS)-LCAO method, which was used later in our chemisorption studies. This non-empirical method has been developed by Ros, Baerends and coworkers and it has been tested already for a series of small molecules and some transition metal complexes. The $[Fe_4S_4(SH)_4]^{n-}$ cubane complex can serve as a model for the active sites in the non-heme iron-sulphur protein catalysts high potential iron protein and ferredoxin. On this fairly large complex we have tested particularly the (spin-restricted) core pseudopotential version of the HFS method, which has been developed recently by Snijders and Baerends. In the calculations on the paramagnetic $[Cu(dtc)_2]$ complex we have used also the spin-unrestricted version of the HFS method; we have calculated magnetic coupling parameters, g tensor, (an)isotropic Cu and S hyperfine tensors, and optical excitation energies. The results appear to be in good agreement with the detailed experimental data from electron paramagnetic resonance (EPR) measurements and from optical spectroscopy.

For more details about the problems treated and the results obtained we refer to the individual chapters, which have their own abstracts and introductions.

Hartree-Fock-Slater-LCAO calculations on $[Fe_4S_4(SH)_4]^{0,2-,3-}$: a model for the 4-Fe active site in high potential iron protein and ferredoxin.

P.J.M. Geurts, J.W. Gosselink, A. van der Avoird
Institute of Theoretical Chemistry
University of Nijmegen
Toernooiveld, Nijmegen, The Netherlands

and

E.J. Baerends, J.G. Snijders
Scheikundig Laboratorium der Vrije Universiteit
De Boelelaan 1083, Amsterdam, The Netherlands

ABSTRACT

The electronic structure of the complexes $[Fe_4S_4(SH)_4]^{0,2-,3-}$ which model the 4-Fe active site in high potential iron protein and ferredoxin, has been calculated with the Hartree-Fock-Slater-LCAO method (in its frozen core and core pseudopotential versions). Results are in agreement with the measured electronic absorption spectrum and magnetic behaviour. The electric field gradient on the Fe nuclei is larger than expected from the observed Mössbauer quadrupole splitting, but the (small) change in this quantity in going from the dianion to the trianion is well described. The Fe-S bonding is mainly covalent and direct Fe-Fe bonding is weak; these conclusions also follow from extended Hückel calculations which we have made in parallel. The self-consistent HFS-LCAO calculations show that in redox reactions the Fe atoms act as charge redistributors. The core pseudopotential version of the method yields results which generally agree with those of the frozen core calculations.

1. INTRODUCTION

The non-heme iron-sulphur proteins with 1-Fe, 2-Fe and 4-Fe active sites play an important role as electron carriers in many biological systems [1-3]. Especially, the 4-Fe active sites of the two biocatalysts high potential iron protein (HP) and ferredoxin (Fd) and their synthetic analogues, $[Fe_4S_4(SR)_4]^{2-,3-}$ (R=alkyl, aryl) which have been prepared recently [4-7] have been subject to much experimental study (see also ref. 1-7): X-ray diffraction [4,8-10], electrochemical measurements [6,8,11,12], electronic absorption spectroscopy [6,8,9,11-14], XPS [8,13], Mössbauer spectroscopy [5,8,10,13-15], magnetic susceptibility measurements [5,8,10] and ^{1}H NMR shifts [8,9,16,17].

The relationship between the biologically important oxidation states of the proteins and their analogues is indicated in the following scheme (s-red= super-reduced, red=reduced, ox=oxidized, s-ox=super-oxidized):

$$Fd_{red} \leftrightarrow Fd_{ox} \leftrightarrow Fd_{s\text{-}ox}$$

$$HP_{s\text{-}red} \leftrightarrow HP_{red} \leftrightarrow HP_{ox}$$

$$[Fe_4S_4(SR)_4]^{3-} \leftrightarrow [Fe_4S_4(SR)_4]^{2-} \leftrightarrow [Fe_4S_4(SR)_4]^{-}$$

The central role is played by Fd_{ox}, HP_{red} and the dianion analogue $[Fe_4S_4(SR)_4]^{2-}$. Formally the latter can be viewed as a mixed valence compound with two of the Fe atoms in the 2+ and two in the 3+ oxidation state (bridging S^{2-} and terminal SR^-); in Mössbauer spectroscopy [8,13-15] only one quadrupole splitting (doublet), has been observed, however, which shows the four iron atoms to be equivalent (formal oxidation state $Fe^{2.5+}$). From these Mössbauer data, but also from NMR and magnetic susceptibility measurements at low temperature [8,16] it follows further that the dianion has a singlet spin ground state (S=0) with antiferromagnetically coupled iron centres; at higher temperatures the increasing ^{1}H NMR shifts and susceptibilities point to the population of non-singlet states. A qualitative MO description of the iron core ($4\text{-}Fe^{2.5+}$) results in the electron configuration $(a_1+e+t_2)^{12}$ $(e+t_1+t_2)^{10}$ $(t_1+t_2)^0$ with the second set of orbitals neither bonding nor antibonding [4]. In Mössbauer spectra of the other biologically important oxidation state, the trianion, in first instance a broadened quadrupole doublet [14,15] has been observed. Later on two doublets have been found with on the average a similar splitting as for the dianion (at low temperature) [5,10]; this is indicative for two inequivalent subsites in $[Fe_4S_4(SR)_4]^{3-}$ and localization of the extra

electron at one subsite. Magnetic susceptibilities [5,10] are consistent with an antiferromagnetic spin doublet ground state ($S=\frac{1}{2}$) but again indicate the population of higher spin states, even at the lowest temperatures in this case [10].

In this work we investigate the $[Fe_4S_4(SH)_4]^{3-,2-,0}$ cubane cluster by three different molecular orbital methods: the restricted Hartree-Fock-Slater-LCAO-frozen core (HFS-FC) method [18] and the same method but using a core pseudopotential [19] (HFS-PS) instead of the frozen core and the extended Hückel (EH) method [20]. The reason that we also include the (biologically irrelevant) neutral cluster in our study is to examine the influence of the negative charge on the calculated positive occupied orbital energies in the dianion; see sections 3.2 and 3.3.

The purpose of this study is twofold. On the one hand to obtain more information about the electronic structure of the cubane cluster and to interpret the optical excitation spectrum, the Mössbauer parameters and the temperature behaviour of the magnetic moment and the ^1H NMR shifts. On the other hand, we wanted to test the core pseudopotential version of the HFS-LCAO method and to compare this method with the HFS-scattered wave (SW) method [21,22] (which has been applied recently [23] to the related cluster $[Fe_4S_4(SCH_3)_4]^{2-}$) and the EH method on a realistic test system with more than one transition metal atom. This analysis is important in view of other possible applications of these methods, for instance to the study of chemisorption clusters.

Other theoretical studies of Fe-S non-heme proteins have concentrated on the 1-Fe active site using EH [24-28], HFS-SW [29] and GVB [30,31] methods and on the 2-Fe active site using the EH [32,33] and HFS-SW [34] methods.

2. *METHOD AND CALCULATIONS*

In all three computational methods used in this study (HFS-FC, HFS-PS and EH) only valence electrons are treated variationally; we have considered the 3d and 4s electrons on Fe, the 3s and 3p electrons on S and the 1s electron on H; the Slater type orbital (STO) basis was taken from the tables of Clementi and Roetti [35]: double zeta quality with an additional set of 4p functions on Fe (the exponents of the 4p basis functions were taken equal to those of the 4s functions).

As one can find detailed information about the HFS-LCAO method elsewhere, regarding the principles [18,19,36] and the application to small molecules and

transition metal complexes [36], we will mention here only the basic features. The HFS-LCAO matrix elements are calculated numerically; the scaling parameter α in the local exchange (X_α) potential is taken to be equal to 0.7. Mainly to simplify the calculation of the Coulomb potential in each integration point, the electron density $\rho(1) = \sum_{\mu,\nu} P_{\mu\nu} \chi_\mu(1) \chi_\nu(1)$ is expanded in one-centre fit functions with angular parts including $\ell \neq 0$ (in contrast to the HFS-SW method we do not introduce the muffin-tin approximation). This electron density is iterated to self-consistency. In the HFS-FC version the core orbitals are frozen (using double zeta STO's [35]) and the valence orbitals are orthogonalized to the core by adding extra core functions to the basis (single zeta STO's [35]); this of course requires additional density fit functions. In the HFS-PS version a pseudopotential is added to the one-electron HFS operator, which makes the core orbitals degenerate with the valence orbital to be calculated; the problem of which valence orbital has to be chosen is essentially solved by taking the average energy of the occupied valence levels and applying a perturbation correction to the valence orbital energies through second order [19]; the advantage of the pseudopotential approach is that we need less basis and fit functions.

We have compared the HFS-FC and HFS-PS methods, we have tested different density fit bases and we have investigated the effect of the perturbation correction in case of HFS-PS. All these tests were first performed for FeS, which can be considered as a subunit of the main cluster, and then for the $[Fe_4S_4(SH)_4]^{2-}$ dianion.

For FeS the internuclear distance has been taken equal to 2.45Å [37]. The HFS calculations on $[Fe_4S_4(SH)_4]^{3-,2-,0}$ were carried out in T_d symmetry (fig. 1; sulphur atoms which bridge iron atoms are indicated as S^*), although the

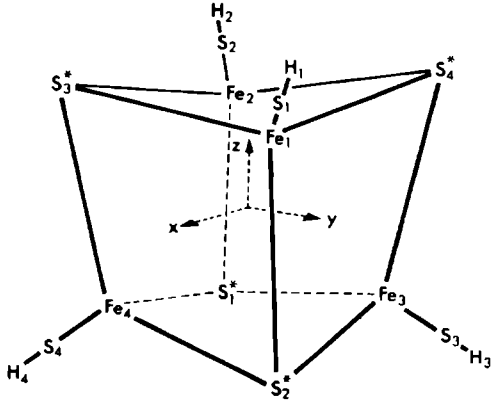

Figure 1. T_d geometry and atom numbering of $[Fe_4S_4(SH)_4]^{n-}$; sulphur atoms which bridge iron atoms are indicated as S^*.

real structure of the complex deviates slightly from T_d and actually has D_{2d} symmetry; by means of EH calculations (which were done in both T_d and D_{2d} symmetry), we have shown that this approximation has no drastic influence on the results.

The coordinates of the Fe and S atoms in the D_{2d} symmetry were taken from parameters for the crystal structure of $[(CH_3CH_2)_4N]_2[Fe_4S_4(SCH_2C_6H_5)_4]$ [4]; in T_d symmetry they were determined by averaging. The coordinates of the H atoms were chosen such that the S-H distances are equal to those in the H_2S molecule [38]; in T_d the Fe-S-H angle is 180^o (imposed by symmetry) and in D_{2d} it is equal to the Fe-S-C angle in $[(CH_3CH_2)_4N]_2[Fe_4S_4(SCH_2C_6H_5)_4]$ [4] ($\simeq$ 100 degrees).

Calculations on the 1-Fe and 2-Fe active sites have shown that replacing CH_3 groups by H atoms [25,29,32] does not influence the results essentially.

A problem we have in our calculations is to determine the electronic ground state configuration of the complexes $[Fe_4S_4(SH)_4]^{n-}$. In principle one could do this by comparing, for different electron configurations, the total energies. These are defined in the HFS scheme just as in the Hartree-Fock (HF) method except that the HF total exchange energy has been replaced by a statistical expression depending on the electron density only ($\sim \rho^{4/3}$) [21]. In practice the HFS total energies are affected by two kinds of errors (in addition to the errors present in the HF total energies):

1. the inaccuracy caused by the numerical integration scheme and by the electron density fit procedure (explained above);
2. for open shell electron configurations the HFS method does not calculate the total energies of the different possible spin multiplet states but some average over these states [36,39].

For the large $[Fe_4S_4(SH)_4]^{n-}$ clusters where the number of numerical integration points and density fit functions are necessarily rather limited, while different possible electron configurations lie very close in energy, the comparison of total energies is not a good criterion to decide which is the electronic ground state. Instead, we have defined the ground state as the state where all the molecular orbitals with the lowest energies are occupied with electrons, in a fully self-consistent manner.

3. *RESULTS AND DISCUSSION*

3.1. *FeS*

In order to test the core pseudopotential and the density fit basis to be

Table 1. Orbital energies and population analysis for FeS with spdfg fit basis

Method: HFS-		FC	PS[a)]
Orbital and Energy (Hartree)			
	σ	-0.542	-0.546
	σ	-0.235	-0.233
	σ	-0.169	-0.176
	π	-0.191	-0.189
	π	-0.153	-0.154
	δ	-0.194	-0.180
Gross atomic charges	Fe	0.39	0.33
Gross atomic	Fe : 3d	6.13	6.20
orbital populations	4s	1.22	1.21
	4p	0.25	0.27
	S : 3s	1.97	1.96
	3p	4.43	4.37
Net atomic and	Fe	7.44	7.45
atom-atom overlap	S	6.23	6.10
populations	Fe-S	0.33	0.45

a) HFS-PS results with perturbation corrections

used we have performed several calculations on FeS in the valence configuration $\sigma^2\sigma^2\sigma^2\pi^4\pi^2\delta^1$. Results for the orbital energies and the Mulliken population analysis [40,41] calculated with the most extensive fit bases are shown in table 1.

It can be concluded that there is good agreement between HFS-FC and HFS-PS. The perturbation corrections to the pseudopotential improve the orbital energies by less than 5% (about 0.02 Hartree), which is in agreement with the conclusions in the literature [19].

The influence of the fit basis is the following. The differences between the energies calculated with only s-type fit functions and those calculated

with s- and p-type functions are 6% at most. Adding a d-type fit function has almost no effect (3%) on the σ and π levels but improves the δ level by 15% which is still less than 0.03 Hartree. The changes caused by adding fit functions of still higher angular momentum, f- and g-type (and at the same time some more s- and p-type functions), are minor (3%). The influence of the fit basis on the populations is negligible. Clearly the charge density can be fitted with functions which need not necessarily go as high in angular momentum as the basis functions would suggest (otherwise atomic orbitals up to d-type would require charge density functions up to g).

In the large cubane cluster we have limited the fit basis to s- and p-type functions only.

3.2. *HFS-FC calculations on* $[Fe_4S_4(SH)_4]^{2-}$

Calculations have been done with s-type fit functions only (s fit basis) and with s- and p-type fit functions (sp fit basis). We have investigated three different valence electron configurations: $3t_1^6 4e^4 8t_2^0$, $3t_1^6 4e^0 8t_2^4$ and $3t_1^4 4e^0 8t_2^6$; the first one gives rise to a singlet spin state, whereas the second and third configurations can lead to singlets and triplets.

The HFS-SW calculation of Yang et al. [23] for the similar complex $[Fe_4S_4(SCH_3)_4]^{2-}$ resulted in the ground state configuration $t_1^6 e^0 t_2^4$. In our calculations, independently of the fit basis used (s or sp), we have found the ground state (defined by a self-consistent occupation of the lowest orbitals, see section 2) to be $t_1^6 e^4 t_2^0$; the other two configurations led to empty orbitals lying lower than occupied ones. So, our ground state configuration disagrees with that found by HFS-SW for the methyl analogue of the cluster, but it is in agreement with our EH calculations (for T_d and D_{2d} symmetry).

Comparing the results for the three different configurations with each other (using the sp fit basis) we observe that the orbital energies are shifted to lower values going from $t_1^6 e^4 t_2^0$ to $t_1^6 e^0 t_2^4$ (by about 0.4 eV) and again from the latter to $t_1^4 e^0 t_2^6$ (about 0.2 eV). The effect of enlarging the fit basis from s to sp is an almost constant shift of all levels (upwards by about 1.5 eV for the higher valence levels).

In fig. 2 we have shown the MO scheme corresponding to the $t_1^6 e^4 t_2^0$ configuration in the sp fit basis. The character of the orbitals indicated in this figure was determined by a Mulliken population analysis [40,41]; the uppermost valence levels have mainly Fe(3d) character and they are separated by a gap of about 1 eV from levels which mainly consist of S(3p) orbitals; another gap of about 1 eV separates the latter from a cluster of mainly

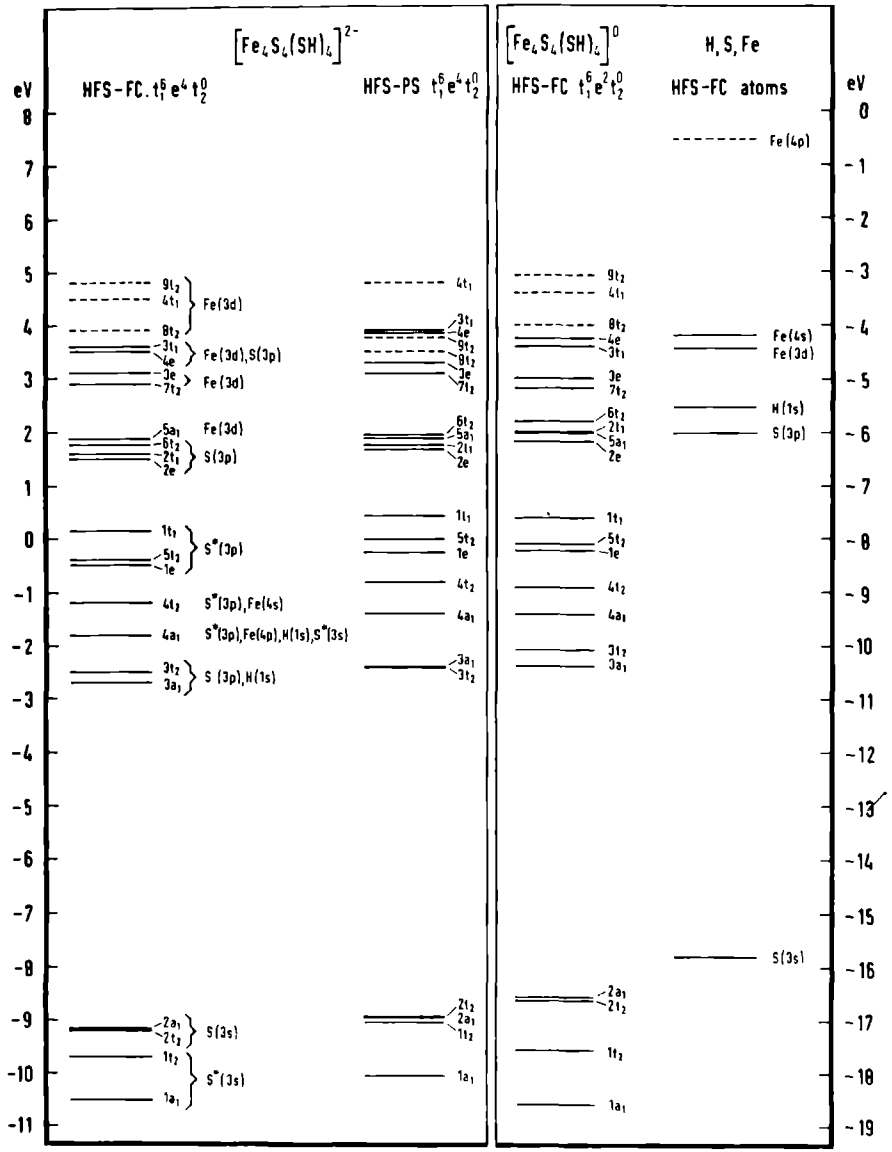

Figure 2. MO level scheme and characterization of orbitals for HFS calculations in T_d symmetry; on request a list of detailed information about MO coefficients or MO population data is available from the authors.

$S^*(3p)$ levels. The occupation of the MO's with mainly Fe(3d) character: $5a_1^2$, $7t_2^6$, $3e^4$, $4e^4$, $3t_1^6$, $8t_2^0$, $4t_1^0$, $9t_2^0$, confirms the qualitative MO description [4] $(a_1+e+t_2)^{12}$ $(e+t_1+t_2)^{10}$ $(t_1+t_2)^0$. In the HFS-SW calculation [23] only one distinct gap is found with a somewhat greater width, while the highest occupied orbitals consist of a mixture of orbitals with predominantly Fe(3d) character and orbitals with Fe(3d)-S(3p) character. Whereas the HFS-SW results [23] in these respects seem to be sensitive to the exact occupation of the highest valence levels, our results do not change qualitatively, and only slightly quantitatively, when changing the electron configuration (e.g. from $t_1^6e^4t_2^0$ to $t_1^6e^0t_2^4$).

A peculiar point in the calculation of the dianion $[Fe_4S_4(SH)_4]^{2-}$ is the large number of positive orbital energies.

Schwarz [42] has found for the O^- and F^- ions that local density schemes, such as HFS, yield positive orbital energies, while in Hartree-Fock (HF) theory all orbital energies are negative; he concluded that this difference in the energies practically does not lead to a difference in the wavefunctions. In general, positive orbital energies are reached with smaller ionicity in HFS than in HF theory, because of the higher orbital energies in the former. HFS-DV (discrete variational) calculations for the $(MgO_6)^{10-}$ cluster [43] also showed positive orbital energies for the occupied levels. If the crystal field of bulk MgO was included in the calculation, however, all levels were stabilized (showing an almost constant downward shift of about 55 eV).

3.3. *HFS-FC calculations on $[Fe_4S_4(SH)_4]^{0,3-}$*

In order to investigate the origin of the positive orbital energies obtained for the dianion without taking into account the stabilizing field of the positive counterions explicitly we have performed [44] a calculation on the neutral cluster with configuration $t_1^6e^2t_2^0$ in the sp fit basis; the results are presented in fig. 2. Note that in essence all levels are shifted by a constant amount ($\sim$ 8 eV) to lower energies, such that all occupied orbitals have negative energies; also the relation with atomic Fe, S and H levels can be seen now; the cluster valence levels are somewhat stabilized compared to the corresponding free atom levels, due to bonding interactions. So the positive orbital energies in the dianion are correlated with the overall net charge and can be expected to vanish when the positive counterions are taken into account explicitly.

The calculations on the trianion (configuration $t_1^6e^4t_2^1$) show a further shift of the levels of the dianion towards positive energy. The magnitude of

this shift (2- → 3-) is indeed about half of the shift (0 → 2-).

3.4. HFS-PS calculations on $[Fe_4S_4(SH)_4]^{2-}$

The pseudopotential calculations have been performed with an sp fit basis for the configuration $t_1^6 e^4 t_2^0$ without and with perturbation corrections (see section 2) and for the configuration $t_1^6 e^0 t_2^4$ with corrections; the level scheme for $t_1^6 e^4 t_2^0$ with corrections is shown in fig. 2.

The corrected energies of the occupied orbitals do not differ significantly from the uncorrected ones, mostly by less than about 0.5 eV or 0.02 Hartree; this is in agreement with the findings for FeS. Larger differences have been found for the virtual levels: without perturbation, the empty $6a_1$ orbital lies between the filled $7t_2$ and 3e orbitals, whereas in the scheme with perturbation (see fig. 2) this $6a_1$ orbital (not drawn) has moved up above the filled levels and now the empty $8t_2$ and $9t_2$ orbitals lie between the filled 3e and 4e levels.

The presence of these virtual orbitals between the occupied ones could not be removed by choosing a different orbital occupancy; always the self-consistent result showed a level ordering which was not consistent with the occupancy. So we must conclude that the PS method in this case does not lead to a unique ground state as defined in section 2. The case of $[Fe_4S_4(SH)_4]^{2-}$ is a difficult one, however, since the highest occupied and the lowest empty orbitals lie very close indeed (cf. the situation in metals with partly filled bands). Moreover, we have found that the PS method is still useful even for this system, since the different electron configurations only show a more or less constant energy shift of the occupied MO levels and the electronic charge distribution (section 3.6) calculated with the PS method (for all these configurations) is in good agreement with the FC results. In other possible applications of the PS method, e.g. to chemisorption clusters the precise occupation of the highest (metal) levels is not important (see also section 4).

3.5. EH calculations on $[Fe_4S_4(SH)_4]^{2-}$

As already mentioned we have used an idealized T_d structure of the complex in all HFS calculations in order to save computation time. To study the effect of this idealization we have performed two non-iterative EH calculations, one in T_d and the other in the real D_{2d} symmetry. Table 2 gives the VSIP's and basis functions (STO's) as taken from ref. [45,46]; the 3d orbital on Fe is represented by a contracted set of two d functions; the Wolfsberg-Helmholz parameter κ was set to 2.5 [46].

When comparing the EH-MO scheme for T_d symmetry in fig. 3 with the HFS

Table 2. Parameters for extended Hückel calculations[a)]

Atom	AO	VSIP	ζ
Fe	3d	-8.70	5.35/2.20[b)]
Fe	4s	-7.90	1.40
Fe	4p	-4.55	1.56
S*,S	3s	-20.67	2.1223
S*,S	3p	-11.58	1.8273
H	1s	-13.60	1.0

a) from ref. [45,46]

b) the contraction coefficients are: 0.565088 and 0.584953

schemes in fig. 2, we see the great differences between the two methods; for instance the large gap in EH between Fe(3d) and S(3p), S*(3p) levels separates into two smaller gaps in HFS; the latter level distribution corresponds much better with the experimental electronic spectrum (section 3.7). The ground state configuration derived from the EH results is the same, however, as that from the HFS-FC results: $t_1^6 e^4 t_1^0$. Also the splitting between the highest occupied molecular orbital (HOMO) and the lowest unoccupied molecular orbital (LUMO) differs little, but note that in EH the LUMO is the $4t_1$ orbital whereas in HFS it is the $8t_2$ orbital.

Finally, we see from fig. 3 that in going from T_d to D_{2d} symmetry, the MO scheme does not change much; the obvious effect is a (small) lifting of degeneracy. Also the charge distribution is not much affected (section 3.6). So one can safely use results from calculations in T_d symmetry also in case of the HFS calculations.

3.6. Population analysis and electron density plots

We have represented the charge distribution of the cluster by a Mulliken population analysis [40,41] (see tables 3 to 5). The character of each MO as indicated in figs. 2 and 3 was obtained by analyzing these data per MO. Moreover, we have made some electron density and density difference plots (density of the complex, minus the sum of atomic densities) for several planes through the $[Fe_4S_4(SH)_4]^{2-}$ cubane. Results for two planes are shown in figs. 4 and 5.

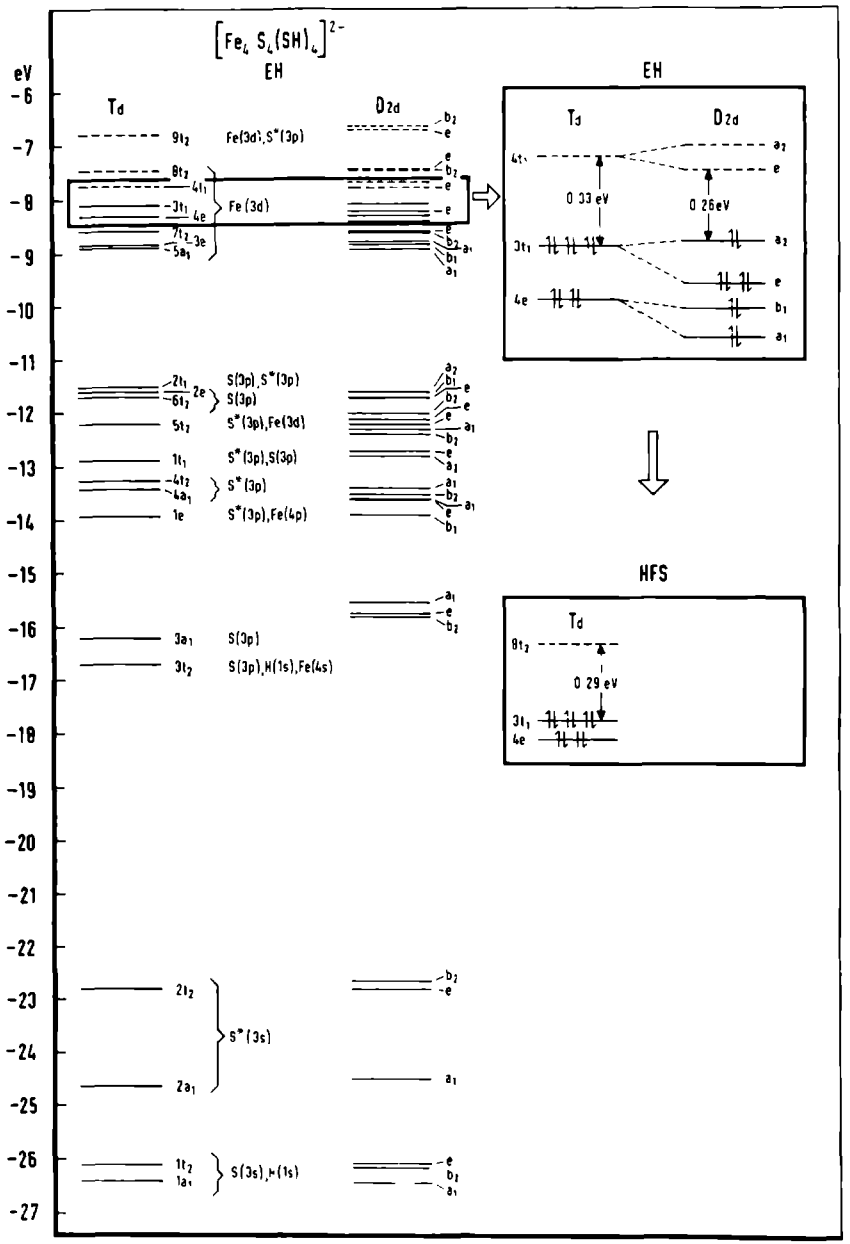

Figure 3. MO level scheme and characterization of orbitals for EH calculations in T_d and D_{2d} symmetry. Comparison of HOMO-LUMO splittings.

Looking at tables 3 to 5 and comparing the electron density plots (not shown) for different HFS calculations, we see that there is generally good agreement between these calculations. The results for the FC s fit basis (not shown) deviate somewhat. The perturbation correction in the HFS-PS calculations has no significant effect on the populations. A minor effect is obtained by changing the electron configuration: going from $t_1^6 e^4 t_2^0$ via $t_1^6 e^0 t_2^4$ to $t_1^4 e^0 t_2^6$ one finds mainly an increase of Fe net population and a decrease of the Fe-Fe, Fe-S^* and S-H overlap populations. This can be understood from the Fe(3d) and S(3p) character of the orbitals involved (see fig. 2).

The two EH calculations (in T_d and D_{2d} symmetry) also agree very closely. Qualitatively the EH results show the same features as the HFS results but there are some discrepancies regarding the net and overlap populations discussed below.

From table 3 we see that the atomic charges on Fe ($\simeq +0.25$), S^*($\simeq -0.30$) and S($\simeq -0.60$) are much smaller than their ionic values, $Fe^{2.5+}$, S^{2-}. This indicates mainly covalent bonding. From table 4 it appears that 0.55 electron is donated by the sulphur ligands to the 4s orbital of Fe, 0.89 electron to the 4p orbitals (both of which are empty in $Fe^{2.5+}$) and 0.80 electron to the Fe 3d shell (in addition to the 5.5 d electrons in $Fe^{2.5+}$). The outer S atoms possess a larger electron density than the bridging S^* atoms, which clearly originates from the populations of the 3p orbitals. In agreement with this, figs. 4a and 5a show that the density is polarized along the Fe-Fe and Fe-S bonds more than along the Fe-S^* bond. The population of the Fe 4p orbitals, which indicates a strong sp hybridization on Fe, confirms the picture of directional Fe-S bonds. Also, the greater Fe-S overlap population compared to that of Fe-S^* (table 5) underlines this conclusion.

In table 5 we observe a remarkable difference between HFS and EH. In particular, there is a rather large shift of electrons from the Fe net to the Fe-Fe overlap population. The same shift has been found to a smaller extent between different HFS calculations (see above). A detailed analysis has shown that the large negative Fe-Fe overlap population and the extremely high Fe net population in HFS, are caused mainly by the $4t_2$(S^*(3p), Fe(4s)) and $7t_2$(Fe(3d)) orbitals, suggesting an antibonding Fe-Fe interaction. The density difference plots in figs. 4b and 5b demonstrate the contrary however, namely a slight accumulation of electron density between the Fe atoms. So one can conclude that the four Fe atoms in the tetrahedral arrangement are non-bonding or weakly bonding. As observed earlier [47] the Mulliken population analysis looses some of its significance when used with a larger than minimal basis set.

Table 3. Gross atomic charges[a)]

Complex	$[Fe_4S_4(SH)_4]^{2-}$		$[Fe_4S_4(SH)_4]^{0}$	$[Fe_4S_4(SH)_4]^{3-}$	$[Fe_4S_4(SH)_4]^{2-}$	
Method	HFS-FC	HFS-PS[b)]	HFS-FC		EH-T_d	EH-D_{2d}
Configuration	$t_1^6e^4t_2^0$		$t_1^6e^2t_2^0$	$t_1^6e^4t_2^1$	$t_1^6e^4t_1^0$	
Fe	0.26	0.27	0.29	0.23	-0.05	0.01
S*	-0.31	-0.31	-0.11	-0.40	-0.16	-0.16
S	-0.60	-0.58	-0.47	-0.63	-0.35	-0.40
H	0.15	0.12	0.29	0.05	0.07	0.06

a) HFS results with sp fit basis

b) HFS-PS results with perturbation corrections

Table 4. Gross atomic orbital populations[a)]

Complex	$[Fe_4S_4(SH)_4]^{2-}$		$[Fe_4S_4(SH)_4]^{0}$	$[Fe_4S_4(SH)_4]^{3-}$	$[Fe_4S_4(SH)_4]^{2-}$	
Method	HFS-FC	HFS-PS[b)]	HFS-FC		EH-T_d	EH-D_{2d}
Configuration	$t_1^6e^4t_2^0$		$t_1^6e^2t_2^0$	$t_1^6e^4t_2^1$	$t_1^6e^4t_1^0$	
Fe 3d	6.30	6.28	6.30	6.32	6.35	6.35
Fe 4s	0.55	0.62	0.60	0.52	0.53	0.52
Fe 4p	0.89	0.83	0.81	0.92	1.17	1.12
S* 3s	1.93	2.01	1.95	1.91	1.57	1.57
S* 3p	4.38	4.30	4.16	4.49	4.60	4.60
S 3s	1.82	1.87	1.84	1.83	1.37	1.46
S 3p	4.79	4.71	4.63	4.81	4.98	4.94
H 1s	0.85	0.88	0.71	0.95	0.93	0.94

a) HFS results with sp fit basis

b) HFS-PS results with perturbation corrections

Table 5. Net atomic and atom-atom overlap populations[a)]

Complex	$[Fe_4S_4(SH)_4]^{2-}$		$[Fe_4S_4(SH)_4]^{0}$	$[Fe_4S_4(SH)_4]^{3-}$	$[Fe_4S_4(SH)_4]^{2-}$	
Method	HFS-FC	HFS-PS[b)]	HFS-FC		EH-T_d	EH-D_{2d}
Configuration	$t_1^6e^4t_2^0$		$t_1^6e^2t_2^0$	$t_1^6e^4t_2^1$	$t_1^6e^4t_1^0$	
net						
Fe	13.64	11.68	13.79	14.27	6.82	6.80
S*	6.24	6.29	6.03	6.37	5.36	5.35
S	6.25	6.22	6.06	6.40	5.59	5.68
H	0.77	0.82	0.54	1.01	0.55	0.56
overlap						
Fe-Fe	-4.14	-2.84	-4.28	-4.49	0.03	0.04[c)]
Fe-S*	0.21	0.16	0.19	0.19	0.56	0.56[c)]
Fe-S	0.64	0.62	0.58	0.63	0.75	0.66
S-H	0.42	0.39	0.53	0.22	0.79	0.81

a) HFS results with sp fit basis

b) HFS-PS results with perturbation corrections

c) averaged over non-equivalent pairs

The population analysis of the model clusters for 1-Fe [25,28] and 2-Fe [32,33] active sites show the same overall results for gross atomic charges and orbital populations. The weak direct Fe-Fe bonding has been reported also for a 2-Fe active site using the HFS-SW method [34].

Finally, we compare the results for the dianion and neutral cluster. From tables 3 to 5 it is clear that the two outgoing electrons originate almost entirely from the S*(3p)-S(3p)-H(1s) part of the cluster. This, at first sight, is unexpected since these two electrons are taken from the 4e level which has mainly Fe(3d) character. Apparently, after removal of the double negative charge, the orbitals relax in such a way that the total charge density around

(a) (b)

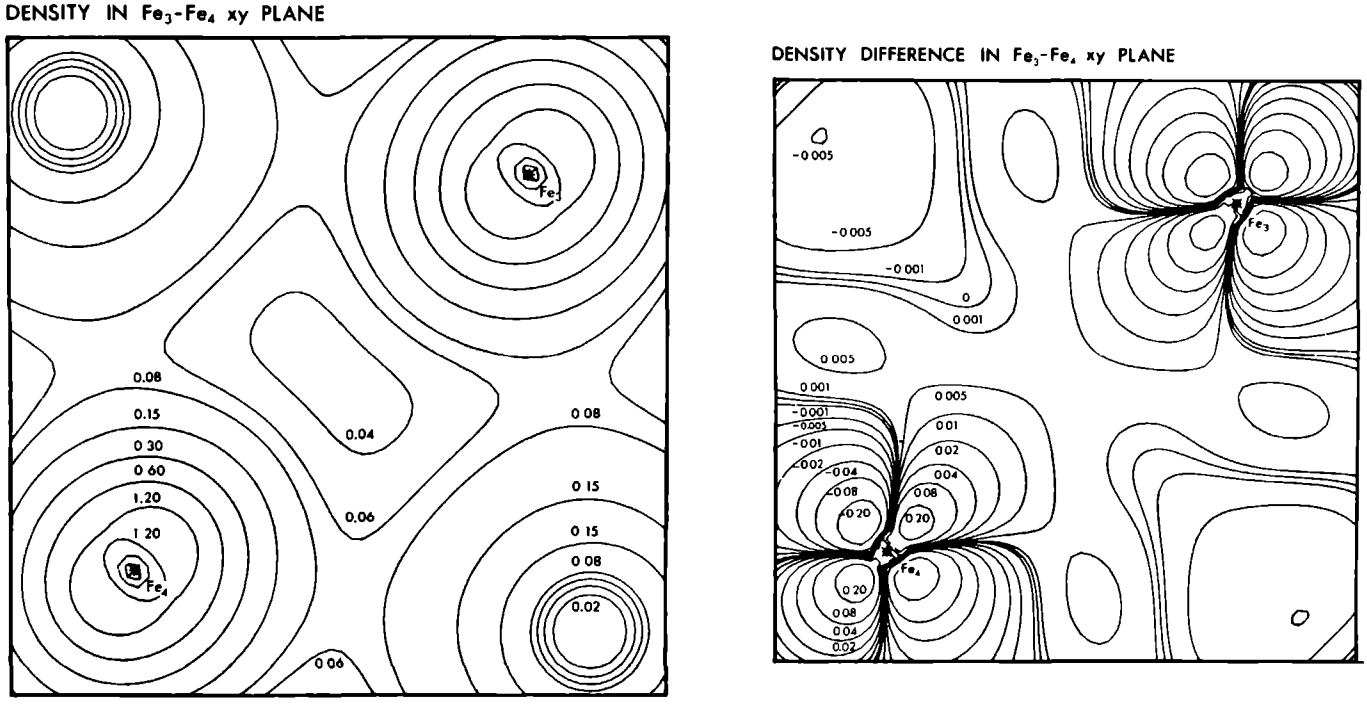

Figure 4. Electron density plot (a) and electron density difference plot (b) in Fe3-Fe4 xy plane for $[Fe_4S_4(SH)_4]^{2-}$ calculated with the HFS-FC method in the $t_1^6e^4t_2^0$ configuration with an sp fit basis; values in e/bohr^3.

(a)

(b)

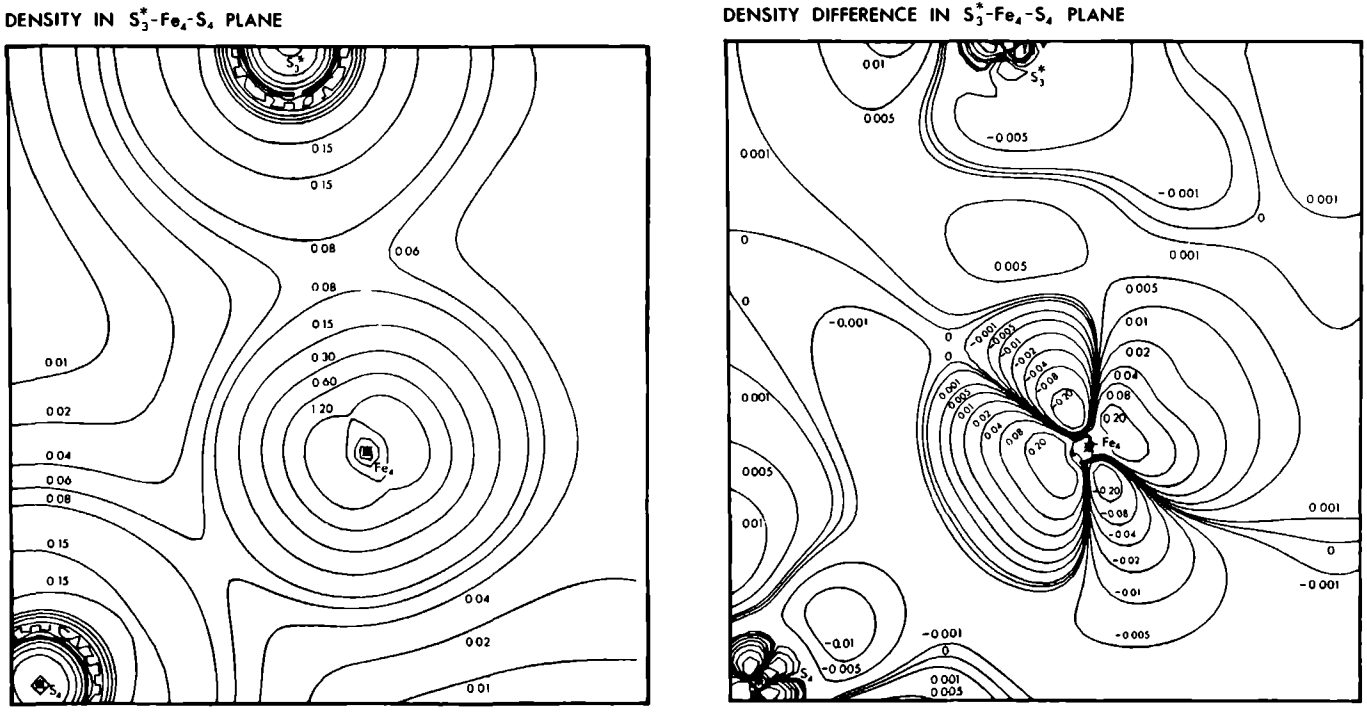

Figure 5. Electron density plot (a) and electron density difference plot (b) in S_3^*-Fe_4-S_4 plane for $[Fe_4S_4(SH)_4]^{2-}$ calculated with the HFS-FC method in the $t_1^6e^4t_2^0$ configuration with an sp fit basis; values in e/bohr^3.

the Fe centres is not changed essentially; this is confirmed by a population analysis. Going to the trianion, the third electron goes into the $8t_2$ level, which has almost purely Fe(3d) character. Again we observe the same trend, namely that also in this case the Fe atoms act mainly as charge redistributors. Thus we can understand the almost unchanged quadrupole splitting (cf. section 3.8) upon electron addition or removal [5,8,10,13-15]. Similar observations have been made for the 1-Fe and 2-Fe active site clusters, $[Fe(SH)_4]^{1-,2-}$ [31] and $[Fe_2S_2(SH)_4]^{0,1-}$ [32] and in the series $[Fe_2(CO)_6(PH_2)_2]^n$, n=0,-1,-2 [48]. These results should be quite important in explaining the redox behaviour of the Fe-S proteins (and their synthetic analogues).

3.7. Electronic excitation spectrum

In the experimental optical absorption spectrum of $[Fe_4S_4(SR)_4]^{2-}$ in solution [6,8,11,14] two bands, at 4.2 eV and 3.0 eV, have been attributed to S→Fe charge transfer transitions; shoulders have been observed around 3.5 eV and at 1.9 eV. In addition, the spectrum of the solid [13] shows absorption bands at 2.5 eV and 1.6 eV. See fig. 6.

We have calculated excitation energies:

a) from the ground state levels (GS);

b) from transition state calculations [21,49] for some excitations (TS).

The transition state procedure accounts for the orbital relaxation effects which occur upon excitation (in this respect it is similar to the ΔSCF method [50]), and it has shown to yield results in quantitative agreement with the experimental spectra for a series of transition metal oxo-complexes [51]. The subtraction of ground state energy levels (method a) can not be justified theoretically, but the results show that there is very little difference (less than 3%) between a) and b). This is related to the observation (sections 3.2 and 3.3) that changes in the electron configuration just cause a practically constant shift of all levels in this large complex. Fig. 6 shows all possible symmetry allowed excitations from the $t_1^6e^4t_2^0$ ground state corresponding with the HFS-FC results in the sp fit basis.

By looking at the character of the orbitals involved (fig. 2) one can assign the experimentally observed bands at 1.9 and 1.6 eV to Fe(3d)→Fe(3d) transitions. The bands at 3.0 and 2.5 eV are S(3p)→Fe(3d) charge transfer excitations, probably mixed with the relatively high lying $5a_1 \rightarrow 4t_1$ and $5a_1 \rightarrow 9t_2$ d-d transitions; also the shoulder around 3.5 eV will be a charge transfer band. The absorption around 4.2 eV has mainly $S^*(3p) \rightarrow Fe(3d)$ charge transfer

character. From our calculations we predict some symmetry-allowed d-d transitions at lower energies as well, but we have not calculated the intensities. A lower energy band is observed in the spectrum of HP_{red} at 1.2 eV [52] but it seems to have no counterpart in $[Fe_4S_4(SR)_4]^{2-}$.

An analysis for other configurations or from the PS results is hampered by the circumstance that some of the empty levels are lying lower than filled ones; disregarding these empty levels yields, as could be expected, an incom-

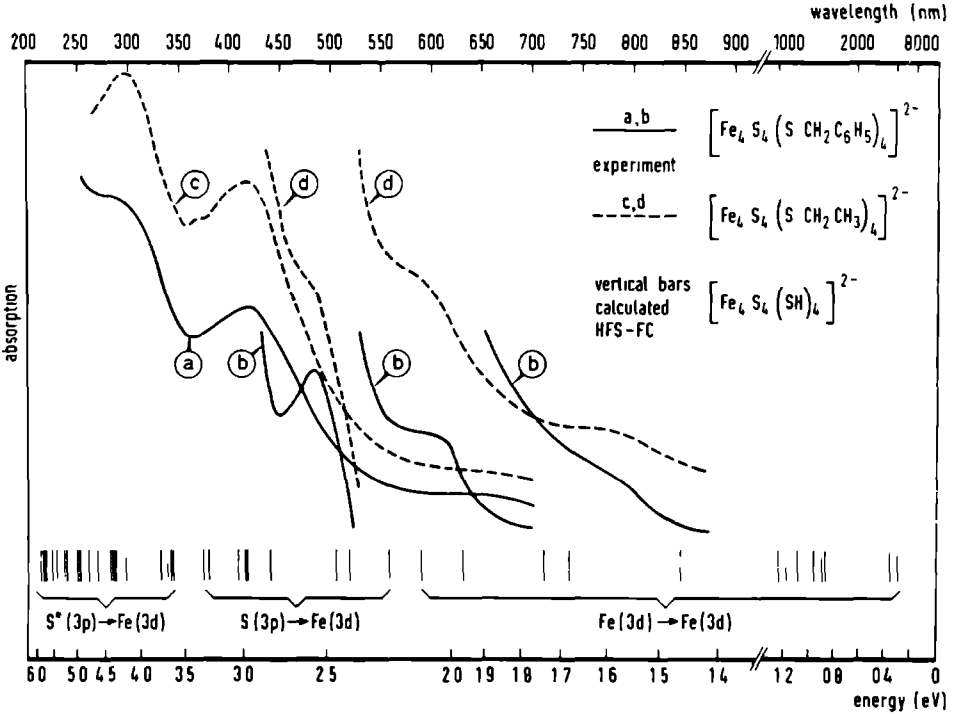

Figure 6. Calculated electronic transitions (HFS-FC, $t_1^6e^4t_2^0$, sp fit basis) of $[Fe_4S_4(SH)_4]^{2-}$ (vertical bars) compared with experimental electronic absorption spectra of $[(CH_3CH_2)_4N]_2[Fe_4S_4(SCH_2C_6H_5)_4]$ (——) in acetonitrile solution (a) [6,14] and as a thin film (b) [13] and of $[(CH_3CH_2CH_2)_4N]_2[Fe_4S_4(SCH_2CH_3)_4]$ (---) in DMF solution (c) [11] and as a thin film (d) [13]. Dotted vertical bars represent transitions which are symmetry forbidden in T_d but which will be allowed in D_{2d}.

plete and less satisfactory picture.

An analysis of the EH results (see fig. 3) shows immediately that these do not agree with the measured electronic spectrum although the correct order of the bands is predicted. In particular they yield much too high frequencies for some of the charge transfer bands; e.g. no absorptions are found in the range from 2.2 to 3.8 eV due to the large gap discussed in section 3.5.

In the experimental spectrum of the trianion $[Fe_4S_4(SR)_4]^{3-}$ one observes a shift of about 0.4 eV, relative to the dianion spectrum, of the band at 3.0 eV to higher energy, while the other bands stay practically at the same positions [6,14]. In our HFS-FC calculations on the trianion (ground state) we observe a change in the excitation energies which reflects this behaviour almost quantitatively.

3.8. Quadrupole splitting

From Mössbauer measurements on $[Fe_4S_4(SR)_4]^{2-}$ at low temperature (4.2 K) [8,13-15] a quadrupole splitting of the ^{57}Fe Mössbauer levels of 1.26 mm/sec has been obtained. Moreover, one has derived that the electric field gradient on the Fe nucleus has a positive principal component V_{zz} and an asymmetry parameter $\eta \equiv (V_{xx} - V_{yy})/V_{zz} < 0.4$. From the fact that only one quadrupole doublet was observed, it has been concluded that all four Fe atoms are equivalent to each other. For the trianion the situation is different. At first, a broadened spectrum with a similar quadrupole splitting as for the dianion has been seen at low temperature [14,15]. Subsequent experiments [5] and especially a detailed analysis [10] have shown that the spectrum consists of two distinct quadrupole doublets, indicating two inequivalent subsites in $[Fe_4S_4(SR)_4]^{3-}$. In our calculations we have applied symmetry restrictions to the nuclear framework and to the electron distribution which prevent us from distinguishing between both subsites. Therefore we can compare our calculated quadrupole splitting for the trianion only with an average of the two splittings observed experimentally. Specifically, this average for $[(CH_3CH_2)_4N]_3[Fe_4S_4(SCH_2C_6H_5)_4]$ in frozen solution (again at 4.2 K) amounts to 1.57 mm/sec [10]; the average value of 1.17 mm/sec for the crystalline compound corresponds with a more strongly distorted structure [10].

We have calculated the electric field gradient from the HFS molecular orbitals in the following way. Each STO in the atomic orbital basis has been expanded as a linear combination of 3, 4 or 5 Gaussian type orbitals (GTO's) using the exponents and coefficients from Stewart's maximum overlap fits [53]. These expansions have been substituted into the MO's obtained from the HFS calculations and the components and principal values of the electric field gradient

Table 6. Electric field gradient and quadrupole splitting

	$[Fe_4S_4(SR)_4]^{2-}$									$[Fe_4S_4(SR)_4]^{3-}$	
	HFS-FC[a] T_d			HFS-PS[a] T_d			EH T_d | D_{2d}		Experimental (low T)[b]	HFS-FC T_d	Experimental (low T)[c]
	one-centre		Total	one-centre		Total	one-centre			one-centre	
	STO	STO-3GTO	STO-3GTO	STO	STO-3GTO	STO-3GTO	STO	STO		STO	
V_{zz} (10^{22} N/mC)	4.2	3.8[d]	3.0[e]	3.4	3.3[f]	3.0	1.1	1.2	> 0	4.3	-
η[g]	0	0	0	0	0	0	0	0.3	< 0.4	0	-
Quadrupole splitting[h] (mm/sec)	9.1 (5.8)	8.3 (5.3)	6.6 (4.2)	7.4 (4.7)	7.1 (4.5)	6.6 (4.2)	2.3 (1.5)	2.6 (1.7)	1.25	9.5 (6.1)	1.57

a) values are given for the configuration $t_1^6 e^4 t_2^0$ calculated with an sp fit basis

b) from ref. [8,13-15]

c) from ref. [10]; see also text

d) STO-4GTO expansion: V_{zz} = 4.0; STO-5GTO expansion: V_{zz} = 4.1

e) STO-4GTO expansion: V_{zz} = 3.2

f) STO-4GTO expansion: V_{zz} = 3.3; STO-5GTO expansion: V_{zz} = 3.3

g) in T_d symmetry η = 0 since the local symmetry on Fe is C_{3v}

h) calculated with Q = 0.21 barns (quadrupole moment of the I = 3/2 excited state of the ^{57}Fe nucleus [55]; values in brackets have been obtained by correcting for core polarization using the approximate Sternheimer factor (1-R) = 0.64 [56,57]

tensor on the Fe nucleus have been calculated with the one-electron properties package of the program POLYATOM [54] including all multi-centre contributions. The one-centre contributions have been directly calculated with the STO basis also, in order to verify that the STO-3,-4 or -5GTO expansion did not significantly influence the results. For the EH molecular orbitals we have only calculated these one-centre terms (after first orthogonalizing the EH basis orbitals to the core orbitals [45]) since the multi-centre contributions appeared to be small (less than 20%).

From table 6 where the results are listed we observe that particularly the HFS absolute values for the Fe quadrupole splitting are much too large. However, the HFS calculations predict correctly that the change in the quadrupole splitting in going from the dianion to the trianion is small [5,8,10,13-15]. This is consistent with the picture emerging from these calculations that the Fe atoms mainly act as charge redistributors for the extra electron. The results from different HFS calculations on the same (2^-) complex, FC or PS, different density fit bases, different electron configurations do not vary much.

The overestimate of the quadrupole splitting can be ascribed in part to the lack of core polarization effects in the HFS-FC and HFS-PS calculations as well as in the EH calculation. Correcting for these effects by the use of an approximate Sternheimer factor, which has been calculated for a 3d-electron in the Fe^{2+} ion, [56,57], brings the EH results into reasonable agreement with experiment; the HFS values are still too high. This is probably related to the very high Fe net atomic population and negative Fe-Fe overlap population resulting from the HFS but not from the EH calculations (see section 3.6). The Mössbauer quadrupole splitting is a very sensitive measure of the charge distribution around the Fe atom (it depends mainly on the differences in 3d orbital populations). The HFS results with the charge density represented only by s- and p-type fit functions (during the iterations to self-consistency) may not be sufficiently accurate to reproduce this detailed d-electron charge distribution. The good agreement with experiment for the much simpler EH method must then be regarded as fortuitous, although it seems to occur more generally [24,26,28,33].

3.9. *Magnetic properties*

From the Mössbauer spectra [8,13-15], the ^1H NMR shifts of SCH_2 protons [8,16] and the magnetic susceptibility [8] at low temperature it follows that the ground state of the complex $[Fe_4S_4(SR)_4]^{2-}$ is a singlet spin state or, in

other words, that the Fe centres are antiferromagnetically coupled. At higher temperature the ^{1}H NMR shifts and the susceptibility increase [8,16], indicating a thermal population of excited non-singlet spin states. The magnetic moment per iron atom nearly obeys an exponential law $M \sim \exp(-\Delta E/kT)$ in the temperature range 140K < T < 300K with an excitation energy ΔE of about 0.02 eV.

From the HFS calculations as well as from the EH calculations we have found indeed a singlet closed shell ($3t_1^6 4e^4$) ground state. The distance $\Delta\varepsilon$ to the first excited level is 0.29 eV in the HFS-FC results† (in T_d symmetry), but this value will probably be reduced somewhat by the symmetry lowering to D_{2d}, (see fig. 3; in EH there is indeed such a reduction of $\Delta\varepsilon$ from 0.33 eV to 0.26 eV). What is more important is that, in contrast with the optical spectrum where we look at singlet-singlet transitions, we are interested here in the excitation energy ΔE to the lowest non-singlet state (e.g. triplet) which is lower (according to Hund's rule) than the excitation energy calculated by the restricted HFS method which in fact lies in between the singlet-triplet and the singlet-singlet excitation energies. Therefore we can only consider the HFS value $\Delta\varepsilon$ = 0.29 eV as an upper bound for the excitation energy ΔE. The result ΔE < 0.29 eV is not very useful in practice but at least it is not in contradiction with the experimental result $\Delta E \simeq$ 0.02 eV.††

In the HFS-SW calculations [23] the lowest energy in T_d symmetry was found to correspond with the $t_1^6 e^0 t_2^4$ configuration, leading to a non-singlet ground state. By invoking the symmetry distortion to D_{2d} symmetry [23] one could obtain a closed shell (antiferromagnetically coupled) ground state in agreement with experiment.

---

† *The excitation energy ΔE should in fact be obtained as the level difference $\Delta\varepsilon$ in a transition state calculation but this will not much affect the result (cf. section 3.7).*

†† *Also in the calculated optical transition energies we find errors of about 0.5 eV relative to the experimental spectrum; still we can regard the agreement between the HFS results (section 3.7) and experiment as quantitative since the measured spectrum consists of rather broad bands which are correctly reproduced.*

4. CONCLUSIONS

Summarizing, we can conclude that the Hartree-Fock-Slater-LCAO method yields results for the $[Fe_4S_4(SH)_4]^{2-,3-}$ complex which are in fair agreement with the experimental electronic absorption spectrum and magnetic behaviour. Extended Hückel results are not in agreement with the optical spectrum. The HFS value for the electric field gradient on the Fe nucleus is considerably larger than the experimental value from Mössbauer quadrupole splitting; this may be due to the insufficient accuracy of the present HFS calculation (which uses only s- and p-type fit functions for representing the electronic charge density during the iterations) in describing the detailed charge distribution around the Fe nucleus. It is probably fortuitous that the EH value for this electric field gradient agrees better with experiment. The small relative change in quadrupole splitting when going from the dianion to the trianion is correctly predicted by the HFS method.

The Fe-S bonding in this Fe-S cubane complex is mainly covalent; the charges on the Fe atoms and especially the bridging S^* atoms are quite small. Direct Fe-Fe bonding or antibonding is weak. In relation to the practically important redox behaviour of this complex in the biocatalysts high potential iron protein and ferredoxin it is interesting that we have found that electrons taken away from or added to this complex will originate mainly from or will be going to the sulphur ligands, although the molecular orbitals which donate or receive these electrons are composed strongly of Fe(3d) orbitals in the original complex; the Fe atoms mainly act as charge redistributors.

About the HFS-core pseudopotential (PS) method we can conclude the following. Most results agree closely with the frozen core (FC) calculations: electronic charge distribution, Mössbauer quadrupole splitting, positions of the occupied levels. This holds even if we omit the perturbation procedure to correct the pseudopotential for the position of each individual valence level (starting with a pseudopotential for the average valence level energy). Somewhat larger deviations occur for some of the virtual levels. For the large 4-Fe complex considered here, with only a very small gap between the highest occupied levels and the lowest virtual ones, some of the virtual levels are found between the occupied ones in the PS calculation. Since this occurs for any electron configuration chosen during the iteration to self-consistency it is not possible to determine the ground state configuration by the PS method. Although we do not wish to disregard this problem, we observe, on the other hand, that the PS method can still be very useful since some rearrangement of

electrons betweeen the MO's around the "Fermi level" hardly changes the overall charge distribution and the relative positions of the occupied MO's. We have reached the same conclusion in HFS calculations for the chemisorption of acetylene on transition metal clusters, where the exact occupancy of the levels in the metal "d-bands" practically did not affect the results found for the acetylene bonding.

ACKNOWLEDGEMENT

We thank Prof.dr. P. Ros and Dr. H.L.M. van Gaal for valuable discussions.

The investigations were supported (in part) by the Netherlands Foundation for Chemical Research (SON) with financial aid from the Netherlands Organization for the Advancement of Pure Research (ZWO).

REFERENCES

[1] W.H. Orme-Johnson, Annu. Rev. Biochem. 42 (1973) 159.

[2] G. Palmer, The Enzymes, Vol. XII, Part B, 3rd ed., P.D. Boyer, Ed., Academic Press, New York, N.Y., 1975, p. 1.

[3] W. Lovenberg, Ed., Iron-Sulfur Proteins, Vol. I-III, Academic Press, New York, N.Y., 1973, 1973, 1977.

[4] B.A. Averill, T. Herskovitz, R.H. Holm, J.A. Ibers, J. Am. Chem. Soc. 95 (1973) 3523.

[5] R.W. Lane, A.G. Wedd, W.O. Gillum, E.J. Laskowski, R.H. Holm, R.B. Frankel, G.C. Papaefthymiou, J. Am. Chem. Soc. 99 (1977) 2350.

[6] J. Cambray, R.W. Lane, A.G. Wedd, R.W. Johnson, R.H. Holm, Inorg. Chem. 16 (1977) 2565.

[7] R.H. Holm, J.A. Ibers, Iron-Sulfur Proteins, Vol. III, W. Lovenberg, Ed., Academic Press, New York, N.Y., 1977, Chapter 7.

[8] T. Herskovitz, B.A. Averill, R.H. Holm, J.A. Ibers, W.D. Phillips, J.F. Weiher, Proc. Nat. Acad. Sci. USA 69 (1972) 2437.

[9] L. Que, Jr., M.A. Bobrik, J.A. Ibers, R.H. Holm, J. Am. Chem. Soc. 96 (1974) 4168.

[10] E.J. Laskowski, R.B. Frankel, W.O. Gillum, G.C. Papaefthymiou, J. Renaud, J.A. Ibers, R.H. Holm, J. Am. Chem. Soc. 100 (1978) 5322.

[11] B.V. DePamphilis, B.A. Averill, T. Herskovitz, L. Que, Jr., R.H. Holm, J. Am. Chem. Soc. 96 (1974) 4159.

[12] C.L. Hill, J. Renaud, R.H. Holm, L.E. Mortenson, J. Am. Chem. Soc. 99 (1977) 2549.

[13] R.H. Holm, B.A. Averill, T. Herskovitz, R.B. Frankel, H.B. Gray, O. Siiman, F.J. Grunthaner, J. Am. Chem. Soc. 96 (1974) 2644.

[14] R.B. Frankel, T. Herskovitz, B.A. Averill, R.H. Holm, P.J. Krusic, W.D. Phillips, Biochem. Biophys. Res. Commun. 58 (1974) 974.

[15] R.B. Frankel, B.A. Averill, R.H. Holm, J. Phys. (Paris) 35 (1974) C6-107.

[16] R.H. Holm, W.D. Phillips, B.A. Averill, J.J. Mayerle, T. Herskovitz, J. Am. Chem. Soc. 96 (1974) 2109.

[17] J.G. Reynolds, E.J. Laskowski, R.H. Holm, J. Am. Chem. Soc. 100 (1978) 5315.

[18] E.J. Baerends, D.E. Ellis, P. Ros, Chem. Phys. 2 (1973) 41.

[19] J.G. Snijders, E.J. Baerends, Molec. Phys. 33 (1977) 1651.

[20] R. Hoffmann, J. Chem. Phys. 39 (1963) 1397.

[21] J.C. Slater, Quantum Theory of Molecules and Solids, Vol. 4, McGraw-Hill, New York, 1974.

[22] K.H. Johnson, Annu. Rev. Phys. Chem. 26 (1975) 39.

[23] C.Y. Yang, K.H. Johnson, R.H. Holm, J.G. Norman, Jr., J. Am. Chem. Soc. 97 (1975) 6596.

[24] G.H. Loew, D.Y. Lo, Theoret. Chim. Acta (Berl.) 32 (1974) 217.

[25] G.H. Loew, M. Chadwick, D.A. Steinberg, Theoret. Chim. Acta (Berl.) 33 (1974) 125.

[26] G.H. Loew, D. Lo, Theoret. Chim. Acta (Berl.) 33 (1974) 137.

[27] G.H. Loew, M. Chadwick, D. Lo, Theoret. Chim. Acta (Berl.) 33 (1974) 147.

[28] L. Eisenstein, D.R. Franceschetti, Chem. Phys. Letters 50 (1977) 167.

[29] J.G. Norman, Jr., S.C. Jackels, J. Am. Chem. Soc. 97 (1975) 3833.

[30] R.A. Bair, W.A. Goddard III, J. Am. Chem. Soc. 99 (1977) 3505.

[31] R.A. Bair, W.A. Goddard III, J. Am. Chem. Soc. 100 (1978) 5669.

[32] G.H. Loew, D.A. Steinberg, Theoret. Chim. Acta (Berl.) 23 (1971) 239.

[33] G.H. Loew, D.A. Steinberg, Theoret. Chim. Acta (Berl.) 26 (1972) 107.

[34] J.G. Norman, Jr., B.J. Kalbacher, S.C. Jackels, J.C.S. Chem. Comm. (1978) 1027.

[35] E. Clementi, C. Roetti, Atomic Data and Nuclear Data Tables, Vol. 14, Academic Press, New York, 1974, p. 177.

[36] E.J. Baerends, P. Ros, Int. J. Quantum Chem. S12 (1978) 169; and references therein.

[37] W.B. Pearson, Ed., Structure Reports for 1970, Vol. 35A, Oosthoek, Scheltema & Holkema, Utrecht, 1975, p. 140.

[38] R.C. Weast, Ed., Handbook of Chemistry and Physics, 55th ed., CRC Press, Cleveland, Ohio, 1974, p. F-202.

[39] T. Ziegler, A. Rauk, E.J. Baerends, Theoret. Chim. Acta (Berl.) 43 (1977) 261.

[40] R.S. Mulliken, J. Chem. Phys. 23 (1955) 1833.

[41] R.S. Mulliken, J. Chem. Phys. 23 (1955) 1841.

[42] K. Schwarz, Chem. Phys. Letters 57 (1978) 605.

[43] C. Satoko, M. Tsukada, H. Adachi,
J. Phys. Soc. Japan 45 (1978) 1333.

[44] We acknowledge Dr. P.S. Bagus for a useful discussion on this point.

[45] J.L.K.F. de Vries, C.P. Keijzers, E. de Boer,
Inorg. Chem. 11 (1972) 1343; and references therein.

[46] C.P. Keijzers, Thesis, Nijmegen, 1974.

[47] F. Mulder, M. van Hemert, P.E.S. Wormer, A. van der Avoird,
Theoret. Chim. Acta (Berl.) 46 (1977) 51.

[48] B.K. Teo, M.B. Hall, R.F. Fenske, L.F. Dahl,
Inorg. Chem. 14 (1975) 3103.

[49] E.J. Baerends, P. Ros, Chem. Phys. 2 (1973) 52.

[50] P.S. Bagus, Phys. Rev. 139 (1965) A619.

[51] T. Ziegler, A. Rauk, E.J. Baerends, Chem. Phys. 16 (1976) 209.

[52] M. Cerdonio, R.-H. Wang, J. Rawlings, H.B. Gray,
J. Am. Chem. Soc. 96 (1974) 6534.

[53] R.F. Stewart, J. Chem. Phys. 52 (1970) 431.

[54] D.B. Neumann et al., QCPE 11, 199 (1971).

[55] J.G. Stevens, V.E. Stevens, Ed., Mössbauer Effect Data Index,
Covering the 1976 Literature, IFI/Plenum, New York, N.Y., 1978, p. 51.

[56] R. Ingalls, Phys. Rev. 128 (1962) 1155.

[57] A.J. Freeman, R.E. Watson, Phys. Rev. 131 (1963) 2566.

CHAPTER III

Hartree-Fock-Slater-LCAO calculations on the Cu(II) bis(dithiocarbamate) complex; magnetic coupling parameters and optical spectrum.

P.J.M. Geurts, P.C.P. Bouten and A. van der Avoird
Institute of Theoretical Chemistry
University of Nijmegen
Toernooiveld, Nijmegen, The Netherlands

ABSTRACT

The electronic structure of the copper(II) bis(dithiocarbamate) complex has been calculated by the non-empirical Hartree-Fock-Slater-LCAO method and, from the resulting molecular orbitals, the g tensor and the copper and sulphur hyperfine tensors have been obtained. The bonding between the Cu atom and the four ligand S atoms is mainly covalent and the unpaired electron is delocalized over these atoms. All the magnetic parameters are in fair agreement with the experimental EPR results and also the electronic excitation energies agree rather well with the optical spectrum.

1. *INTRODUCTION*

Transition metal complexes with dithiocarbamato ligands have been the subject of extensive studies in our department [1] and elsewhere [2]. Especially about the complex bis(N,N'-diethyldithiocarbamato)copper(II), $[Cu(et_2dtc)_2]$, rather complete information is available; from EPR we know the g tensor and the (an)isotropic metal and sulphur hyperfine tensors [3-5], the polarized optical spectrum has been measured [6] and the redox potentials have been obtained [7]. Extended Hückel (EH) molecular orbital calculations have been performed [8,9] by adjusting two of the EH parameters such that the calculated principal values of the g tensor agree with experiment; this gave quite good agreement also between the calculated anisotropic hyperfine tensors and the experimental values so that we can assume that the (valence) MO picture thus obtained is realistic. Still, other properties, e.g. the electronic excitation energies, are badly represented by the EH method and, moreover, it is rather uncertain whether the parameter choice obtained from this "calibration" proce-

dure [8] has any general significance. Therefore, there is a need for ab initio quantum theoretical methods applicable to transition metal complexes, which are necessarily more complicated than the simple semi-empirical EH method, but which may provide more generally reliable information about the electronic structure of such complexes even if only few data are available from experiment. Such a method is the non-empirical Hartree-Fock-Slater (HFS)-LCAO method developed by Ros and Baerends [10,11] which has already been tested on a series of small molecules and some transition metal complexes [12]. Sofar, no attention has been given to the calculation of magnetic properties by this method. The $[Cu(dtc)_2]$ complex seems a very suitable case to test this method for ligands of a different type and also to look at the accuracy of some procedures proposed for calculating magnetic coupling parameters from the HFS molecular orbitals.

2. METHODS

2.1. Molecular Orbital method

The Hartree-Fock-Slater (HFS)-LCAO method has been described in detail elsewhere [10,11]. Its most characteristic features are the replacement of the Hartree-Fock one-electron exchange operator by a local ($X\alpha$) potential depending on the (spin) density [13] and the representation of this (spin) density by a linear combination of exponential (Slater type) functions centered on the nuclei (we have included density fit functions of s-,p-,d-,f- and g-type; no spherical averaging of the density or the potential around the nuclei takes place, in contrast with the HFS-scattered wave method [14] which uses a muffin-tin potential). A similar density fitting procedure in terms of s-type Gaussian functions has been proposed by Sambe and Felton [15]. The matrix elements of the Coulomb and exchange operators derived from this (fitted) density are calculated numerically [10]. The exchange parameter α was kept at 0.7 as in all previous calculations with this method [11,12].

We have used both the spin-polarized, unrestricted (UHFS) and the restricted (RHFS) versions of the method [12]. The atomic orbital basis set used in most calculations comprised the 3d,4s,4p orbitals for Cu, 3s,3p for S, 2s, 2p for C and N, 1s for H, each represented by two Slater type orbitals (STO's, double zeta basis); the core orbitals (represented by near Hartree-Fock functions [16]) were frozen, i.e. a constant contribution from the core electrons has been included in the Coulomb and exchange potentials, while all valence orbitals have been orthogonalized to the core by adding linear combinations of

STO's, one for each core orbital. In one calculation these single zeta core orbitals on Cu were explicitly included in the secular problem in order to observe the effect of core (spin) polarization. All orbital exponents have been taken from the tables by Clementi and Roetti [16]. Computer timings for this HFS-LCAO method applied to transition metal complexes compare favorably with the Hartree-Fock (HF)-LCAO method [17].

2.2. *Expressions for magnetic coupling parameters*

— The g tensor

The system we are dealing with has a spin-doublet ground state with no orbital degeneracy (Cu $3d^9$ if the complex were completely ionic). We can write the following approximate second order perturbation formula for the g tensor [18,19]. (Δg_{ij} is the deviation from the free-electron result g_e; i,j = x,y,z)

$$\Delta g_{ij} = g_e \sum_{\substack{m,\sigma \\ \text{occupied spin-orbitals}}} \sum_{\substack{n,\sigma' \\ \text{virtual spin-orbitals} \\ (\sigma'=\sigma)}} \sum_{A} \sum_{B} \frac{\langle \chi_m^A | \xi^A(r_A) L_i^A | \chi_n^A \rangle \langle \chi_n^B | L_j^B | \chi_m^B \rangle}{\varepsilon_m - \varepsilon_n} \qquad (1)$$

Actually, the second order contribution to Δg is only gauge invariant together with a first order term; expression (1) corresponds to a particular gauge in which this first order term is negligible [18,19]. Furthermore, one must make the following assumptions in deriving it:

(i) Spin-orbit coupling can be described by an (effective) one-electron operator, i.e. the two-electron coupling terms [20,21] can be taken into account by an effective one-electron potential. This approximation seems consistent with the HFS (independent particle) formalism used for the calculation of the molecular (spin)orbitals. The functions $\chi_{m,n}^{A,B}$ occurring in formula (1) are the restrictions of the molecular orbitals $\Psi_{m,n}$ to the atoms A,B; they include the MO coefficients. We have taken these orbitals, both the occupied, Ψ_m, and the virtual ones, Ψ_n, and the corresponding orbital energies, ε_m and ε_n, from a ground state HFS calculation. In this respect, it is important to remember that the excited wave functions are not necessarily the best descriptions of the physical excited states of the system; the only condition required by perturbation theory is that they form (or, in practice, approach) a complete set together with the ground state functions. Expression (1) with this choice of $\Psi_{m,n}$ and $\varepsilon_{m,n}$ corresponds with uncoupled Hartree-

Fock(-Slater) perturbation theory [22].

(ii) The effective one-electron potential occurring in the spin-orbit coupling terms is a scalar potential which can be additively constructed from contributions spherical around the nuclei; the corresponding electric field felt by the electrons is:

$$\vec{E} = \frac{2m^2c^2}{e\hbar^2} \sum_{\substack{A \\ \text{atoms}}} \xi^A(r_A)\vec{r}_A \qquad (2)$$

The operators L_i^A, L_j^B are components of the angular momentum around the nuclei A, B.

(iii) Only one-centre integrals are retained.

It has been shown by Moores and McWeeny [21] that the approximations (i) to (iii) produce results for the spin-orbit splitting in NO and CH and the g tensor in NO_2 and CN which are in good agreement with the results of complete ab initio calculations including all two-electron spin-orbit coupling terms and many-centre integrals. If the empirical values for the atomic spin-orbit parameters, λ^A, are introduced for the radial matrix elements over $\xi^A(r_A)$, the results are in excellent agreement also [21] with the molecular experimental data. This explains the success of the usual semi-empirical description of spin-orbit coupling effects by the operator $\sum_A \lambda^{A \to A} \vec{L} \cdot \vec{S}$ [18,23]. Extending formula (1) with many-centre terms seems easy, but it requires the ab initio calculation of matrix elements for which we need explicitly the effective scalar and vector potential accounting for all two-electron coupling terms, while the results would probably be less accurate [21]. So we have chosen to use formula (1) with the empirical atomic spin-orbit parameters from table 1. The only problem then is

Table 1. Spin-orbit coupling parameters λ [a)]

atom	orbital	λ[cm^{-1}]
Cu	3d	828
S	3p	382
C	2p	28
N	2p	76

a) from refs. [8,24]

that we have a double zeta representation for each AO which leads to three different (two diagonal and one off-diagonal) radial matrix elements over $\xi^A(r^A)$ while only one empirical parameter λ^A is available per AO. We have solved this problem by assuming that $\xi^A(r^A)$ depends on r^A as $(r^A)^{-3}$ Z_{eff} [20], calculating the three matrix elements over $(r^A)^{-3}$ and distributing λ^A proportionally over the corresponding $\xi^A(r^A)$ matrix elements. The error which we possibly introduce by this procedure must remain very small, since by far the largest contribution to λ^A arises from the single diagonal element over the most compact basis orbital and, moreover, the coefficients of the two exponential functions are not very different in the atom and in the molecule.

— The hyperfine coupling tensor

The first, isotropic, hyperfine coupling contribution is the Fermi-contact term, which is directly proportional to the spin density at the nucleus, B.

$$a^B = \frac{8\pi}{3}\frac{\mu_0}{4\pi}\, g_e g_B \mu_b \mu_n \Big[\sum_{\substack{m,(\sigma=\alpha)\\ \text{occupied}\\ \text{spin-}\\ \text{orbitals}}} |\psi_m(B)|^2 - \sum_{\substack{m',(\sigma=\beta)\\ \text{occupied}\\ \text{spin-}\\ \text{orbitals}}} |\psi_{m'}(B)|^2 \Big], \qquad (3)$$

where μ_b is the Bohr magneton, μ_n is the nuclear magneton, g_B is the gyromagnetic ratio of nucleus B and μ_0 is the vacuum permeability. Next we have a first order (anisotropic) electron-spin-nuclear-spin dipole-dipole term plus two second order terms due to the additional coupling with the orbital angular momentum. If we make the same assumptions as in deriving the g tensor, we obtain the following expression (derived for the spin-restricted case in refs. [24,25]):

$$A^B_{ij} = \frac{\mu_0}{4\pi}\, g_e g_B \mu_b \mu_n \Big[\Big(\sum_{\substack{m,(\sigma=\alpha)\\ \text{occupied}\\ \text{spin-}\\ \text{orbitals}}} \langle \chi^B_m | T^B_{ij} | \chi^B_m \rangle - \sum_{\substack{m',(\sigma=\beta)\\ \text{occupied}\\ \text{spin-}\\ \text{orbitals}}} \langle \chi^B_{m'} | T^B_{ij} | \chi^B_{m'} \rangle \Big)$$

$$+ \sum_{\substack{m,\sigma\\ \text{occupied}\\ \text{spin-}\\ \text{orbitals}}} \sum_{\substack{n,\sigma'\\ \text{virtual}\\ \text{spin-}\\ \text{orbitals}\\ (\sigma'=\sigma)}} \sum_{\substack{A\\ \text{atoms}}} \Big(\frac{2\langle \chi^A_m | \xi^A(r^A) L^A_i | \chi^A_n \rangle \langle \chi^B_n | (r^B)^{-3} L^B_j | \chi^B_m \rangle}{\varepsilon_m - \varepsilon_n} + \qquad +$$

$$+ \sum_{k,\ell} i\epsilon_{k\ell i} \frac{\langle \chi_m^A | \xi^A(r^A) L_k^A | \chi_n^A \rangle \langle \chi_n^B | T_{\ell j}^B | \chi_m^B \rangle}{\epsilon_m - \epsilon_n}] \qquad (4)$$

where T_{ij}^B is the dipole-dipole coupling tensor of an electron with nucleus B and $\epsilon_{k\ell i}$ is the antisymmetric Levi-Cevita symbol [26]. The second order terms in A_{ij}^B contain an isotropic (pseudocontact) contribution which must be added to the Fermi-contact term (3).

Finally we must remark that, of course, the many-electron ground state wave function (Slater determinant) constructed with the molecular orbitals from a spin-unrestricted HFS calculation does not exactly correspond with a doublet spin eigenstate. The results show that the differences between orbitals for spin α and orbitals for spin β in our unrestricted calculations are quite small, however, and, therefore, we have not tried to correct the results for this defect. (This could be done by spin projection of the total wave function after the SCF calculation [27] which is a cumbersome and still not very satisfactory procedure). In our formula's for the magnetic coupling parameters we have assumed that the two components of a Kramers doublet can be represented by the wave functions resulting from two (formally) different UHFS calculations, one with an extra "unpaired" spin α and one with an extra spin β. Moreover, we have only considered those excitations in the second order terms of formula's (1) and (4), which yield non-zero contributions if the α and β orbitals were exactly equal [24,25] (i.e. the excitations of the "unpaired" electron to higher MO's and the excitations from lower MO's to the unpaired hole). In parallel with the spin-unrestricted calculations, we have also performed restricted HFS calculations.

2.3. *Electronic excitation energies*

In the HFS method the electronic excitation energies can be calculated as the difference between the relevant orbital energies in a transition state calculation [13], where the transition state for each excitation is obtained by transferring half an electron (without changing spin). If the relaxation effects accompanying this electron transfer are small one can also estimate the excitation energies from ground state orbital energy differences.

3. *CALCULATIONS AND RESULTS*

The EPR results have been obtained from studies of $[Cu(et_2dtc)_2]$ doped into single crystals of the diamagnetic $[Ni(II)(et_2dtc)_2]$ complex [3-5]. Since

these results have indicated [3,4] that the structure of the guest molecules $[Cu(et_2dtc)_2]$ is close to the $[Ni(et_2dtc)_2]$ structure, we have based our calculations on the structure of the latter compound [28]. The molecular symmetry of this compound is C_i but it deviates only slightly from D_{2h} symmetry and we have assumed this higher symmetry in our HFS-LCAO calculations, using the atomic coordinates shown in fig. 1. Extended Hückel calculations which have been done previously [8,9] in C_i symmetry and which we have now repeated in D_{2h} symmetry (see fig. 2 and tables 2 and 3) yield practically identical results. Moreover, we have replaced the terminating ethyl groups by hydrogen atoms. Experiments with different alkyl-substituted ligands [29] and extended Hückel calculations [24] have shown that this replacement has no significant effect on the optical and magnetic properties studied in this paper.

The unrestricted HFS calculation with frozen cores on Cu, S, C and N and the AO basis described above yields the MO level scheme in fig. 2. Relaxing

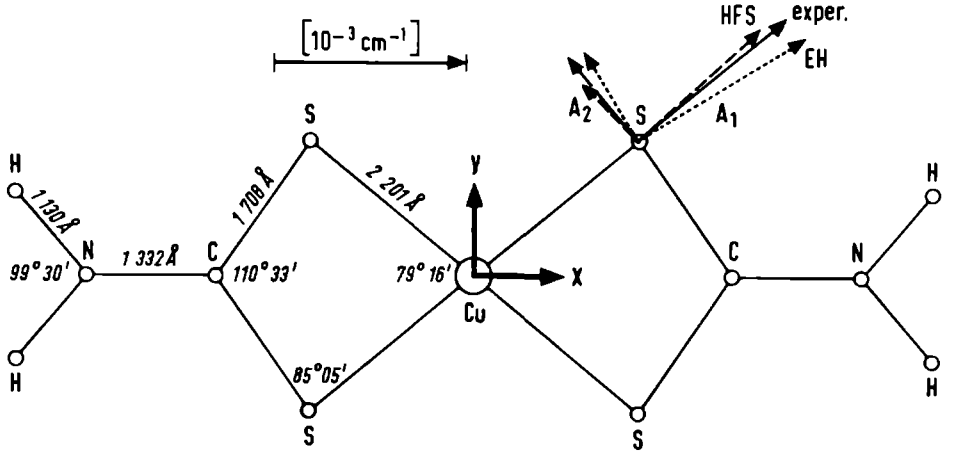

Figure 1. Molecular structure (D_{2h}) of $[Cu(dtc)_2]$. Principal axes and values of hyperfine tensor on S (A_3-axis in the z-direction).

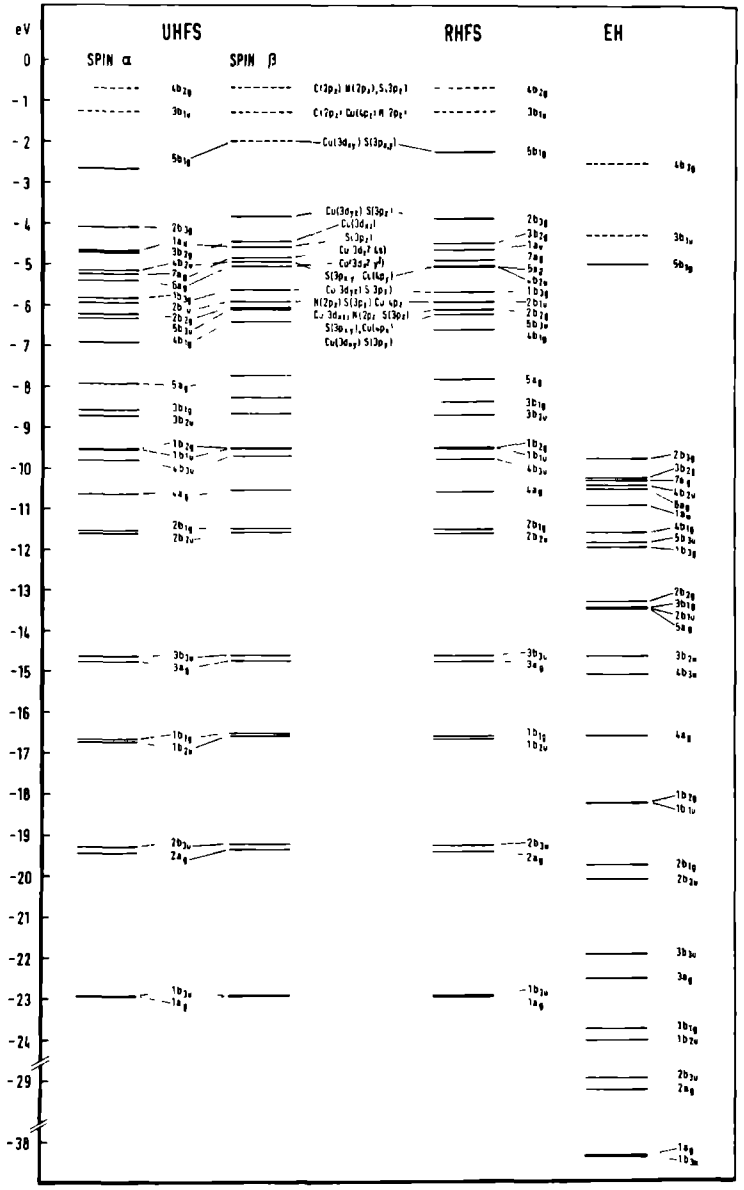

Figure 2. Molecular orbital level scheme and main atomic orbital contributions to the highest occupied and lowest unoccupied orbitals for HFS (with frozen cores) and EH results in D_{2h} symmetry. Occupied levels have been drawn (———), virtual levels have been dashed (- - -); the $5b_{1g}$ level holds one (unpaired) electron.

Table 2. Population analysis[a]

	UHFS			RHFS	EH
	spin α	spin β	total	total	total
Gross atomic populations or charges[b]					
Cu	5.38(0.34)	4.97	0.66(0.34)	0.65(0.40)	0.01
S	3.10(0.17)	2.93	-0.02(0.17)	-0.01(0.15)	-0.28
C	2.24(0.00)	2.25	-0.49(0.00)	-0.49(0.00)	0.49
N	2.80(0.00)	2.80	-0.60(0.00)	-0.60(0.00)	-0.50
H	0.30(0.00)	0.30	0.40(0.00)	0.40(0.00)	0.28
Gross atomic orbital populations					
Cu $3d_{z^2}+3d_{x^2-y^2}$	1.93 (0)	1.93	3.86 (0)	3.85 (0)	3.97 (0)
$3d^{xy}$	1.00(0.34)	0.58	1.58(0.34)	1.60(0.40)	1.58(0.53)[c]
$3d^{xz}$	0.99 (0)	0.98	1.97 (0)	1.97 (0)	1.99 (0)
$3d_{yz}$	1.00 (0)	1.00	2.00 (0)	2.00 (0)	2.00 (0)
4s	0.26 (0)	0.27	0.53 (0)	0.53 (0)	0.53 (0)
$4p_x$	0.04 (0)	0.04	0.08 (0)	0.08 (0)	0.30 (0)
$4p_y$	0.09 (0)	0.10	0.19 (0)	0.19 (0)	0.49 (0)
$4p_z$	0.07 (0)	0.07	0.14 (0)	0.14 (0)	0.13 (0)
S 3s	0.95(0.00)	0.94	1.89(0.00)	1.89(0.00)	1.55(0.01)[c]
$3p_x$	0.67(0.09)	0.59	1.26(0.09)	1.25(0.08)	1.44(0.14)[c]
$3p_y$	0.64(0.08)	0.57	1.21(0.08)	1.20(0.07)	1.57(0.05)[c]
$3p_z$	0.84 (0)	0.83	1.67 (0)	1.67 (0)	1.73 (0)
C 2s	0.65 (0)	0.65	1.30 (0)	1.30 (0)	1.01 (0)
$2p_x$	0.49 (0)	0.49	0.98 (0)	0.98 (0)	0.82 (0)
$2p_y$	0.58(0.00)	0.58	1.16(0.00)	1.16(0.00)	0.92(0.01)[c]
$2p_z$	0.52 (0)	0.53	1.05 (0)	1.05 (0)	0.75 (0)
N 2s	0.79 (0)	0.79	1.58 (0)	1.58 (0)	1.19 (0)
$2p_x$	0.59 (0)	0.59	1.18 (0)	1.17 (0)	1.19 (0)
$2p_y$	0.64(0.00)	0.64	1.28(0.00)	1.28(0.00)	1.38(0.00)[c]
$2p_z$	0.78 (0)	0.78	1.56 (0)	1.56 (0)	1.74 (0)
H 1s	0.30(0.00)	0.30	0.60(0.00)	0.60(0.00)	0.72(0.00)[c]
Net atomic populations					
Cu	5.31(0.41)	4.83	10.14(0.41)	10.16(0.48)	10.22(0.53)
S	3.07(0.24)	2.84	5.91(0.24)	5.91(0.23)	5.69(0.20)
C	2.08(0.00)	2.12	4.20(0.00)	4.20(0.00)	2.14(0.01)
N	2.42(0.00)	2.43	4.85(0.00)	4.85(0.00)	4.38(0.00)
H	0.19(0.00)	0.19	0.38(0.00)	0.39(0.00)	0.42(0.00)
Atom-atom overlap populations					
Cu-S	0.16(-0.04)	0.20	0.36(-0.04)	0.35(-0.04)	0.45
S-C	0.17(0.00)	0.17	0.34(0.00)	0.34(0.00)	0.96
C-N	0.27(-0.00)	0.25	0.52(-0.00)	0.52(-0.00)	1.01
N-H	0.30(0.00)	0.29	0.59(0.00)	0.59(0.00)	0.67
Cu-C	-0.26(0.00)	-0.27	-0.53(0.00)	-0.54(0.00)	-0.12
S-S[d]	-0.21(-0.09)	-0.13	-0.34(-0.09)	-0.33(-0.09)	-0.12

a) values in parentheses refer to the unpaired electron only ($5b_{1g}$ MO)
b) values for spin α, spin β and in parentheses are populations; other values represent charges
c) EH values in parentheses are net (instead of gross) atomic orbital populations
d) two S atoms belonging to the same ligand

Table 3. Magnetic coupling parameters[a]

		UHFS[a] frozen cores	UHFS[a] relaxed Cu core	RHFS[a] frozen cores	EH[a]	Experimental[b]
	Δg_{xx}	0.0264	0.0271	0.0272	0.0179	0.0177(0.0207)
	Δg_{yy}	0.0330	0.0335	0.0367	0.0225	0.0227(0.0285)
	Δg_{zz}	0.1074	0.1124	0.1115	0.0755	0.0817(0.1053)
Cu	A_{xx}	43.2 (56.5)	44.3 (58.2)	38.5 (52.3)	40.0 (47.9)	43.0 (43.8)
	A_{yy}	44.0 (55.1)	45.0 (56.8)	41.1 (52.3)	39.1 (47.9)	37.0 (34.3)
	A_{zz}	-87.2(-111.5)	-89.3(-115.0)	-79.6(-104.7)	-79.1(-95.9)	-80.0(-78.2)
	A_{iso}	5.4 (-16.7)	-56.9 (-80.0)	22.9 (0)[c]	8.1 (0)[c]	-79.0(-64.2)
S[d]	A_1	7.8	7.8	7.8	10.2(10.2)	9.9
	A_2	-4.0	-4.0	-3.9	-5.0(-5.1)	-5.5
	A_3	-3.8	-3.8	-3.9	-5.1(-5.1)	-4.4
	A_{iso}	16.8	17.0	12.2	11.6(11.4)	11.7
C	A_{xx}	0.27	0.27	-0.00	-0.26(-0.22)	
	A_{yy}	-0.14	-0.14	0.01	0.47 (0.44)	< 2[e]
	A_{zz}	-0.13	-0.13	-0.00	-0.22(-0.22)	
	A_{iso}	-4.8	-4.8	0[c]	-0.02 (0)[c]	
N	A_{xx}	0.08	0.08	-0.03		
	A_{yy}	0.16	0.16	0.05		
	A_{zz}	-0.24	-0.24	-0.03		
	A_{iso}	-0.57	-0.56	0[c]		

a) calculated A values [10^{-4} cm^{-1}] represent the sum of the first and second order terms (formula's (3) and (4)), with the first order contribution indicated in parentheses (for A_{iso} the first order contribution is the Fermi-contact term (3)); exceptions are the HFS results for S, C and N which contain only the first order contributions, as the second order terms are small (cf. the EH results)

b) for [$Cu(et_2dtc)_2$] in [$Ni(et_2dtc)_2$]: Δg values and A values on Cu from ref. [3], A values on S from ref. [4]; in parentheses values for [$Cu(et_2dtc)_2$] in [$Zn(et_2dtc)_2$] from ref. [24,30]

c) the Fermi-contact contribution is zero in this case because the MO of the unpaired electron ($5b_{1g}$) has zero density at the nucleus

d) principal axes are shown in Fig. 1

e) the C^{13} hyperfine splitting has not been observed, so it was concluded that it was buried in the copper hyperfine linewidth [34] (the splitting found in ref. [4] must be ascribed to so-called hydrogen spin-flip transitions [35])

the core orbitals on Cu makes no visible difference in this (valence level) scheme (and in most other properties, except for the Fermi-contact term, see below), whereas a restricted HFS calculation yields about the average result of the α and β levels from the unrestricted calculation (see fig. 2). The ground state orbital occupancy can be read from this figure, with the "unpaired" electron occupying the $5b_{1g}$ orbital. This occupancy agrees with the EH calculations. The Cu-S bonding is mainly covalent, with rather small changes on the atoms and considerable positive overlap populations (see table 2). The unpaired electron is distributed rather evenly over the Cu $3d_{xy}$ orbital and the $3p_x$ and $3p_y$ orbitals of the four S atoms.

This picture is confirmed by the fair agreement between the calculated magnetic coupling parameters and the experimental values from EPR. The g tensor of the complex and the hyperfine coupling tensors with the Cu, S, C and N nuclei have been calculated according to the formula's (1), (3) and (4). Because of the D_{2h} symmetry of the complex and the positions of the nuclei, the principal axes of these tensor coincide with the molecular symmetry axes, except for the S hyperfine coupling tensor; the latter has been diagonalized, yielding the principal axes drawn in fig. 1. The calculated principal values, together with the experimental ones have been listed in table 3. This table contains results from both restricted and unrestricted HFS calculations with frozen cores and, since we expected spin polarization of the core electrons to be important especially for the Fermi-contact interaction with the Cu nucleus, we have also relaxed the Cu core orbitals in one calculation.

The excitation energies for the transitions $2b_{3g} \rightarrow 5b_{1g}(d_{yz} \rightarrow d_{xy})$ and $3b_{2g} \rightarrow 5b_{1g}(d_{xz} \rightarrow d_{xy})$ obtained from transition state calculations as well as from the ground state have been listed in table 4, together with the experimental

Table 4. Electronic excitation energies [cm^{-1}]

Transition	UHFS ground state	UHFS transition state	Experimental[a)]
$2b_{3g} \rightarrow 5b_{1g}(3d_{yz} \rightarrow 3d_{xy})$	14820	15990	14480
$3b_{2g} \rightarrow 5b_{1g}(3d_{xz} \rightarrow 3d_{xy})$	19840	21670	18600

a) from ref. [6]; our assignment of the experimentally observed bands is the reverse of that given by the authors (see text)

electronic frequencies measured on $[Cu(et_2dtc)_2]$ diluted in $[Zn(et_2dtc)_2]$ crystals [6]. In D_{2h} symmetry the d-d transitions would be electric dipole forbidden but the symmetry of $[Cu(et_2dtc)_2]$ in the $[Zn(et_2dtc)_2]$ crystal strongly resembles the molecular symmetry in pure $[Cu(et_2dtc)_2]$ [30,31], which is close to C_{2v} (compared with the D_{2h} structure of fig. 1, the metal nucleus is somewhat lifted out of the molecular plane) and the transitions $d_{yz} \rightarrow d_{xy}$ and $d_{xz} \rightarrow d_{xy}$ become allowed.

For the charge transfer transitions the difference between the excitation energies from transition state calculations and those from ground state calculations is larger than for the d-d transitions (probably due to the larger charge displacements). The lowest (forbidden) $5b_{1g} \rightarrow 3b_{1u}$ charge transfer transition which according to the ground state level diagram (fig. 2) would be at lower frequency than the lowest d-d band, shifts to considerably higher energy in a transition state calculation. Its frequency becomes comparable with the d-d transition frequencies; its intensity is probably very low as it is forbidden even in C_{2v} symmetry. The other charge transfer bands will be at higher frequencies.

4. *DISCUSSION*

The calculated g tensor and hyperfine coupling tensors agree fairly well with the experimental data. The g tensor and the anisotropic hyperfine tensors on Cu and S do not differ much for the different HFS calculations (restricted/unrestricted, frozen core/relaxed Cu core); so these properties are not much affected by the spin polarization of the "doubly occupied" orbitals (which is small anyway, cf. the first two columns in table 2). The anisotropic hyperfine tensors, in particular, are mainly determined by the distribution of the unpaired electron. By contrast, the (isotropic) Fermi-contact interaction depends very strongly on spin polarization: in the restricted HFS calculation this term is exactly equal to zero for Cu (in D_{2h} symmetry; in the real molecular C_i symmetry a very small positive value has been found from EH calculations [8]). The spin polarization of the valence orbitals makes this term negative (but still too small in absolute value), while the corresponding interaction on the S atoms remains positive (in agreement with the experimental results). The spin polarization of the Cu core increases the negative value for the isotropic Cu hyperfine coupling and it becomes in satisfactory agreement with experiment, considering the very small spin polarization responsible for this contact interaction. The remaining discrepancy could be due to the rather simple (single

zeta) representation of the core orbitals and to the defect that the unrestricted HFS wave function is not an eigenfunction of the total spin operator. Also in the g tensor and anisotropic hyperfine tensors the remaining deviations from experiment are fairly small and could well be caused by the approximate formula's used for the calculation of these magnetic coupling parameters (e.g. the neglect of many-centre integrals).

Also the deviations could originate from the difference between the assumed $[Ni(et_2dtc)_2]$ structure for the copper complex and the actual molecular $[Cu(et_2dtc)_2]$ structure (e.g. the difference between the Cu-S bond length and the Ni-S bond length is about 0.1Å [32]) or from the interactions with neighbours in the crystal. In this respect, it is very interesting to compare also the EPR parameters measured on $[Cu(et_2dtc)_2]$ in $[Zn(et_2dtc)_2]$ (see table 3), which happen to agree even better with the HFS calculations than the nickel crystal parameters.

Because of the fair overall agreement we conclude that the MO picture emerging from the HFS-LCAO calculations, the charge distribution, the degree of covalency, the delocalization of the unpaired electron, are realistic. This picture agrees with the EH results [8,9], calculated with two of the parameters fitted to the experimental g tensor, and it confirms some more empirical interpretations of the EPR results [33].

The excitation energies from our HFS calculations agree quite well with the experimental optical spectrum; the assignment of the d-d transitions also agrees with EH [8]. So the assignment by Rajasekharan et al. [6] is probably incorrect. (This assignment could not be based on the polarization of the measured electronic spectrum since the molecules in the crystal are not oriented along the polarization directions. Instead, the authors [6] have invoked an approximate electrostatic model). Surprisingly, the excitation energies from the ground state HFS calculation are even better than those from transition state calculations. We may ascribe this to neighbour effects or geometry distortions in the $[Cu(et_2dtc)_2]$ molecules, built into $[Zn(et_2dtc)_2]$ crystals (the actual molecular symmetry being close to C_{2v}, while the HFS calculations have been performed on D_{2h} symmetry molecules). All HFS results are considerably better than the EH excitation energies, which are unrealistically high (38650 cm^{-1} and 42420 cm^{-1} for the d-d transitions).

Concluding we may say that our results for $[Cu(dtc)_2]$ illustrate that the non-empirical HFS-LCAO method can be well used to calculate not only the charge distribution in transition metal complexes, but also various magnetic and optical properties.

ACKNOWLEDGEMENT

We thank Prof.dr. P. Ros, Dr. E.J. Baerends and Dr. W. Heijser for making available and for assistance in using the HFS-LCAO program. We are grateful to Dr. C.P. Keijzers for stimulating discussions and for making available his programs to calculate the magnetic coupling tensors in the restricted Hartree-Fock case.

The investigations were supported (in part) by the Netherlands Foundation for Chemical Research (SON) with financial aid from the Netherlands Organization for the Advancement of Pure Research (ZWO).

REFERENCES

[1] J. Willemse, J.A. Cras, J.J. Steggerda and C.P. Keijzers, Structure and Bonding 28, 83 (1976).

[2] D. Coucouvanis, Progr. Inorg. Chem. (in press).

[3] M.J. Weeks and J.P. Fackler, Inorg. Chem. 7, 2548 (1968).

[4] R. Kirmse and B.V. Solovev, J. Inorg. Nucl. Chem. 39, 41 (1977).

[5] Hyunsoo So and R. Linn Belford, J. Am. Chem. Soc. 91, 2392 (1969).

[6] M.V. Rajasekharan, C.N. Sethulakshmi, P.T. Manoharan and H. Gudel, Inorg. Chem. 15, 2657 (1976).

[7] J.G.M. van der Linden, Thesis, Nijmegen (1972).

[8] C.P. Keijzers, H.J.M. de Vries and A. van der Avoird, Inorg. Chem. 11, 1338 (1972).

[9] C.P. Keijzers and E. de Boer, Mol. Phys. 29, 1007 (1975).

[10] E.J. Baerends, D.E. Ellis and P. Ros, Chem. Phys. 2, 41 (1973).

[11] E.J. Baerends and P. Ros, Chem. Phys. 2, 52 (1973).

[12] E.J. Baerends and P. Ros, Intern. J. Quantum Chem. S12, 169 (1978).

[13] J.C. Slater, Quantum Theory of Molecules and Solids, Vol. 4, McGraw-Hill, New York (1974).

[14] K.H. Johnson, J. Chem. Phys. 45, 3085 (1966).

[15] H. Sambe and R.H. Felton, J. Chem. Phys. 62, 1122 (1975).

[16] E. Clementi and C. Roetti, Atomic Data and Nuclear Data Tables, Vol. 14, Academic Press, New York (1974) p. 177 ff.

[17] E.J. Baerends and P. Ros, Mol. Phys. 30, 1735 (1975).

[18] A.J. Stone, Proc. Royal Soc. A271, 424 (1963).

[19] C.P. Slichter, Principles of Magnetic Resonance, Harper & Row, New York (1963).

[20] J.C. Slater, Quantum Theory of Atomic Structure, Vol. 2, McGraw-Hill, New York (1960) p. 189 ff.

[21] W.H. Moores and R. McWeeny, Proc. Royal Soc. A332, 365 (1973).

[22] P.W. Langhoff, M. Karplus and R.P. Hurst, J. Chem. Phys. 44, 505 (1966).

[23] E. Ishiguro and M. Kobori, J. Phys. Soc. (Japan) 22, 263 (1967).

[24] C.P. Keijzers, Thesis, Nijmegen (1974).

[25] C.P. Keijzers and E. de Boer, J. Chem. Phys. 57, 1277 (1972).

[26] A. Lichnerowicz, Elements of Tensor Calculus, Methuen, London (1962).

[27] T. Amos and L.C. Snyder, J. Chem. Phys. 41, 1773 (1964).

[28] M. Bonamico, G. Dessy, C. Mariani, A. Vaciago and L. Zambonelli, Acta Cryst. 19, 619 (1965).

[29] C.P. Keijzers, G.F.M. Paulussen and E. de Boer, Mol. Phys. 29, 973 (1975).

[30] C.P. Keijzers, P.L.A.C.M. van der Meer and E. de Boer, Mol. Phys. 29, 1733 (1975).

[31] C.P. Keijzers and E. de Boer, Mol. Phys. 29, 1743 (1975).

[32] M. Bonamico, G. Dessy, A. Mugnoli, A. Vaciago and L. Zambonelli, Acta Cryst. 19, 886 (1965).

[33] T.R. Reddy and R. Srinivasan, J. Chem. Phys. 43, 1404 (1965).

[34] H.J. Stoklosa and J.R. Wasson, Inorg. Nucl. Chem. Lett. 10, 377 (1974).

[35] D. Attanasio, Inorg. Chem. 16, 1824 (1977).

CHAPTER IV

Hartree-Fock-Slater-LCAO studies of the acetylene-transition metal interaction. I. Chemisorption on Ni surfaces; cluster models.

Petro Geurts and Ad van der Avoird
Institute of Theoretical Chemistry
University of Nijmegen
Toernooiveld, Nijmegen, The Netherlands

ABSTRACT

The interaction of C_2H_2 with Ni surfaces has been studied by the Hartree-Fock-Slater-LCAO method (with core pseudopotentials). Different adsorption sites (π,di-σ,μ_2,μ_3) at the Ni(111) surface have been modelled by clusters of 1 to 4 Ni atoms; the structure of C_2H_2 and the Ni-C distance have been varied (3 structures, 2 distances). The acetylene-metal bonding can be interpreted in terms of π to metal donation and, especially, metal to π^* back donation effects which considerably weaken the C-C bond. These effects become increasingly important when more metal atoms are directly involved in the adsorption bonding: π<di-σ<μ_2<μ_3. The calculated shifts in the ionization energies are in fair agreement with the experimentally observed shifts (by UPS) for C_2H_2 adsorbed on Ni(111) (and other Ni surfaces); these shifts do not depend very sensitively on the bonding situation, however, so that we could not assign the structure of adsorbed C_2H_2 solely on this basis. From the comparison between the measured C-C stretch frequency (by ELS) and the calculated C-C overlap populations, using a relation calibrated on Ni-acetylene complexes, we find that μ_3 bonding of C_2H_2 with a Ni-C distance of about 1.9Å is most probable on the Ni(111) surface; the CCH angle is estimated to be somewhat smaller than 150°. We have suggested an explanation for the surface specific dissociation of C_2H_2: C_2 fragments (C-H bond breaking) have been observed on stepped Ni surfaces (at low temperature), CH fragments (C-C bond breaking) have been found on ideal surfaces (at higher temperatures).

1. *INTRODUCTION*

During the past few years much attention has been given to the adsorption and reaction of small organic molecules on films and single crystal surfaces of transition metals, mainly to get insight in the fundamental aspects of more complicated catalytic processes. A simple and at the same time interesting mo-

lecule in this respect is acetylene, while among the first row transition metals, nickel has been studied most with regard to the adsorption of acetylene.

Different experimental techniques have been used to study C_2H_2 adsorbed on Ni: field emission microscopy (FEM) [1], gas phase analysis [2], ultraviolet photoelectron spectroscopy (UPS) [3-7], low energy electron diffraction (LEED) [5,8-10], Auger electron spectroscopy (AES) [8,9], electron energy loss spectroscopy (ELS) [11-16], temperature programmed desorption (TPD) [5,11,12] and measurements of work function changes [1,4,5,7,11,12]. From these studies follows that molecular adsorption takes place at low temperature ($T \approx 100K$) on the low index planes, whereas dissociation products will form at higher temperatures ($T > 300K$ to 400 K) and higher coverages on these planes; on stepped surfaces fragmentation starts already at low temperature.

A first important question is: how is the molecular C_2H_2 bound to the nickel surface, what is its geometrical and electronic structure? The answer to this question will probably have some bearing upon the possibilities for dissociation, too. The experimental data alone do not provide a complete picture and, moreover, the conclusions based on these data have been different. Several attempts have been made to obtain additional insight via quantumtheoretical studies. Demuth and Eastman [17] and Demuth [7,18] have performed Hartree-Fock (HF)-LCAO calculations on free C_2H_2 and C_2H_2 bound to one Be atom in order to observe the effect of distortions in the molecular geometry on the electron binding energies;they have used the results for the interpretation of the UPS spectra measured for adsorbed C_2H_2. Upton and Goddard [19] have optimized the geometry of C_2H_2 in contact with one Ni atom by means of GVB-CI calculations (minimizing the total energy). A HF-LCAO study of C_2H_2 interacting with a Ni atom at a fixed geometry has been performed by Itoh and Kunz [20]. Clusters of nickel atoms with adsorbed C_2H_2 have been studied by the semi-empirical Extended Hückel (EH) [21,22] and CNDO/2 [23] methods. Kasowski [24] has obtained energy bands for a layer of C_2H_2 molecules (without metal) by the LCMTO method. These studies and similar ones for C_2H_2 on Be [25], Mn [26], Fe [27,28] and Pt [29,30] are hampered by the following problems. On the one hand, the ab initio calculations consider only one (transition) metal atom (or none at all), while the binding of C_2H_2 to nickel surfaces probably takes place with two or three neighbouring metal atoms. On the other hand, the semi-empirical treatments are not sufficiently accurate to yield, for example, reliable electron binding energies which can be compared with UPS spectra.

Therefore, we have undertaken a systematic study of C_2H_2 interacting in different manners with 1,2,3 or 4 Ni atoms. Although we realize that more Ni atoms are necessary to represent all the characteristics of a Ni surface and to obtain, for instance, accurate adsorption energies, level broadenings etc., these few nickel atoms form a first representation of different possible adsorption sites. And, since we shall look mainly at the properties of the C_2H_2 molecule itself and their changes upon adsorption, a model which includes the directly interacting metal atoms will already show most of the features upon which we concentrate in this paper. Geometry distortions of C_2H_2 have been taken into account and two different metal-C_2H_2 distances have been considered. The method that we have used is the non-empirical spin-restricted Hartree-Fock-Slater (HFS)-LCAO method [31], which has shown to yield fairly reliable molecular properties, in particular ionization energies [32,33]. We have not only looked at the electronic structure of molecularly adsorbed C_2H_2 on Ni, but we have also suggested an explanation for the two different pathways of dissociative chemisorption, which have been found on ideal surfaces and on stepped surfaces, respectively [5,13,15,16]. The bonding of the dissociation products, the relation with C_2H_2 bound to mono- and dinuclear Ni complexes (containing other ligands as well), and the adsorption of C_2H_2 on different transition metals (Fe and Cu) are subjects of subsequent papers [34].

2. *METHOD AND CALCULATIONS*

The self-consistent HFS-LCAO method developed by Ros, Baerends and coworkers, has been described in detail elsewhere [31-33]. Its most important features are the local exchange approximation [35] ($X\alpha$, with α fixed at 0.7), the representation of the electron density by one-centre fit functions and the numerical integration of the matrix elements over the HFS operator. We have used the core pseudopotential version of the method [36] (without perturbation corrections, cf. [37]), which treats the valence electrons in the Coulomb and exchange field of the frozen cores, with projectors assuring core-valence orthogonality. The atomic orbital basis consists of 3d, 4s and 4p orbitals on Ni, 2s and 2p on C and 1s on H, each represented by two Slater type orbitals (STO's, double zeta basis). Also the frozen core shells are represented by such double zeta STO's. The exponents have been taken from Clementi and Roetti [38] (for Ni from the $3d^8 4s^2\ ^3F$ state); the 4p functions on Ni have been given the same exponents as the 4s, while the exponents for the hydrogen 1s functions (0.783003 and 1.383180) are optimal atomic HFS values. For the

density fit functions one also uses STO's; we have included all angular functions (s-,p-,d-,f- and g-type) required by the AO basis, i.e. no spherical averaging of the density or the potential takes place (in contrast with the scattered wave implementation of the HFS method [39]). A somewhat more extended basis set has also been tested on the free C_2H_2 molecule, but this had hardly any effect on the electron binding energies and populations. The HFS-LCAO method has shown to yield rather good electronic properties for a number of small molecules and transition metal complexes, e.g. [33], in particular also ionization energies. The core pseudopotential version has been tested on several atoms and diatomics [36] and on a fairly large transition metal cluster complex, $[Fe_4S_4(SH)_4]^{2-}$ [37]†.

From structure determinations of transition metal complexes, it has been found that C_2H_2 (or substituted acetylenes) can bind in several manners to one, two, three or four transition metal atoms [40-47]. Analogous binding sites have been proposed for C_2H_2 on transition metal surfaces [5,11,12,14, 21-23,29,30,48-51] and the Ni clusters which we have considered, see fig. 1, actually model these sites on the Ni(111) surface (some of them occur on other planes too). The μ_2 binding can be understood as a double π bond, each of the two perpendicular acetylene π orbitals interacting with one metal atom. The μ_3 bond can be imagined as a superposition of a π bond, for one of the acetylene π orbitals, and a di-σ bond, for the other π orbital. The interaction between each π orbital of acetylene and the metal can be interpreted in terms of the well known Dewar-Chatt-Duncanson model [53,54], which involves π to metal donation and metal to π^* back donation of electrons.

The nickel-carbon distance in our models was taken to be about 1.9Å, which corresponds with the value observed in nickel-alkyne complexes [40-45]; in most cases we have also studied a distance of about 2.4Å, which has been derived from the LEED analysis of the metastable C_2H_2 species on Pt(111) [49]

---

† *The only problem with this version is that the energies of the virtual MO's are somewhat less accurate than those of the occupied ones. In large complexes with sets of nearly degenerate MO's, one finds sometimes, after iteration, empty orbitals lying slightly lower than the highest occupied ones, but this may occur also in HFS calculations without pseudopotential. Different occupancies lead to the same situation; the differences in the total energy are too small (in view of the accuracy of the latter) to make a definite choice. In our application to C_2H_2 adsorbed on Ni clusters, this causes the problem that we can not determine with certainty which of the orbitals around the Fermi level should be occupied. This problem only concerns the nearly degenerate anti-bonding metal orbitals, however, and we have always checked, in cases of doubt, that the different possible occupancies do not lead to any significant difference in the results for C_2H_2 adsorption.*

SITE GEOMETRIES

		$\angle_{CCH}$ (degr)	180	150	120
		C-C (Å)	1.204	1.271	1.337
		C-H (Å)	1.056	1.071	1.086
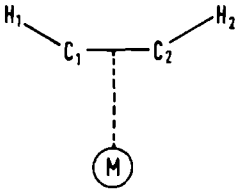	π	M-$C_{1,2}$ (Å)	1 897	1 908	1.919
			2 405	2.413	2.422
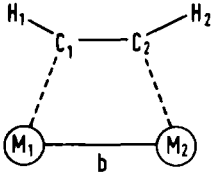	di-σ	M_1-C_1=M_2-C_2 (Å)	1.911	1.900	1.890
			2.416	2.407	2.399
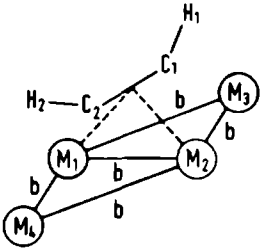	M_1+M_2 : μ_2				
	M_1+M_2+M_3 : $\mu_{2(+1)}$				
	M_1+M_2+M_3+M_4 : $\mu_{2(+2)}$				
			1 897	1.908	1 919
		$M_{1,2}$-$C_{1,2}$ (Å)	2.405	2.413	2 422
		M_3-C_1=M_4-C_2(Å)	2.026	2 001	1.976
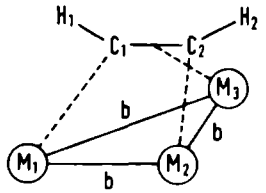	μ_3	M_1-C_1 = M_2-C_2(Å)	1 911	1 900	1 890
			2 416	2 407	2 399
		M_3-$C_{1,2}$ (Å)	1.897	1.908	1.919
			2 405	2.413	2 422

Figure 1. Model clusters for different C_2H_2 adsorption sites. For Ni the bulk nearest neighbour distance [52] is: b = 2.492Å. The plane of (bent) C_2H_2 is always perpendicular to the metal surface plane. The metal-carbon distances are essentially 1.9 and 2.4Å as described in the text. Small differences are caused by the changes in the C-C distance upon distortion of the C_2H_2 molecule, at constant height above the "surface".

(distance reduced by 0.1Å for Ni). Acetylene has been distorted from a linear molecule (with the free molecule bond distances [52]) to a bent one with CCH angles of 150° and 120°. In the 120° case the C-C and C-H bond lengths of ethylene [55] have been used, in the 150° case they are obtained by linear interpolation. In the model for μ_2 bonding, we have added also one or two extra metal atoms to the cluster, $\mu_{2(+1)}$ and $\mu_{2(+2)}$, in order to observe their effects.

The questions,which are the preferred adsorption sites for C_2H_2 on Ni surfaces and what are the geometries of the adsorbed molecules, could in principle be answered on the basis of total (adsorption) energy calculations. The differences are probably very sublte, however, and the computations would become very time-consuming since many structural parameters may have to be relaxed in order to find maximum binding energy. It is worthwile to explore this approach in further studies, using procedures [56] which greatly improve the accuracy of the HFS binding energy calculations. In the present work, the calculated (adsorption) binding energies adopt unrealistic values due to numerical problems and we have chosen a different procedure. The results of our calculations for the different adsorption sites, different C_2H_2 distortions and different metal-carbon distances have been compared with the UPS and ELS data measured for C_2H_2 adsorbed on Ni. Ionization energies (corresponding with peak positions in UPS) can be calculated within the HFS scheme by the transition state method [32,35]. Vibrational frequencies (measured by ELS) can be compared with calculated force constants, but the direct computation of the latter is hard since it implies the knowledge of the total energy surface. Instead, we have used the almost linear relationship which has been found [57] between molecular stretch frequencies and calculated Mulliken [58,59] atom-atom overlap populations. This relation has been calibrated for the C-C stretch in acetylene by means of HFS calculations on nickel complexes with C_2H_2 as a ligand [34, paper III] and comparison with infrared frequencies. The correlation between our results calculated for the different structures and the measured UPS and ELS spectra has been used to indicate the most probable structure of C_2H_2 on Ni(111).

3. *RESULTS*

3.1. *Free acetylene*

Acetylene in its ground state has the valence electron configuration $2\sigma_g^2 2\sigma_u^2 3\sigma_g^2 1\pi_u^4$. The $2\sigma_g$ orbital is primarily a C-C (2s-2s) bonding MO, the $2\sigma_u$

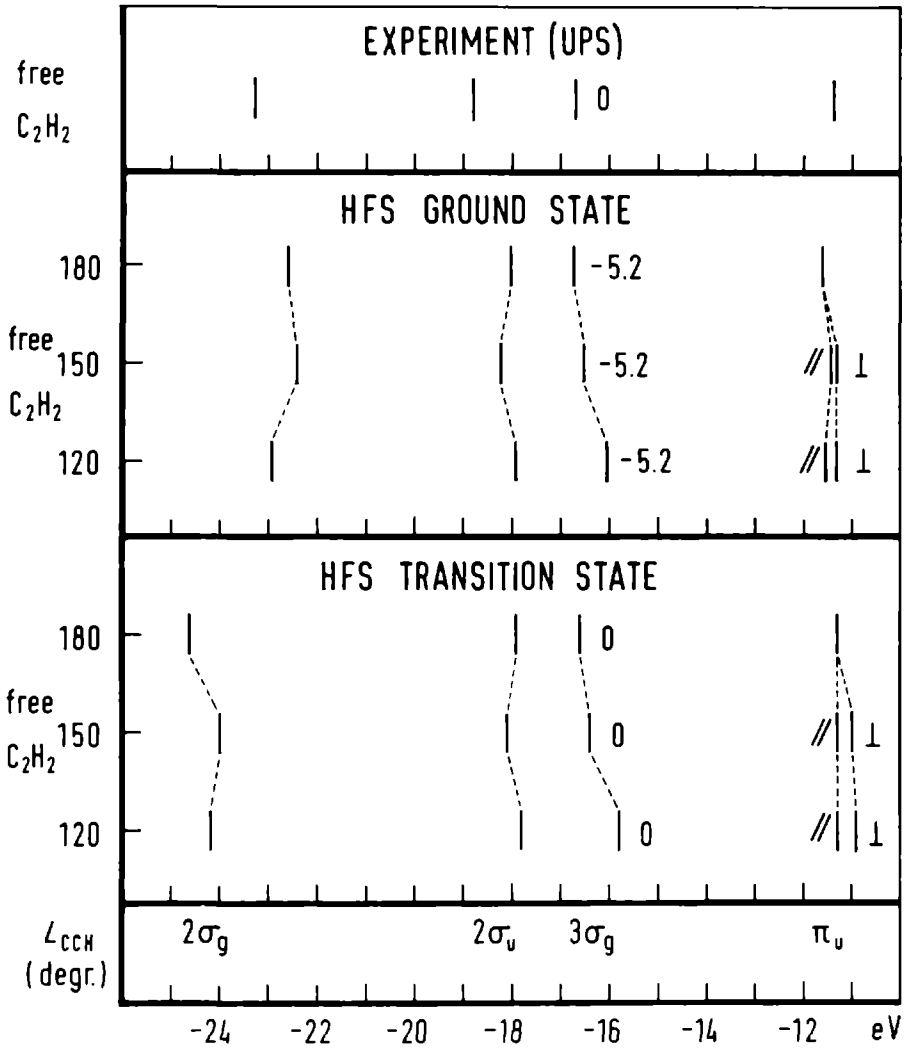

Figure 2. Acetylene MO schemes from HFS ground state and transition state calculations, compared with the experimental (UPS) ionization energies [18,60]. The ground state spectra have been shifted (by the amount indicated in eV) in order to bring the $3\sigma_g$ level of free C_2H_2 (CCH angle 180°) to the same position as the experimental level.

Table 1. Population analysis for free C_2H_2

CCH angle		180°	150°	120°
net atomic populations	C	3.00	3.18	3.41
	H	0.30	0.31	0.32
gross atomic charges	C	-0.32	-0.33	-0.34
	H	0.32	0.33	0.34
atom-atom overlap populations	C-C	1.89	1.59	1.21
	C-H	0.75	0.74	0.73

an odd combination of C-H bonding orbitals; $3\sigma_g$ is C-H bonding and C-C bonding (with more 2p character on C). Fig. 2 shows the valence MO schemes from ground and transition state calculations on free C_2H_2 (CCH angle 180°), together with the experimental ionization energies measured by UPS [18,60]. We observe that the transition state results are in fairly good absolute agreement with experiment. A similar agreement is found for the levels from the ground state calculation if we look at the relative positions (in the figure these levels are shifted, by -5.2 eV, to bring the $3\sigma_g$ level at the correct position). Apparently, the relaxation effect on the different ionization energies is rather uniform, except for the lower lying $2\sigma_g$ orbital. In spite of this satisfactory agreement, the deviations between the calculated and the experimental values are of the same magnitude as the ionization energy shifts observed upon adsorption. Therefore, we shall look in the next section at the adsorption shifts in the calculated and experimental levels, rather than at the level positions.

Fig. 2 also shows the effects of geometry distortion of the C_2H_2 molecule on the calculated ionization energies. These effects are almost identical in the ground and transition states. The π orbital in the plane of bending† is destabilized more than the one perpendicular to it. Also the $2\sigma_g$ and $3\sigma_g$ levels are destabilized, but the $2\sigma_u$ level is stabilized at the CCH angle of 150°; for 120° the picture changes again.

From the population analysis [58,59] in table 1 it follows that the C_2H_2 bending causes a charge shift from the C-C overlap population to the net atomic C populations, while the other populations remain almost unaffected. This can be understood since the C_2H_2 bending is accompanied by an increase in the C-C bond length, which is substantially larger than the increase of the C-H bond length.

---

†*Note that this orbital is indicated as $\pi_\perp$ since, upon adsorption, it is the one perpendicular to the surface. The π orbital perpendicular to the plane of the bent C_2H_2, but parallel to the surface, is indicated as $\pi_{//}$.*

3.2. *Adsorbed acetylene: ionization energies, relation with UPS*

The ionization energies, I_{ads}, measured for an adsorbed molecule can be related to the free molecule ionization energies, I_{free}, by the following expression (i labels the different ionized states):

$$I^i_{ads} = I^i_{free} + \Delta E^i.$$

Experimentally, the ionization energies I_{ads} are measured relative to the work function of the substrate-adsorbate system, which can be written as the clean metal work function, ϕ, plus changes, $\Delta\phi$, caused by adsorption. The ionization energy shift ΔE^i is often thought to be composed of two components: $\Delta E^i = \Delta E^i_b + \Delta E^i_r$. This decomposition is related to the interpretation of the ionization energy as a molecular orbital energy (Koopmans' theorem [61]) plus a relaxation energy, caused by the relaxation of the orbitals of the ion. The bonding (initial state) shift ΔE^i_b is then the change in that molecular orbital energy upon adsorption, due to the interaction with the metal. The relaxation (final state) shift ΔE^i_r is the difference in relaxation energy between the free ion and the adsorbed ion, mainly caused by the screening or partial filling of the electron hole by the metal electrons. In the HFS method, which we have used, Koopmans' theorem does not hold, so, formally, we cannot make this distinction. The total shifts ΔE^i can be obtained from the molecular orbital levels in transition state calculations. Still, we can also use the relative positions of the ground state MO levels, if the transition state relaxation effects in the HFS calculations (which should not be confused with ΔE^i_r defined above) are the same for the different levels. In the free molecule this has been found, except for the lowest valence level, $2\sigma_g$ (see section 3.1).

In figs. 3 to 6 we have shown the ground state and transition state MO levels calculated for (distorted) C_2H_2 on different adsorption sites. The interactions between C_2H_2 and the metal are not so strong that we cannot distinguish the pure C_2H_2 MO's anymore. We have drawn only those levels which are primarily composed of the occupied valence MO's of C_2H_2[†]; these levels happen to be the lowest occupied valence orbitals in all adsorption clusters. Since we want to look at the adsorption shifts ΔE^i, we have included the dia-

---

† *We have also used the same symbols as in the free C_2H_2 molecule to denote these MO's.*

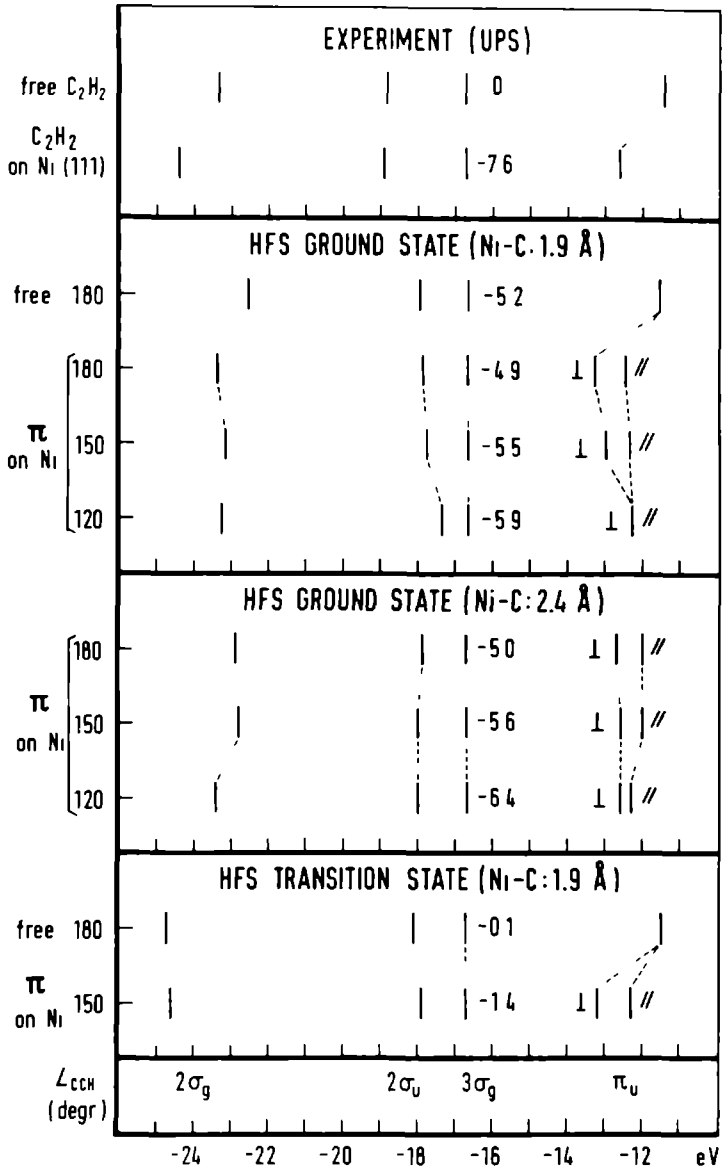

Figure 3. MO schemes for C_2H_2 on the Ni π site from HFS ground state and transition state calculations, compared with the free C_2H_2 level schemes. The same comparison is made for the experimental (UPS) ionization energies of C_2H_2 molecularly adsorbed on Ni(111) [5-7,18] (measured relative to the work function) and the ionization energies of free C_2H_2 [18,60]. All spectra have been shifted by the amount indicated (in eV) next to the $3\sigma_g$ levels in order to bring these $3\sigma_g$ levels into the same position.

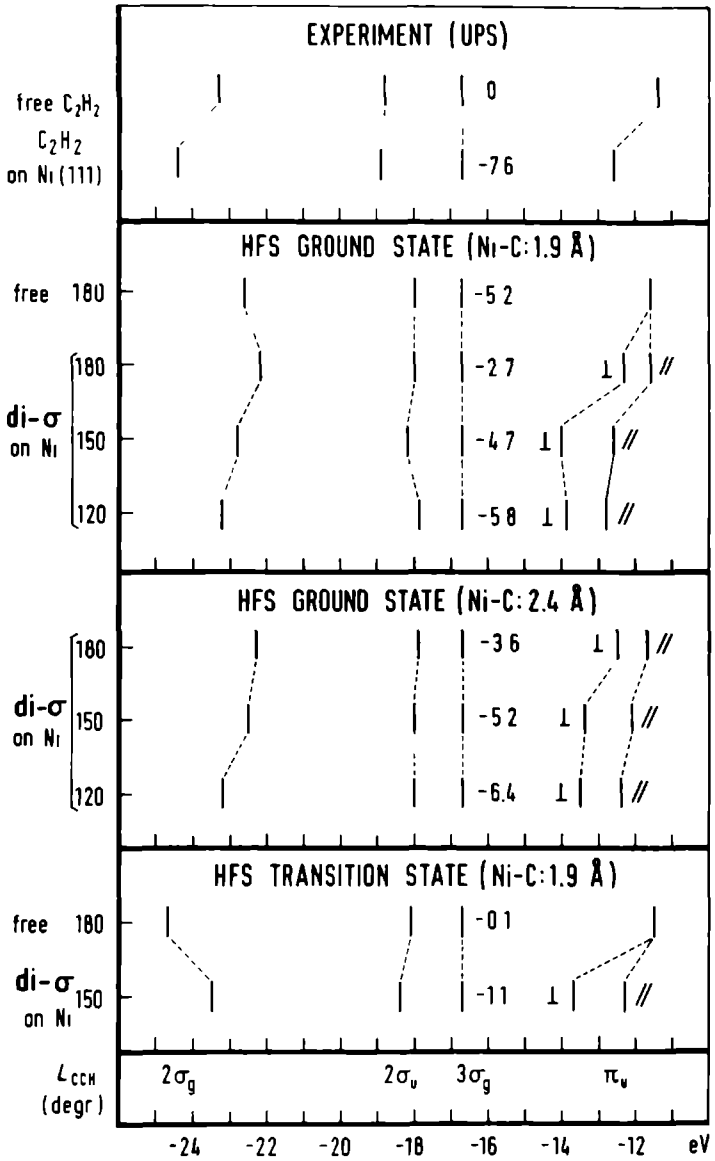

Figure 4. MO schemes for C_2H_2 on the Ni_2 di-σ site; see further the caption of fig. 3.

grams for free, undistorted C_2H_2 and the experimental UPS data for free C_2H_2 [18,60] and C_2H_2 adsorbed on Ni(111) [5-7,18]. These shifts are taken relative to the shift of the $3\sigma_g$ level, as in other interpretations of the UPS spectrum [4-7,17,18,22], but the shifts of this $3\sigma_g$ level (and thus of the whole MO schemes) are also indicated in the figures.

First we conclude that the transition state calculations compared to the corresponding ground state results, show the same behaviour as for free C_2H_2: all levels exhibit a practically uniform relaxation effect, except the $2\sigma_g$ orbital again. So, indeed, we can use the ground state MO schemes to obtain the adsorption shifts in the upper valence levels.

The next conclusion we can draw is that, contrary to the assumption by Demuth et al. [7,17,18], the adsorption shifts ΔE^i are very different from the shifts caused by the distortion of the free acetylene molecule, even for the σ levels. The largest (bonding) shifts are found for the π_u levels and these shifts are in the opposite direction from the effects of the distortion alone. Also the splitting between the $\pi_\perp$ and $\pi_{/\!/}$ levels is in the opposite sense, in most cases, and this is quite understandable if we look at the reason for the π level stabilization, the bonding interaction with the nickel atoms, and at the geometries of the adsorbate-metal systems. The $\pi_\perp$-$\pi_{/\!/}$ splitting is largest if only one π orbital ($\pi_\perp$) is involved in the (σ-type) bonding to the metal (as for the π site, but especially for di-σ bonding). When both the π orbitals of acetylene are involved (μ_2,μ_3 bonding), this splitting is somewhat smaller. This can be understood if we transform the $\pi_\perp$ and $\pi_{/\!/}$ orbitals, which obey the symmetry of the cluster models (fig. 1), to a new set of two rotated π orbitals which point directly to the metal atoms (such a transformation leaves the total wave function invariant if both π orbitals are doubly occupied). In the μ_2 cluster, where these new π orbitals are completely equivalent, the $\pi_\perp$-$\pi_{/\!/}$ splitting is only due to the interaction between the equivalent π-to-metal bonds and to the distortion of C_2H_2 in the 150^o and 120^o cases.

The overall picture for the upper valence levels that emerges from the UPS spectrum of C_2H_2 on Ni(111), i.e. a small change in the $2\sigma_u$-$3\sigma_g$ splitting and a relatively large bonding shift of the π_u levels, is found in many of the models calculated. Also the $\pi_\perp$-$\pi_{/\!/}$ splitting is small enough in various cases to explain the single broadened π_u ionization feature observed. An interesting detail, in this respect, is that, some years ago, two distinct π_u levels with a splitting of about 2 eV have been measured for C_2H_2 on polycrys-

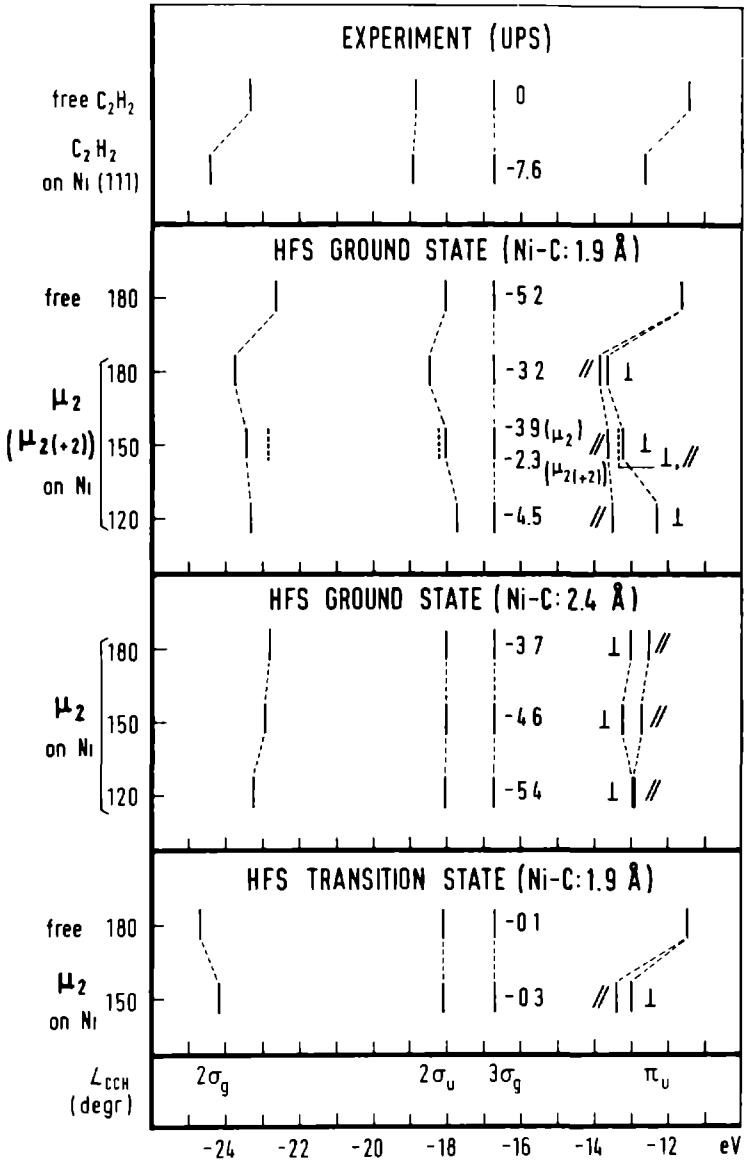

Figure 5. MO schemes for C_2H_2 on the Ni_2 μ_2 and Ni_4 $\mu_{2(+2)}$ (dashed bars) sites; see further the caption of fig. 3.

talline Ni [3]. A definite assignment of the structure and the bonding site of C_2H_2 on Ni(111) cannot be made, however, because the differences between the results calculated for different situations are too small, with respect to the deviations from the experimental UPS spectrum which are still present. We shall come back to this point in section 4 when we have discussed the calculations related to the ELS spectrum.

The (bonding) shift of the $2\sigma_g$ level, which has been measured, is only found in some of the ground state calculations. In the transition state results this shift is compensated by relaxation effects. The relaxation effect in the free C_2H_2 molecule is calculated too large, however, and its reduction in adsorbed C_2H_2 by the screening effects of the metal atoms (which is indeed found) may be somewhat too large also; this would explain that the $2\sigma_g$ bonding shift is not seen in the transition state calculations.

Although we have based our conclusions mainly on the adsorption shifts in the ionization energies, we have compared also their absolute values (I_{ads}) for adsorbed C_2H_2. The experimental ionization energies are measured relative to the work function of the metal-adsorbate system (4.3 eV for C_2H_2 on Ni(111) [4,5,7]), the calculated ones are relative to the vacuum level. In order to compare the results, one can either add the measured work functions to the experimental I_{ads}, or one can subtract the Fermi levels calculated in our cluster models from the theoretical I_{ads} (from transition state calculations). The latter procedure yields an agreement between experiment and calculations to within 2 eV, whereas in the first case the error can be 4 eV. This error is substantially larger than for the free C_2H_2 molecule, which is not surprising if we look at the size of the clusters used to represent the Ni(111) surface. The level shifts are less sensitive to this size, however, as we have checked.

The addition of one ($\mu_{2(+1)}$) or two ($\mu_{2(+2)}$) extra nickel atoms to the μ_2 cluster practically does not change the ionization energies calculated for adsorbed C_2H_2 (the $\mu_{2(+1)}$ results deviate slightly more because the symmetry of the adsorption site is distorted in this model). A similar behaviour has been found for CO on Ni(100) [62]: the adsorbate levels for NiCO and for Ni_5CO (CO in top position) are quantitatively similar. Apparently these ionization energies are primarily affected by the interactions with the nickel atoms directly adjacent to the adsorbate molecules.

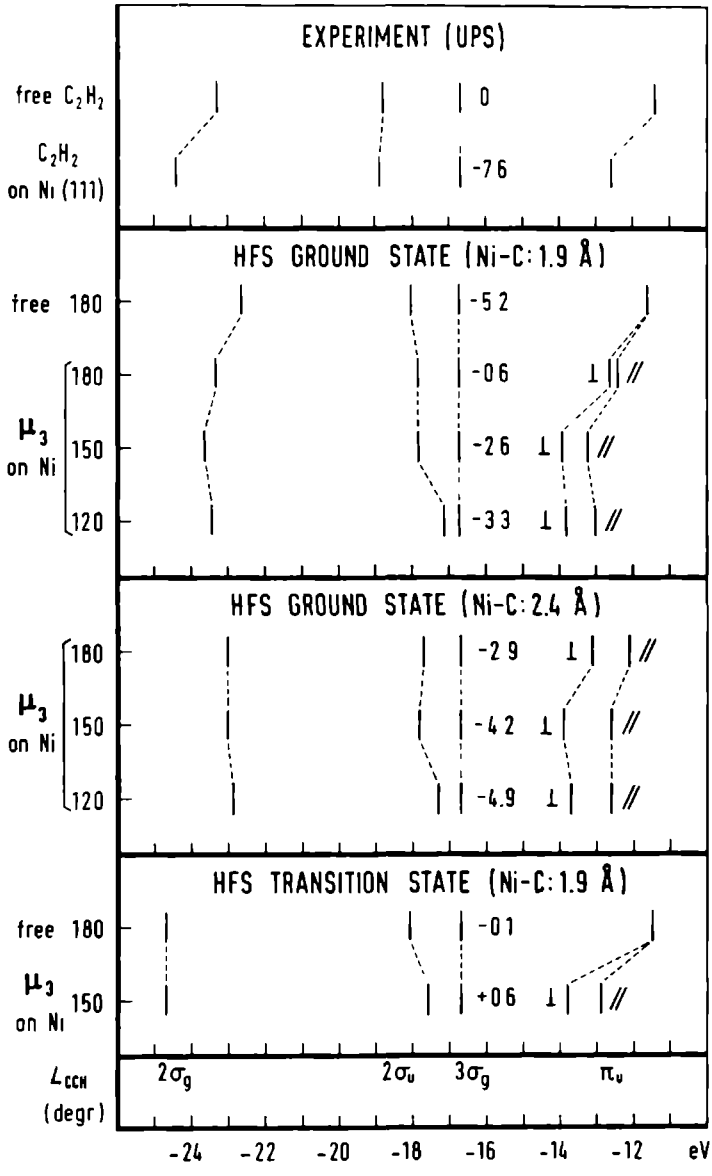

Figure 6. MO schemes for C_2H_2 on the Ni_3 μ_3 site; see further the caption of fig. 3.

3.3. *Adsorbed acetylene: population analysis, relation with FLS*

The most interesting data from a Mulliken population analysis [58,59] of the adsorption clusters studied have been collected in fig. 7 and table 2. Some other results will be mentioned in the text. The gross charges of the H atoms in adsorbed C_2H_2 are about the same as in the free molecule ($\simeq$ 0.3 unit charges); the C atoms have acquired some extra negative charge, however, which ranges from -0.2 to -0.6 unit charges (increasing with distortion angle and in the order π,di-σ<μ_2<μ_3). This negative charge on the adsorbed C_2H_2 molecule, which has been found also from an ab initio HF-LCAO study of C_2H_2 interacting with one Ni atom [20], seems in contradiction with the measured work function lowering [1,4,5,7,11,12]. This comparison is based, however, on a simple surface dipole layer model for the work function change. Maybe this model is not applicable in this case; it has been questioned for C_2H_2 adsorption on a Pt surface also [63]. Another explanation could be that the Mulliken population analysis, which makes a rather arbitrary assignment of the charge to the overlapping orbitals, not corresponding to any physically observable quantity, does not properly reflect the spatial (re)distribution of charge. The total dipole moments calculated for our C_2H_2-metal clusters point with their positive parts away from the metal in some cases, whereas the total Mulliken charge on C_2H_2 is always negative. Also these dipole moments cannot be trusted, however, for an explanation of the observed work function change, since the metal clusters are too small; this leads to artificial edge effects.

The calculated extra charge on the C atoms mainly originates from the Ni 4s orbitals of which the gross populations decrease from about 2.0 to about 1.0 electrons in the series π to μ_3. There is also a (slight) increase in the Ni 3d gross populations from 7.4 to 8.0 electrons, while the amount of Ni 4p electrons is almost constant, about 0.6 (except for the π site where it is 0.2). How this extra charge on the C_2H_2 molecule is accomodated we can see by looking at the populations of the π_u orbitals and their antibonding π_g^* counterparts. These MO (gross) populations have been defined by a transformation of the populations from the AO basis to the MO's of (distorted) C_2H_2, using the MO coefficients of the free C_2H_2 molecule. We observe from table 2 and fig. 7 that there is some donation of electrons from the occupied π_u orbitals of acetylene to the metal orbitals. The back donation of metal electrons to the unoccupied π_g^* orbitals of C_2H_2 is much larger, however, and this explains the negative charge on the carbon atoms. The donation-back donation

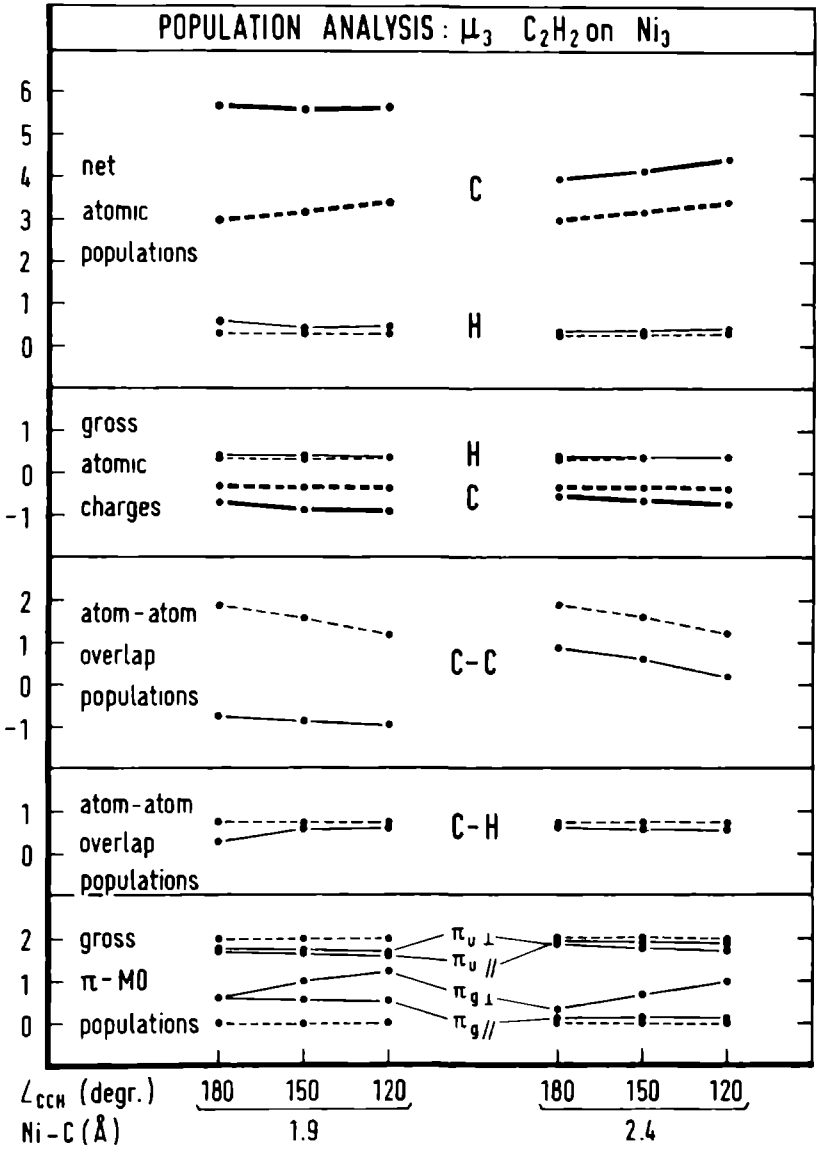

Figure 7. Population analysis data for C_2H_2 on the Ni_3 μ_3 site (▬▬ and ——), compared with free C_2H_2 results (▬ ▬ ▬ and - - -).

effect increases in the order $\pi < di\text{-}\sigma < \mu_2 < \mu_3$ and also we observe that in the cases of μ_2 and μ_3 bonding both the $\pi_\perp$ and the $\pi_{//}$ orbitals become involved. This is in agreement with the bonding shifts and the splitting between the π levels of C_2H_2 as discussed in section 3.2 (in terms of rotated π orbitals which point to the metal atoms). These π orbital populations can be used to define a type of (Mulliken) C-C bond order as the number of electrons in the bonding π_u orbitals minus the number of electrons in the antibonding π_g^* orbitals, divided by two. For free C_2H_2 this π bond order equals two, but it decreases to values smaller than one for μ_2 and μ_3 adsorption (see table 2). A parallel effect is found in the C-C atom-atom overlap population.

When the adsorbed C_2H_2 molecule is distorted we observe the same trend as in the free molecule: a growth of the C net atomic populations at the expense of the C-C overlap population; the absolute value of the latter is much smaller, however, and the C net populations are larger, due to the interaction with the metal atoms (donation-back donation) which we have just discussed. The increase of π^* back donation with increasing distortion angle can (at least in part) be understood from the stabilizing influence of bending on the receiving π_g^* orbitals; in free C_2H_2 the one-electron energies of $\pi_{g\perp}^*$ and $\pi_{g//}^*$ change from +1.39 eV at the CCH angle of 180°, via -1.08 eV($\pi_{g\perp}^*$) and +0.62 eV ($\pi_{g//}^*$) at 150°, to -3.25 eV($\pi_{g\perp}^*$) and -0.04 eV($\pi_{g//}^*$) at 120°. From these values the generally better acceptor ability of $\pi_{g\perp}^*$ compared to $\pi_{g//}^*$ can be explained too (in combination with geometry arguments). The fact that distortion does not have such a pronounced effect on the π_u levels, explains the small variation of π donation as a function of distortion angle; probably geometry arguments are solely important to explain that $\pi_{u\perp}$ donates better than $\pi_{u//}$. Naturally, the donation-back donation interactions increase with decreasing Ni-C distance (from 2.4 to 1.9Å). The C-H overlap populations decrease only slightly, except for the $\mu_{2(+1)}$ and $\mu_{2(+2)}$ adsorption models.

In the $\mu_{2(+1)}$ and $\mu_{2(+2)}$ cases they decrease considerably, e.g. to about -2.49 for $\mu_{2(+1)}$ for the linear adsorbed C_2H_2, compared with the free molecule value of 0.75. This must be due to an extremely strong interaction with the extra nickel atoms (in the $\mu_{2(+1)}$ cluster it happens only at the side of C_2H_2 near the added Ni atom). We can expect this effect if we look at the distances between the H atoms and the extra nickel atoms: 1.39Å, compared with an estimated sum of Van der Waals radii larger than 2.4Å. When the C_2H_2 molecule is distorted to a CCH angle of 150° (Ni-H distance 1.93Å), this interaction dimin-

Table 2. Selected population analysis data for C_2H_2 on Ni clusters

		C-C overlap population		gross π-MO population								π donation		π* back donation		π bond order	
				$\pi_{u\perp}$		$\pi_{u/\!/}$		$\pi^*_{g\perp}$		$\pi^*_{g/\!/}$							
site	Ni-C(Å) → / ↓ CCH angle	1.9	2.4	1.9	2.4	1.9	2.4	1.9	2.4	1.9	2.4	1.9	2.4	1.9	2.4	1.9	2.4
	180°	1.03	1.39	1.77	1.88	1.92	1.97	0.57	0.35	0.11	0.02	0.31	0.15	0.68	0.37	1.51	1.74
π	150°	0.69	0.92	1.78	1.87	1.91	1.97	0.83	0.59	0.09	0.01	0.31	0.16	0.92	0.60	1.39	1.62
	120°	0.40	0.55	2.04	2.00	1.89	1.96	1.00	0.82	0.08	0.01	0.07	0.04	1.08	0.83	1.43	1.57
	180°	0.69	1.28	1.73	1.88	1.91	1.97	0.59	0.29	0.23	0.04	0.36	0.15	0.82	0.33	1.41	1.76
di-σ	150°	0.61	0.88	1.66	1.83	1.88	1.95	0.84	0.65	0.18	0.03	0.46	0.22	1.02	0.68	1.26	1.55
	120°	0.36	0.52	1.79	1.88	1.84	1.93	1.10	0.93	0.17	0.03	0.37	0.19	1.27	0.96	1.18	1.43
	180°	0.16	1.18	1.75	1.88	1.70	1.86	0.48	0.22	0.57	0.16	0.55	0.26	1.05	0.38	1.20	1.68
μ_2	150°	-0.10	0.66	1.68	1.80	1.66	1.81	0.84	0.51	0.53	0.15	0.66	0.39	1.37	0.66	0.99	1.48
($\mu_{2(+2)}$)	(150°)	(0.02)		(1.67)		(1.59)		(1.07)		(0.69)		(0.74)		(1.76)		(0.75)	
	120°	-0.19	0.18	1.73	1.77	1.62	1.77	1.07	0.81	0.50	0.11	0.65	0.46	1.57	0.92	0.89	1.31
	180°	-0.75	0.93	1.74	1.87	1.71	1.92	0.62	0.32	0.59	0.12	0.55	0.21	1.21	0.44	1.12	1.68
μ_3	150°	-0.85	0.68	1.71	1.78	1.66	1.92	1.02	0.68	0.58	0.11	0.63	0.30	1.60	0.79	0.89	1.46
	120°	-0.92	0.20	1.68	1.71	1.58	1.89	1.20	0.99	0.54	0.09	0.74	0.40	1.74	1.08	0.76	1.26

ishes and the C-H overlap population is restored to the more realistic, but still low value of 0.11 for $\mu_{2(+2)}$ and 0.01 for $\mu_{2(+1)}$. Upon further distortion to 120° (Ni-H distance 2.41Å) we find a C-H overlap population of 0.42 for $\mu_{2(+1)}$. We shall come back to these results when we discuss possible C_2H_2 dissociation mechanisms (section 4).

Now we relate the population data to the adsorption shifts in the C_2H_2 vibration frequencies measured by ELS [11,12,14]. From the ELS spectra for C_2H_2 on Ni(111) it has been found that the C-C stretch frequency, $\nu_{C\equiv C}$, is strongly lowered to 1218 cm^{-1} [11,12] or 1215 cm^{-1} [14] (free molecule value 1974 cm^{-1} [64]). By comparing these data to the C-C stretch frequencies for ethylene and ethane it has been concluded that the total ($\sigma+\pi$) C-C bond order should be about 1.15 and that the hybridization of the carbon atoms should be close to sp^3. The change in $\nu_{C\equiv C}$ is in agreement with our calculations (C-C overlap populations decrease considerably). We have also shown, however, that it is dangerous to draw conclusions about the properties of adsorbed C_2H_2 molecules by comparing the measured data with free molecule values, since the interaction with the metal changes the properties in a way which cannot be imitated by considering free molecules. Still, it would be interesting to make a more quantitative comparison between the considerable reduction in the measured $\nu_{C\equiv C}$ and our calculated results for the different adsorption models. We have done this by performing HFS-LCAO calculations on some mono- and dinuclear Ni complexes with C_2H_2 as a ligand, π or μ_2 bonded, in combination with other ligands (isocyanide, carbonyl). For these complexes the shifts in $\nu_{C\equiv C}$ have been measured by infrared spectroscopy. Our calculations show [34, paper III] that there exists an approximate linear relation between $\nu_{C\equiv C}$ and the total C-C overlap population. (A similar relation has been found for the C-O stretch in various carbonyl complexes [57], cf. also [65].) From this relation, calibrated in paper III, and the ELS value $\nu_{C\equiv C} \simeq 1215$ cm^{-1}, we estimate the C-C overlap population for C_2H_2 adsorbed on Ni(111) to be around -0.55 ± 0.25†. Results are calculated close to this value for μ_3 adsorption with a Ni-C distance

† *Negative values for the overlap population seem strange if we think of this overlap population as a measure for the (absolute) bond strength. The Mulliken overlap population is not a physically observable quantity, however, and it has often found [57] to be negative between atoms which are still chemically bonding. Its value depends on the choice of the AO basis set also. One may only relate changes in the overlap population, calculated within the same basis, with changes in the bond strength preferably after calibration, as we have done here.*

of about 1.9Å. From the calculations it also follows that the lowering of the C-C overlap population depends much more strongly on the interaction with the metal atoms than on the geometrical distortion of C_2H_2 itself.

4. *STRUCTURE OF ADSORBED C_2H_2: BONDING, SITE PREFERENCE, DISSOCIATION MECHANISMS*

We have found in the preceding sections that the interaction between a C_2H_2 molecule and a nickel surface, represented by a small collection of nickel atoms, takes place via the Dewar-Chatt-Duncanson [53,54] donation-back donation mechanism. Both, from the MO level shifts and from a population analysis we can conclude that mainly the acetylene π orbitals take part in this mechanism; the populations of the occupied $2\sigma_g$, $2\sigma_u$ and $3\sigma_g$ orbitals hardly change and also the relative σ level positions remain much more constant than the positions of the π levels. In the ground state HFS calculations we find, in some cases, a (small) bonding shift of the $2\sigma_g$ level, in agreement with experiment, but in the transition state results this shift is compensated by a (too large?) relaxation effect. The strength of the metal-acetylene interaction increases when more directly adjacent metal atoms take part in the bonding: $\pi<di\text{-}\sigma<\mu_2<\mu_3$. Especially in the latter two cases both the acetylene π orbitals cooperate in the bonding. We do not know, however, whether the adsorption energy also increases in this order, since we have not calculated accurate total energies.

Although the calculated adsorption shifts in the ionization energies agree fairly well with the shifts measured by UPS, the comparison of the UPS spectrum with the calculated ionization spectra is not sufficient to discriminate between all possible structures and binding sites for C_2H_2 on Ni(111). The calculated level schemes do not depend very sensitively on the bonding situation of C_2H_2 to the nickel atoms. (A similar conclusion has been made for CO on Ni(100) [62], where one could not distinguish between a top NiCO or Ni_5CO molecule and a fourfold hollow Ni_5CO binding site). Only certain situations (e.g. di-σ bonding) can be excluded, for example, because they yield a large $\pi_\perp$-$\pi_{/\!/}$ splitting, which has not been found experimentally.

From the comparison of the shifts in the calculated C-C overlap populations, $q_{C\equiv C}$, with the lowering of the C-C stretch frequency $\nu_{C\equiv C}$, found by ELS measurements, we can conclude, however, that C_2H_2 is bonded most probably in a threefold site (μ_3 bonding) on the Ni(111) surface, with a Ni-C distance of about 1.9Å. This comparison can be made semi-quantitatively since we have found (and calibrated) an approximately linear relation between $\nu_{C\equiv C}$ and $q_{C\equiv C}$ in some Ni complexes with acetylene ligands. We cannot be sure about

the geometric distortion of the C_2H_2 molecule, but since the $2\sigma_u$-$3\sigma_g$ splitting does not change very much and the $\pi_\perp$-$\pi_{//}$ splitting is rather small, we think that this distortion will be not much larger than 30° (CCH angle 150°). Values in this range have been found also in some nickel complexes [40-45] (CCH angles from 149° to 126°). A further indication comes from considering the experimental LEED structure [5,9,10], p(2×2), the phase to which also the UPS and ELS results correspond. The occurrence of μ_3 bonding implies internuclear distances between hydrogen atoms of adjacent C_2H_2 molecules which are 1.7Å, 1.9Å and 2.5Å for CCH angles of 180°, 150° and 120° respectively. Looking at the Van der Waals radius of H (1.2Å [66]) we can practically rule out the undistorted linear C_2H_2 structure (Demuth [5] has argued on this basis, that μ_3 sites are excluded, since he assumed, at that time, that adsorbed C_2H_2 is almost linear). Combining the different pieces of information we estimate a CCH angle of somewhat less than 150°. Other studies [11,12,14,18], which do not explicitly include the interaction with transition metal atoms, need still larger distortions to explain the experimental shifts.

Although the different properties calculated for μ_3 site adsorption fit the various experimental data rather nicely, we can, of course, not exclude that another structure holds, which we have not calculated. So, for instance, our calculations indicate that probably also μ_2 adsorption is rather stable. In this case, slightly extrapolating our results, the C_2H_2 molecule on Ni(111) would have to be distorted somewhat stronger in order to find a C-C overlap population agreeing with the ELS data. Again, the C-H groups are probably bent upwards by at least 30° in order to avoid too strong interaction between the H atoms and some of the Ni atoms, which would reduce the C-H overlap population too much (see section 3.3). Also it is possible that the C-C axis is not exactly parallel to the surface,but somewhat tilted [14] or that the C_2H_2 plane is not perpendicular to the surface [12]. Anyway, we can be rather sure that μ_2 type bonding will occur on other surfaces which have no threefold sites such as Ni(111). UPS data are available for molecular C_2H_2 adsorbed on Ni(100) and (110) surfaces [18], but the spectra are rather similar to the (111) results. This shows again the insensitivity of UPS spectra with regard to the exact binding site and structure. Because ELS data are lacking yet, we cannot make an analysis as described above.

Next, we discuss some results of our calculations in relation to the dissociation behaviour of C_2H_2. At somewhat higher temperatures and coverages (T > 300 to 400K) it has been concluded from TPD experiments, LEED and UPS data [5] and from ELS measurements [13,16], that on Ni(111) C_2H_2 dissociates

into (adsorbed) CH species. In the molecularly adsorbed C_2H_2 at low temperature one finds considerable lowering of the C-C stretch frequency already, but not the softening and broadening of the C-H stretch that is present in some other cases of adsorbed hydrocarbons which dehydrogenate at higher temperatures [67]. On a stepped Ni[5(111)×($\bar{1}$10)] surface, ELS shows that dehydrogenation takes place, however, even at temperatures as low as 150K, leaving adsorbed C_2 species [15,16]. This preference for C-C bond breaking in one case, and C-H scission in the other, is very interesting since it is a simple example of a surface specific dissociation process and it takes place at well defined surfaces at low pressure and temperature.

The picture of C-C bond breaking on the Ni(111) surface is consistent with our calculations for the μ_3 adsorption site: the C-C overlap population is strongly reduced, while the C-H value is only slightly smaller than in free C_2H_2. At other surfaces the situation will probably be different and μ_2 type bonding could occur. In that case one might have Ni atoms close to the hydrogen atoms just as in our $\mu_{2(+1)}$ and $\mu_{2(+2)}$ models for the (111) plane. Especially, if the molecules are adsorbed near steps we expect the presence of such extra Ni atoms. Our calculations show that the strong interactions between these additional metal atoms and the H atoms (or the C-H groups) can strongly reduce the C-H overlap populations. The C-H groups could bend away, leading to a restoration of the C-H bond, a further reduction of the C-C bond strength and eventually C-C scission again, but it is also possible that the C-H bonds break first. The latter process would lead, in first instance, to C-C-H and C-C fragments. The C-C fragments will probably not be very stable on flat surfaces, however, since one expects both C atoms to bind to several nickel atoms, leading to a C-C axis nearly parallel to the surface, but the bond angles are rather unfavourable then (the bonds on the C atoms will point to the other C atom and to the surface, i.e. more or less to one side). At steps, we have metal atoms above the surface and the C-C fragments can easily accomodate themselves in positions with the carbon atoms having more favourable bond angles. Thus, we can tentatively explain the formation of C-C fragments from C_2H_2 on stepped Ni surfaces as being due to the presence of nickel atoms nearby, which first reduce the C-H bond strength and, secondly, provide favourable bonding situations for the resulting C-C fragments. The first function could be fulfilled by atoms in the flat surface also, as our calculations have shown.

ACKNOWLEDGEMENT

We thank Prof.Dr. P. Ros, Dr. E.J. Baerends and Dr. J.G. Snijders for making available and for assistance in using the HFS-LCAO program.

Part of this work has been performed at the CECAM workshop "Models and Numerical Methods for the Study of the Structure of Surfaces and Adsorbates on Surfaces", held in Orsay in July and August 1977. One of us (P.G.) thanks Dr. C. Moser for his hospitality. We are also grateful to Dr. J.E. Demuth for stimulating discussions and for making available his results prior to publication.

The investigations were supported in part by the Netherlands Foundation for Chemical Research (SON) with financial aid from the Netherlands Organization for the Advancement of Pure Research (ZWO).

REFERENCES

[1] L. Whalley, B.J. Davis and R.L. Moss, Trans. Faraday Soc. 67 (1971) 2445.

[2] M.K. Al-Noori and J.M. Saleh, J.C.S. Faraday I 69 (1973) 2140.

[3] C.R. Brundle, Faraday Discussions 58 (1974) 138.

[4] J.E. Demuth and D.E. Eastman, Phys. Rev. Letters 32 (1974) 1123.

[5] J.E. Demuth, Surface Sci. 69 (1977) 365.

[6] J.E. Demuth, Phys. Rev. Letters 40 (1978) 409.

[7] J.E. Demuth, IBM J. Res. Develop. 22 (1978) 265.

[8] G. Casalone, M.G. Cattania, M. Simonetta and M. Tescari, Surface Sci. 62 (1977) 321.

[9] M.G. Cattania, M. Simonetta and M. Tescari, Surface Sci. 82 (1979) L615.

[10] J.C. Hemminger, E.L. Muetterties and G.A. Somorjai, J. Am. Chem. Soc. 101 (1979) 62.

[11] J.C. Bertolini, J. Massardier and G. Dalmai-Imelik, J.C.S. Faraday I 74 (1978) 1720.

[12] J.C. Bertolini and J. Rousseau, Surface Sci. 83 (1979) 531.

[13] J.E. Demuth and H. Ibach, Surface Sci. 78 (1978) L238.

[14] J.E. Demuth and H. Ibach, Surface Sci. 85 (1979) 365.

[15] S. Lehwald, W. Erley, H. Ibach and H. Wagner, Chem. Phys. Letters 62 (1979) 360.

[16] S. Lehwald and H. Ibach, Surface Sci. 89 (1979) 425.

[17] J.E. Demuth and D.E. Eastman, Phys. Rev. B 13 (1976) 1523.

[18] J.E. Demuth, Surface Sci. 84 (1979) 315.

[19] T.H. Upton and W.A. Goddard III, J. Am. Chem. Soc. 100 (1978) 321.

[20] H. Itoh and A.B. Kunz, Chem. Phys. Letters 66 (1979) 531.

[21] A.B. Anderson, J. Chem. Phys. 65 (1976) 1729.

[22] A.B. Anderson, J. Am. Chem. Soc. 100 (1978) 1153.

[23] H. Kobayashi, H. Kato, K. Tarama and K. Fukui, J. Catal. 49 (1977) 294.

[24] R.V. Kasowski, Surface Sci. 63 (1977) 370.

[25] W.C. Swope and H.F. Schaefer III, J. Am. Chem. Soc. 98 (1976) 7962.

[26] W.C. Swope and H.F. Schaefer III, Molec. Phys. 34 (1977) 1037.

[27] A.B. Anderson, J. Am. Chem. Soc. 99 (1977) 696.

[28] T.N. Rhodin, C.F. Brucker and A.B. Anderson, J. Phys. Chem. 82 (1978) 894.

[29] A. Gavezzotti and M. Simonetta, Chem. Phys. Letters 48 (1977) 434.

[30] R.C. Baetzold, Chem. Phys. 38 (1979) 313.

[31] E.J. Baerends, D.E. Ellis and P. Ros, Chem. Phys. 2 (1973) 41.

[32] E.J. Baerends and P. Ros, Chem. Phys. 2 (1973) 52.

[33] E.J. Baerends and P. Ros, Intern. J. Quantum Chem. S12 (1978) 169, and references therein.

[34] P. Geurts and A. van der Avoird, papers II, III and IV in this series, submitted for publication in Surface Sci. (II, IV) and Chem. Phys. (III).

[35] J.C. Slater, Quantum theory of molecules and solids, Vol. 4 (McGraw-Hill, New York, 1974).

[36] J.G. Snijders and E.J. Baerends, Molec. Phys. 33 (1977) 1651.

[37] P.J.M. Geurts, J.W. Gosselink, A. van der Avoird, E.J. Baerends and J.G. Snijders, Chem. Phys. 46 (1980) 133.

[38] E. Clementi and C. Roetti, Atomic data and nuclear data tables, Vol. 14 (Academic Press, New York, 1974), p. 177.

[39] K.H. Johnson, Annu. Rev. Phys. Chem. 26 (1975) 39.

[40] R.S. Dickson and J.A. Ibers, J. Organometal. Chem. 36 (1972) 191.

[41] Y. Wang and P. Coppens, Inorg. Chem. 15 (1976) 1122.

[42] O.S. Mills and B.W. Shaw, J. Organometal. Chem. 11 (1968) 595.

[43] V.W. Day, S.S. Abdel-Meguid, S. Dabestani, M.G. Thomas, W.R. Pretzer and E.L. Muetterties, J. Am. Chem. Soc. 98 (1976) 8289.

[44] J.L. Davidson, M. Green, F.G.A. Stone and A.J. Welch, J. Am. Chem. Soc. 97 (1975) 7490.

[45] M.G. Thomas, E.L. Muetterties, R.O. Day and V.W. Day, J. Am. Chem. Soc. 98 (1976) 4645.

[46] R.S. Dickson, H.P. Kirsch and D.J. Lloyd, J. Organometal. Chem. 101 (1975) C48.

[47] L.F. Dahl and D.L. Smith, J. Am. Chem. Soc. 84 (1962) 2450.

[48] L.L. Kesmodel, P.C. Stair, R.C. Baetzold and G.A. Somorjai, Phys. Rev. Letters 36 (1976) 1316.

[49] L.L. Kesmodel, R.C. Baetzold and G.A. Somorjai, Surface Sci. 66 (1977) 299.

[50] H. Ibach and S. Lehwald, J. Vacuum Sci. Technol. 15 (1978) 407.

[51] T.E. Fischer and S.R. Kelemen, Surface Sci. 74 (1978) 47.

[52] R.C. Weast, ed., Handbook of chemistry and physics, 55th Ed. (CRC Press, Cleveland, 1974) p. F-200,201.

[53] M.J.S. Dewar, Bull. Soc. Chim. Fr. 18 (1951) C79.

[54] J. Chatt and L.A. Duncanson, J. Chem. Soc. (1953) 2939.

[55] H.C. Allen, Jr. and E.K. Plyler, J. Am. Chem. Soc. 80 (1958) 2673.

[56] T. Ziegler and A. Rauk, Theoret. Chim. Acta (Berl.) 46 (1977) 1.

[57] E.J. Baerends and P. Ros, Molec. Phys. 30 (1975) 1735.

[58] R.S. Mulliken, J. Chem. Phys. 23 (1955) 1833.

[59] R.S. Mulliken, J. Chem. Phys. 23 (1955) 1841.

[60] D.W. Turner, C. Baker, A.D. Baker and C.R. Brundle, Molecular photoelectron spectroscopy (John Wiley & Sons, London, 1970).

[61] T. Koopmans, Physica 1 (1934) 104.

[62] A. Rosén, E.J. Baerends and D.E. Ellis, Surface Sci. 82 (1979) 139.

[63] T.E. Fischer, S.R. Kelemen and H.P. Bonzel, Surface Sci. 64 (1977) 157.

[64] D. Dolphin and A. Wick, Tabulation of infrared spectral data (John Wiley & Sons, New York, 1977) p. 74.

[65] D.E. Ellis, E.J. Baerends, H. Adachi and F.W. Averill, Surface Sci. 64 (1977) 649.

[66] L. Pauling, The nature of the chemical bond, 3rd Ed. (Cornell University Press, Ithaca, 1960) p. 260.

[67] J.E. Demuth, H. Ibach and S. Lehwald, Phys. Rev. Letters 40 (1978) 1044.

Hartree-Fock-Slater-LCAO studies of the acetylene-transition metal interaction. II. Chemisorption on Fe and Cu; cluster models.

Petro Geurts and Ad van der Avoird

Institute of Theoretical Chemistry

University of Nijmegen

Toernooiveld, Nijmegen, The Netherlands

ABSTRACT

Self-consistent Hartree-Fock-Slater-LCAO studies have been performed for (geometrically distorted) C_2H_2 molecules interacting with Fe and Cu clusters of one to three atoms, which model the π, di-σ, μ_2 and μ_3 adsorption sites on Fe(110), (100) and Cu(111), (100) and (110) surfaces. The results have been compared with previous data for Ni surfaces (paper I). Calculated ionization energies are in fair agreement with the measured ones (from UPS): a bonding shift of the acetylene π_u levels, relative to the $3\sigma_g$ level, is found in all cases, but also a larger splitting of these π_u levels occurring on Cu, compared with Fe and Ni. This difference is due to a different C_2H_2-metal interaction: on Fe and Ni we find π to metal donation and (more substantial) metal to π^* back donation, on Cu the first effect is dominated by a non-bonded interaction between the occupied acetylene π_u (and $3\sigma_g$) levels and the filled metal levels which are present in the same energy range (only in Cu, due to the lower lying 3d and 4s bands). This relatively strong (net repulsive) interaction explains the larger π_u level splitting and, also, the observation that C_2H_2 binds weaker to Cu (it desorbs, at higher temperature, and does not dissociate) than to Fe and Ni.

1. INTRODUCTION

Although most transition metals can be used as catalysts in some chemical reactions, one finds large differences in activity going along the transition series. These differences appear already in simple processes such as the adsorption of H_2, N_2, NO or CO being molecular on some metals, dissociative on others [1-12]. Also the chemisorption of acetylene, which is interesting for the study of catalytic reactions involving hydrocarbons, shows characteristic differences on Ni, Fe and Cu surfaces. These have been observed under well-defined conditions: single crystal surfaces, rather low temperatures and low coverages (less than a monolayer).

On the Ni(111) surface C_2H_2 is adsorbed molecularly at T ≃ 100K [13-18]. At higher temperatures (300 to 400 K) the molecules dissociate into CH fragments [14,19,20]. Also on the Ni(100) and (110) planes molecular C_2H_2 adsorption has been observed at low temperature [16,21]. For Fe, which has a more open bcc lattice (whereas Ni and Cu have the closest packed fcc structure), the activity of the low index planes seems to depend on the packing density. On the densest Fe surface, (110), molecular C_2H_2 adsorption occurs without fragmentation, at temperatures up to 300 K, according to UPS (ultraviolet photoelectron spectroscopy) [7], LEED (low energy electron diffraction) [11] and thermal desorption [11] studies. On the most open low index plane, (111), adsorption is mainly [11] or completely [22] dissociative (at 300 K) with both C-C and C-H bonds breaking. The medium density (100) face adsorbs C_2H_2 at 98 K, first molecularly, and then gradually converts it into fragments [23] (this process is enhanced by raising the temperature to 123 K). If this (100) surface is partially deactivated by preadsorption of carbon or oxygen, adsorbed C_2H_2 remains molecular. Also on polycrystalline Fe films molecular C_2H_2 adsorption has been observed at low temperature (110 K) [24]. On Cu surfaces the situation is rather different. Both, on Cu(100) faces [15] and on polycrystalline Cu films [24], C_2H_2 is molecularly adsorbed from 80 to 300 K. At higher temperatures C_2H_2 desorbs reversibly without any decomposition taking place. So, on the whole, we can conclude that molecular C_2H_2 adsorption is probably weaker on Cu than on Fe and Ni. Whereas the latter two metals can split C_2H_2 into (adsorbed) fragments, Cu cannot. The activity of the Fe and Ni surfaces seems to be highest for the most open (Fe) surfaces. Also stepped Ni surfaces can dissociate C_2H_2 (into C_2 fragments) at low temperature (150 K) [20,25].

These observations, and the available structural (LEED [11,14,26-28]) and

spectroscopic data (UPS spectra for C_2H_2 on Fe, Ni and Cu [7,13-16,21-24,29], ELS spectra for the Ni(111) surface [17-20,25,30]) form an interesting basis for theoretical studies. We have investigated already (see paper I in this series [31]) the molecularly adsorbed state of C_2H_2 on Ni surfaces (mainly the (111) surface, since most experimental information is available there). We have done this by means of self-consistent Hartree-Fock-Slater-LCAO calculations of C_2H_2 interacting with small clusters of Ni atoms which represent the different adsorption sites on the surface. By extending these calculations to Fe and Cu clusters we want to throw some light on the observed activity differences and to explain the differences in the UPS spectra as well.

Other studies which are related to these problems are semi-empirical (Extended Hückel) calculations for C_2H_2 on Fe clusters [32,33] and ab initio Hartree-Fock-LCAO calculations for (geometrically distorted) C_2H_2 (free or bonded to a Be atom) [15,16,34] and C_2H_2 interacting with one Fe or Cu atom [35]. We think that additional insight can still be gained from further systematic theoretical work, however (as we have explained in paper I).

2. *METHOD AND CALCULATIONS*

The non-empirical (spin-restricted) Hartree-Fock-Slater (HFS)-LCAO method used has been described in detail elsewhere [36-38] and, briefly, in paper I. The atomic orbital basis set (double zeta Slater type orbitals [39]) and the density fit functions have been chosen as in I: 3d, 4s and 4p orbitals on Fe (from the $3d^6 4s^2\ ^5D$ state) and Cu (from the $3d^{10} 4s^1\ ^2S$ state), 2s and 2p on C and 1s on H. The core electrons have been replaced by a non-empirical pseudopotential [40].

The structures of the three low index surfaces of bcc Fe and fcc Cu (and Ni) are depicted in fig. 1. Just as for C_2H_2 on Ni we have studied π bonding (C_2H_2 on top of one metal atom), di-σ bonding (C_2H_2 bridging over 2 metal atoms with the C-C axis parallel to the metal-metal axis), μ_2 bonding (a double π bond, with two metal atoms) and μ_3 bonding (a π bond with one metal atom and a di-σ bond with two others), see also fig. 1. So, our metal clusters range from one to three atoms. The cluster models for C_2H_2 adsorption on Cu are the same as for Ni (see paper I, fig. 1), but the metal-metal nearest neighbour distance b_{Cu} = 2.556Å [41] is somewhat larger (b_{Ni} = 2.492Å [41]) and, moreover, we have also considered a μ_3 site, $\mu_3(a)$, which occurs on the Cu(100) surface (for which surface the UPS spectrum has been measured). The distance between two of the metal atoms is equal to $a = b\sqrt{2}$ in this case (see fig. 1). For Fe,

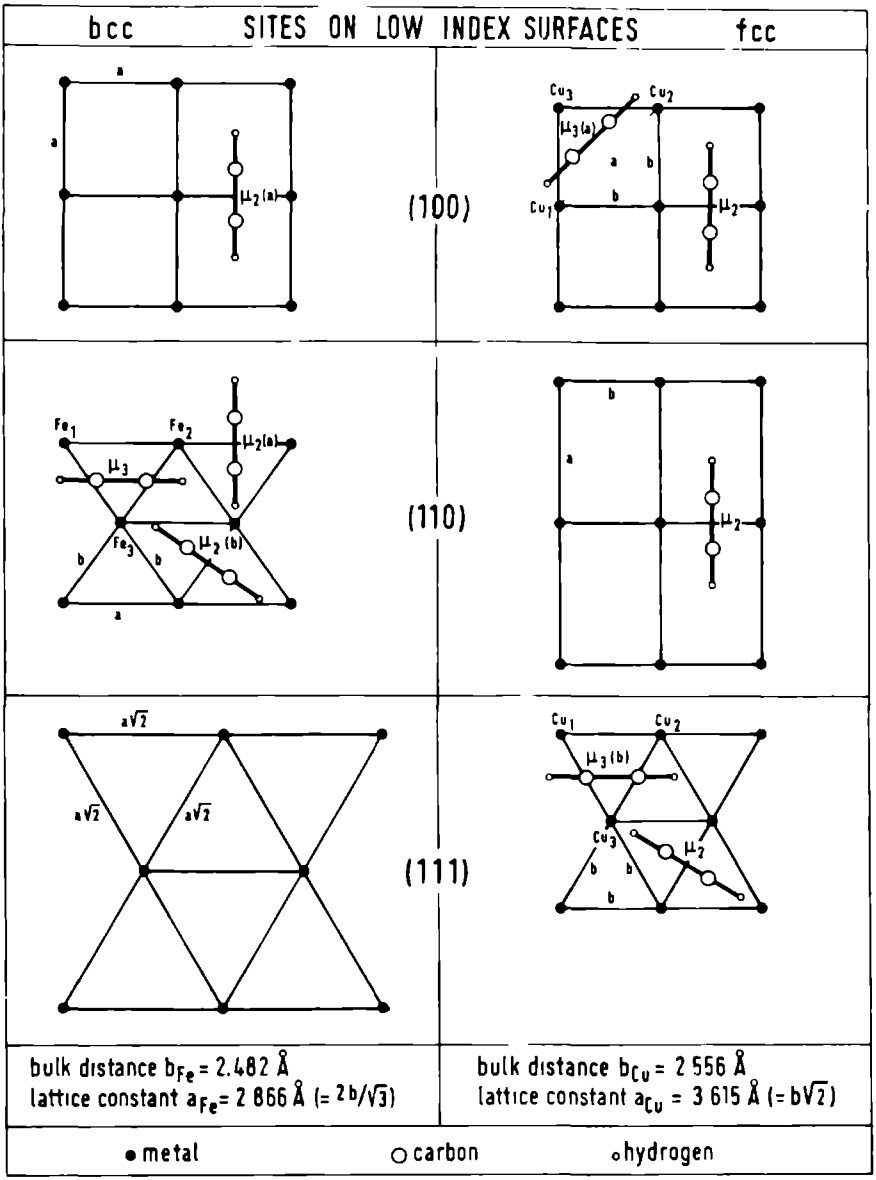

Figure 1. Structures (drawn to scale) of low index surfaces (100), (110) and (111) of bcc iron and fcc copper (bulk nearest neighbour distances, b_{Fe} and b_{Cu}, from ref. [41]). The (projected) positions of C_2H_2 (distorted, CCH angle 150°) for the μ_2 and μ_3 sites have been indicated too.

which has a different lattice structure (bcc) with a slightly smaller neighbour distance b_{Fe} = 2.482Å [41], the μ_3 site occurring on the densest plane (110) is somewhat different, too (see fig. 1). The di-σ and μ_2 sites have been studied for two metal-metal distances, b and a = 2b/√3 (clusters denoted by di-σ(*b*), μ_2(*b*) and di-σ(*a*), μ_2(*a*), respectively). Clusters with larger metal-metal distances (e.g. a√2) have not been studied since the more open Fe surface (111) does not seem to adsorb C_2H_2 molecularly.

In all models the C-C axis is kept parallel to the "surface" with a carbon to metal (internuclear) distance of 1.9Å. The adsorbed acetylene molecule is distorted from the linear structure by bending the CH bonds over 30° (in the vertical plane) and, at the same time, using C-C and C-H bond lengths which are intermediate between the values of free acetylene [41] and those of ethylene [42]. This structure with a CCH angle close to 150° and a metal-carbon distance of 1.9Å has been found as the most probable one in our studies (paper I) for C_2H_2 adsorption on Ni(111); it is in agreement with the X-ray structures of alkyne-transition metal complexes [43-57]. For the π site on Fe surfaces we have considered the linear and the 60° bent C_2H_2 structures, too ($\angle_{CCH}$ = 180° and 120°, respectively). The structural parameters for the adsorption clusters are the same as in our study of C_2H_2 on Ni (except of course the metal-metal distances), see paper I, fig. 1.

The analysis of the results proceeds along the same lines as in paper I. The measured adsorption shifts in the UPS spectrum of C_2H_2 are compared with the shifts in the ionization energies calculated for the cluster models. The latter values are calculated within the HFS formalism in most cases by the transition state method [37,58]. Also the calculated (relative) level positions from ground state HFS calculations can be used, however, since the relaxation effects on the electron binding energies are practically uniform for the upper valence levels of C_2H_2 [31]. The bonding of C_2H_2 to Fe and Cu clusters is discussed, both by looking at the level (bonding/anti-bonding) shifts and at the character of the molecular orbitals involved. This character is expressed by a Mulliken population analysis [59,60] in terms of the atomic orbitals, but also in terms of the MO's of acetylene† (after a linear transforma-

---

†*We use the free acetylene MO nomenclature* ($\sigma_g, \sigma_u, \pi_u, \pi_g^*$) *also for the MO's in the cluster models; actually, the symmetry is lowered, of course. By* $\pi_\perp$ *and* $\pi_{/\!/}$ *we denote* π *orbitals perpendicular and parallel to the "surface", respectively.*

tion). By the latter results we can quantify the Dewar-Chatt-Duncanson donation-back donation effects [61,62]. The data are compared with the Ni results (paper I), but, unfortunately, no ELS spectra are available for C_2H_2 on Fe and Cu,

3. *RESULTS*

3.1. *Adsorption of C_2H_2 on Fe*

The UPS spectrum for C_2H_2 adsorbed on Fe surfaces is similar to the spectrum for Ni surfaces: the π_u levels have a bonding shift relative to the $3\sigma_g$ level, the $2\sigma_u$-$3\sigma_g$ splitting remains almost constant, see figs. 2, 3. This π_u bonding shift is largest for Fe films [24], it is still considerable for the (110) surface [7] but it becomes very small for (100) [23]. On the latter surface, however, the UPS spectrum must be measured immediately after adsorption or on a partially deactivated surface (precovered with carbon or oxygen), since otherwise C_2H_2 becomes dissociated. Only a single π_u peak is observed in the spectra, indicating that the splitting between the two π_u levels should not be too large (smaller than 1 eV probably).

Figs. 2 and 3 also display the calculated adsorption shifts in the electron binding energies for C_2H_2 on Fe clusters. The levels shown are the only ones which are predominantly composed of the occupied C_2H_2 valence levels; they are the lowest valence levels in the C_2H_2-Fe clusters (the same as for Ni, cf. paper I). Only the results for the di-$\sigma(b)$ and $\mu_2(b)$ clusters (see section 2) have been indicated, since those for di-$\sigma(a)$ and $\mu_2(a)$ do not differ significantly. (Note that the Fe-C distances are always 1.9Å, so that for the (a) clusters, with the larger Fe-Fe distance, the C_2H_2 molecule is somewhat closer to the "surface").

The calculated shifts for the μ_2 and μ_3 adsorption clusters are in agreement with the observed UPS spectra. For di-σ bonding the $\pi_\perp$-$\pi_{/\!/}$ splitting becomes too large; this is true also for π bonding, but only in the transition state results. Except for this latter case which is exceptional (we shall discuss it below), the transition state results lead to practically the same shifts of the upper C_2H_2 valence levels as the ground state results, indicating a uniform relaxation effect for these levels. Only the lowest C_2H_2 valence level ($2\sigma_g$) shows a larger relaxation shift (cf. also paper I), but the position of this level has not been measured on Fe surfaces (neither on Cu). The very small π_u bonding shift measured for the (100) surface is not found in any of the cluster models. The molecularly adsorbed C_2H_2, which is not stable on

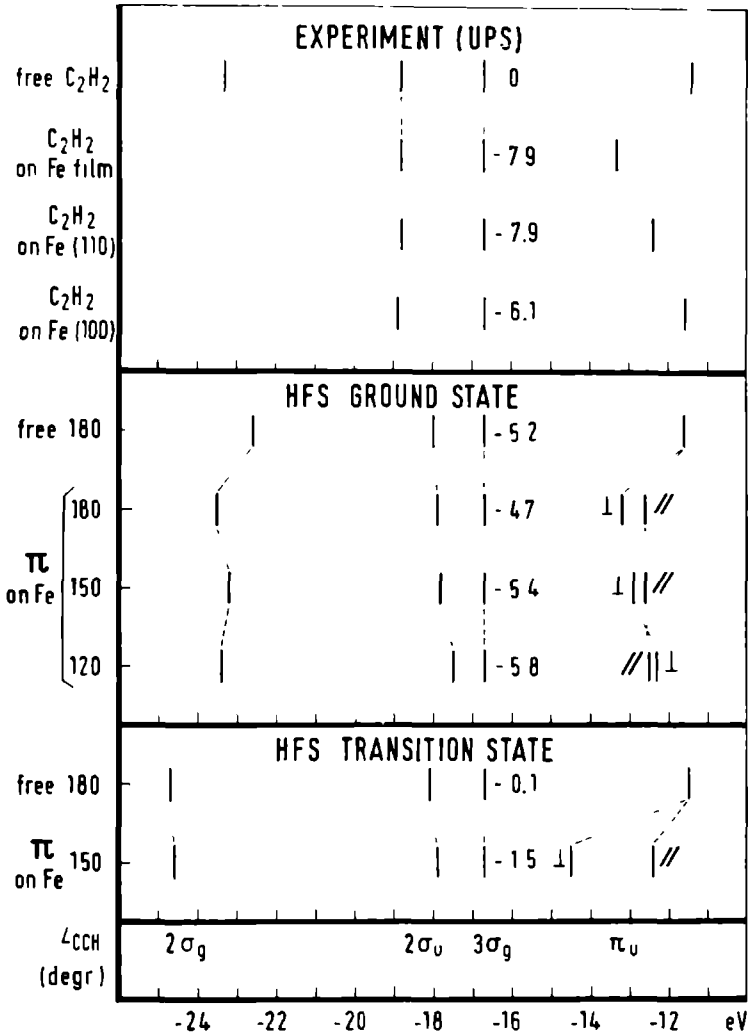

Figure 2. MO schemes for C_2H_2 on the Fe π site from HFS ground state and transition state calculations, compared with the free C_2H_2 level schemes [31]. The same comparison is indicated for the experimental (UPS) ionization energies of C_2H_2 molecularly adsorbed on an Fe film [24], on Fe(110) [7] and on Fe(100) [23] (all measured relative to the work function) and the ionization energies of free C_2H_2 [16,63]. All spectra have been shifted by the amount indicated (in eV) next to the $3\sigma_g$ levels in order to bring these $3\sigma_g$ levels into the same position.

this surface and possibly bound weaker [23,33], might occupy a position (farther away from the surface?) which is not represented by our models.

Let us now look at the electronic charge distribution in the clusters. The Mulliken gross populations of the Fe 3d orbitals are 4.2(π), 5.2(di-σ), 5.4(μ_2) and 5.7(μ_3), the 4s populations are 2.3 (π site, $\angle_{CCH} = 150^{\circ}$), 2.1(di-$\sigma$), 1.5($\mu_2$) and 1.6($\mu_3$) and the 4p populations range from 0.3 to 0.7 electrons. The populations on the adsorbed C_2H_2 molecule are shown in fig. 4, see also table 1; the $2\sigma_g$, $2\sigma_u$ and $3\sigma_g$ populations remain practically equal to two. Generally the results are very similar to the Ni results (paper I), There is some donation of acetylene π_u electrons to the metal and a more substantial back donation of metal electrons to the antibonding π_g^* orbitals. The combination of these two effects leads to a considerable decrease in the C-C overlap population, a growth of the C net atomic population and an increased negative charge on C. The magnitude of these effects increases in the order π<di-σ<μ_2<μ_3 just as for Ni; in the μ_2 and μ_3 cases both the $\pi_\perp$ and the $\pi_{/\!/}$ orbitals of C_2H_2 become involved (see paper I) and this should lead to a considerable decrease in the C-C bond strength. (For Ni [31] this has been compared with the shift in the C-C stretch frequency as measured by ELS [17,18,30]). We have also found some differences with the Ni results, however. The first one is that the lowering in the C-C overlap population (and thus, probably, in the C-C stretch frequency [31,64,65], which has not been measured for Fe, however) for the μ_3 site on the Fe(110) surface is slightly less than for the μ_3 site on Ni(111). (Also the π_u and $2\sigma_g$ bonding shifts are somewhat smaller.) This is understandable when one realizes that for the μ_3 site on Fe(110) two Fe atoms have a somewhat larger distance ($a = 2b/\sqrt{3}$, see fig. 1). Consequently, the difference in interaction strength between the μ_2 and μ_3 sites (although we do not know the interaction energies) seems somewhat smaller on Fe(110) than on Ni(111).

The second difference concerns the π site which yields a somewhat peculiar behaviour for Fe. The Fe 3d population is strikingly low (compared with the other sites) and the population of the acetylene $\pi_{u\perp}$ orbital is larger than two, see table 1. This would point to a negative π donation effect. Although such an effect (which we shall encounter for Cu also) has no direct physical interpretation (it is due to the definition of the Mulliken populations), it points to a specific type of interactions occurring. In this case, it is caused by an occupied Fe orbital which lies only slightly above the occupied acetylene $\pi_{u\perp}$ orbital; these orbitals,which have the same symmetry, strongly inter-

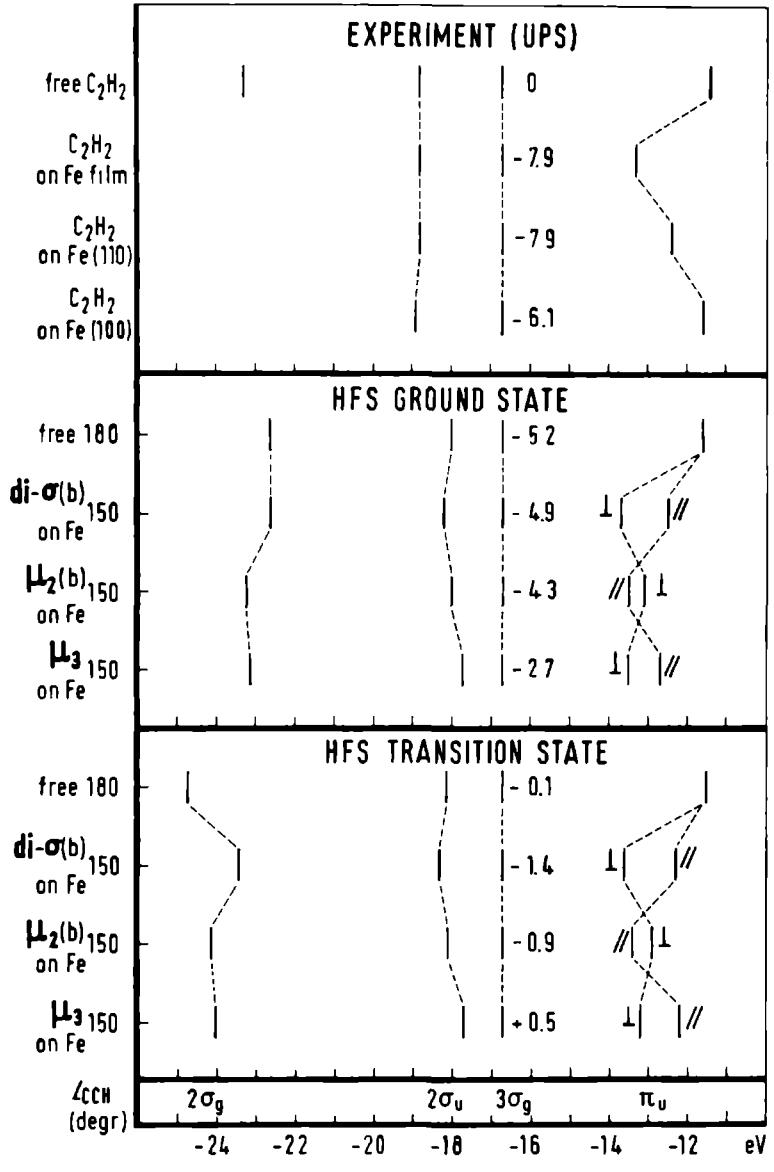

Figure 3. MO schemes for C_2H_2 on the Fe_2 di-$\sigma(b)$ and $\mu_2(b)$ sites and on the Fe_3 μ_3 site; see further the caption of fig. 2.

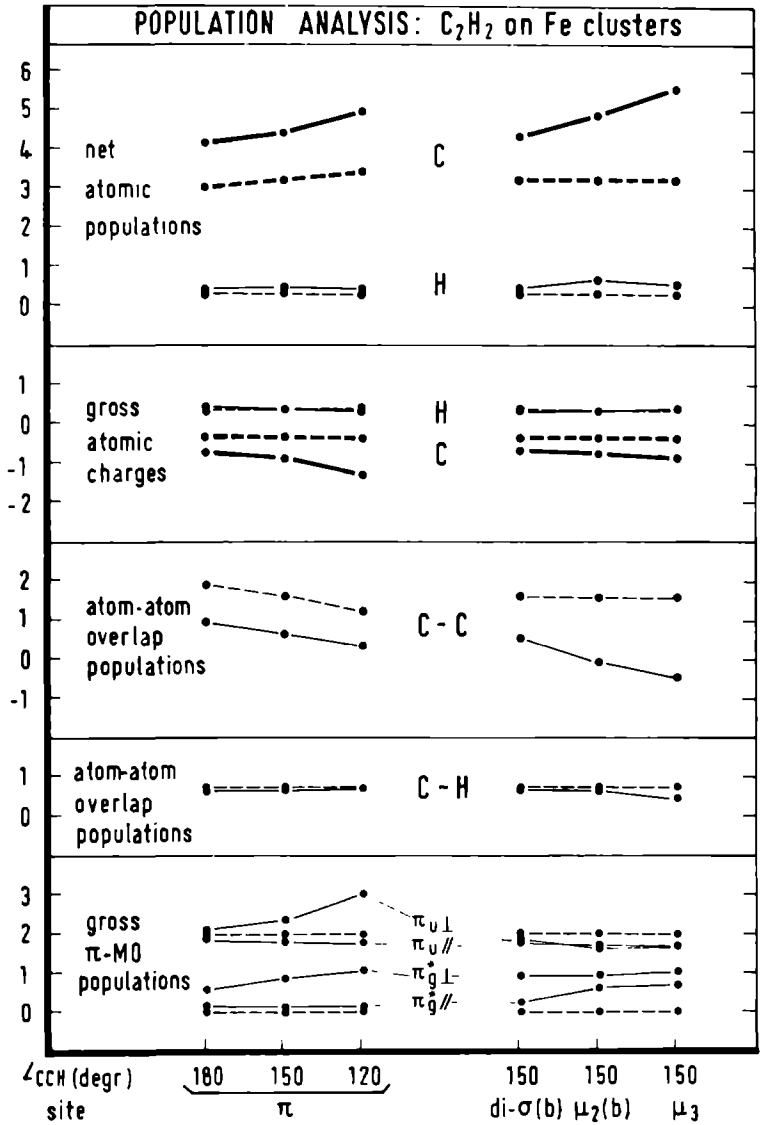

Figure 4. Population analysis data for C_2H_2 on the various Fe sites (▬▬ and ——), compared with free C_2H_2 results [31] (▬ ▬ ▬ and - - -).

act. Since both orbitals are doubly occupied the net interaction will be repulsive, lowering the stability of the C_2H_2-Fe complex. In the transition state for $\pi_{u\perp}$ ionization we extract half an electron from this $\pi_{u\perp}$ orbital, which leads to extra stabilization. This explains the exceptionally large relaxation effect found for the $\pi_{u\perp}$ level (see above). Since all these effects occur only for the π site iron cluster, which consists of a single Fe atom (with level positions which are unrealistic for the metal), we shall not attempt to attribute any physical reality to them in this case. Moreover, it is not very probable in view of our findings, that the π site is preferred by C_2H_2 adsorbing on Fe surfaces.

3.2. Adsorption of C_2H_2 on Cu

In some aspects the UPS spectrum for C_2H_2 on Cu surfaces [15,24], see fig. 5, resembles the spectra for Ni and Fe surfaces: one has observed a bonding shift of the acetylene π_u levels relative to the $3\sigma_g$ level and practically no change in the $2\sigma_u$-$3\sigma_g$ splitting. For Cu, both on the (100) surface [15] and on polycrystalline films [24] one has found a distinct splitting of the acetylene π_u levels, however, which does not occur for Ni and Fe. We compare these results in fig. 5 with the ionization energy shifts calculated for C_2H_2 interacting with Cu clusters.

The calculated results are rather different from the Ni and Fe results. For Ni and Fe we have found a set of orbitals in the C_2H_2-metal clusters (the lowest valence orbitals) which are in one to one relation with the occupied acetylene valence orbitals; each of these cluster MO's contains one C_2H_2 valence MO with large weight. For Cu we notice (in fig. 5) that almost pure Cu MO's are lying lower than the highest valence levels of C_2H_2, but also that some of the occupied C_2H_2-Cu cluster MO's consist of both C_2H_2 and Cu orbitals in different admixtures. Moreover, the acetylene orbitals $\pi_{u\perp}$, $\pi_{u\parallel}$ and (somewhat less) $3\sigma_g$ are mixed among themselves. This strong interaction with the (occupied) low lying Cu orbitals leads to a splitting (and, on the real surface, probably broadening) of the acetylene π_u levels on the larger (tri-atomic) μ_3 clusters, in addition to the $\pi_\perp$-$\pi_\parallel$ splitting observed on Ni and Fe. This can explain the finding of two (π) peaks in the UPS spectrum of C_2H_2 on Cu, whereas there is only one on Ni and Fe. The bonding shift of these (mainly) π_u levels relative to the $3\sigma_g$ level and the small change of the $2\sigma_u$-$3\sigma_g$ splitting also emerges from the calculations. Finally, we note that the bonding shift of the acetylene π_u levels (and of the $2\sigma_g$ level, which has not been measured on Cu, however) is smaller for the $\mu_3(a)$ site occurring on the (100) face than

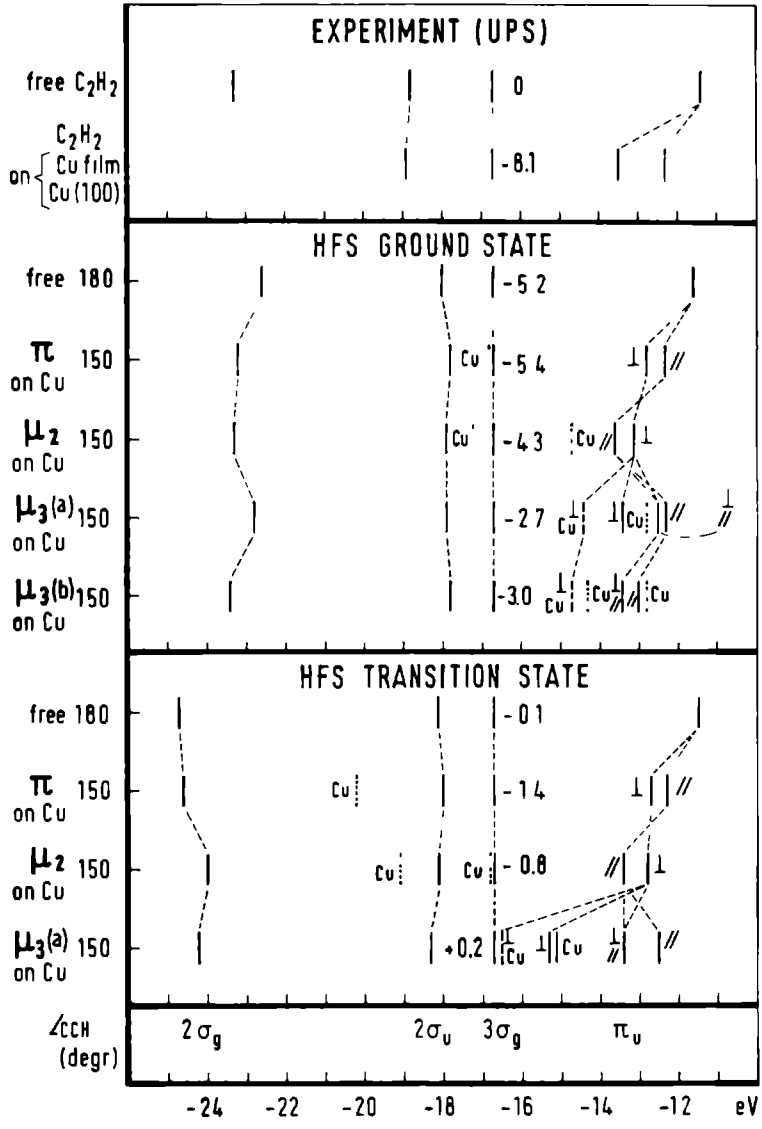

Figure 5. MO schemes for C_2H_2 on the Cu π site, the Cu_2 μ_2 site and the Cu_3 $\mu_3(a)$ and $\mu_3(b)$ sites from HFS ground state and transition state calculations, compared with the free C_2H_2 level schemes [31]. The same comparison is indicated for the experimental (UPS) ionization energies of C_2H_2 molecularly adsorbed on a Cu film [24] and on Cu(100) [15] (coinciding in the figure; both are measured relative to the work function) and the ionization energies of free C_2H_2 [16,63].

Table 1. Selected population data for C_2H_2 on Fe, Ni[a] and Cu clusters

site	∠CCH (degr.)	total $\pi_u(\pi_{u\perp}+\pi_{u/\!/})$ population			total $\pi_g^*(\pi_{g\perp}^*+\pi_{g/\!/}^*)$ population			$3\sigma_g$ population[b]
		Fe	Ni	Cu	Fe	Ni	Cu	Cu
	180	3.95	3.69		0.75	0.68		
π	150	4.16	3.69	3.90	1.02	0.92	0.88	2.56
	120	4.79	3.93		1.21	1.08		
di-σ	150	3.63[c]	3.54		1.19[c]	1.02		
μ_2	150	3.30[d]	3.34	3.24	1.56[d]	1.37	1.39	2.59
μ_3	150	3.38	3.37	5.15[e] 5.63[f]	1.76	1.60	1.74[e] 1.69[f]	2.01[e] 2.03[f]

a) from paper I [31]

b) for adsorption on Fe and Ni, the population of the $3\sigma_g$ orbital is about two (see text and paper I [31]); on Cu the situation is different, see text

c) value for di-σ(*b*)

d) value for μ_2(*b*)

e) value for μ_3(*b*)

f) value for μ_3(*a*)

Figure 5 continued. All spectra have been shifted by the amount indicated (in eV) next to the $3\sigma_g$ levels in order to bring these $3\sigma_g$ levels into the same position. Dotted bars (with the symbol Cu) represent almost pure Cu levels; dashed bars labelled by $\overset{\perp}{Cu}$ stand for about equal mixtures of $\pi_{u\perp}$ and Cu orbitals; levels indicated by $\overset{\perp}{/\!/}$ have about equal $\pi_{u\perp}$ and $\pi_{u/\!/}$ character. Furthermore on the μ_3 sites, all π_u orbitals have small admixtures of Cu character.

for the $\mu_3(b)$ site on (111).

Let us now look at the population analysis again. The Cu 3d populations are 7.4, 8.5 and 8.1 for the π, μ_2 and μ_3 sites, respectively, the 4s populations are 1.9, 1.4 and 1.5 in the same order, and the 4p populations lie between 0.3 and 0.5 electrons. Most of the acetylene data are shown in fig. 6, see also table 1. The essential differences with Ni and Fe are the following. There is an additional shift of electrons from the metal to the carbon atoms, especially for the μ_3 sites. (As pointed out in paper I, this shift in the Mulliken populations does not necessarily correspond with an increase in the work function of the system). These electrons cause the occupied acetylene orbitals to have gross populations considerably larger than 2, suggesting a negative electron donation effect (see table 1). As discussed in section 3.1, this means in fact that there is a (strong) interaction between the occupied low lying metal orbitals and the occupied acetylene orbitals, an interaction which leads to the level splitting and broadening effects which we have just discussed. For the μ_3 sites mainly the acetylene π_u orbitals are involved, for the π and μ_2 sites (less strongly) the $3\sigma_g$ orbitals (see table 1); this corresponds with the presence of copper cluster orbitals with the correct symmetry, lying close in energy to the C_2H_2 orbitals concerned. This interaction between occupied orbitals, which dominates the electron donation effect, should have a net anti-bonding (repulsive) character; it will reduce the C_2H_2-metal bonding caused by the π^* back donation effect (the latter effect is still present on Cu). This may well explain the observation that C_2H_2 desorbs more readily from Cu than from Ni and Fe and does not dissociate [15,24].

Among the μ_3 sites, we notice that the charge shifts and the reduction of C-C overlap population is largest for the $\mu_3(b)$ sites, occurring on the (111) surface; this agrees with the relative π_u and $2\sigma_g$ level bonding shifts. Apparently the $\mu_3(a)$ site, where two of the metal atoms have a considerably larger distance ($a = b\sqrt{2}$) is less effective in interacting with C_2H_2 even though the Cu-C distances are the same (1.9Å). A similar difference, albeit smaller, has been found for the μ_3 site on the Fe(110) surface as compared with the μ_3 site on Ni(111) (see section 3.1).

4. *CONCLUSIONS*

Summarizing the results of the previous sections, we can draw the following conclusions. Acetylene is bound to Fe surfaces via the Dewar-Chatt-Duncanson π to metal donation and metal to π^* back donation mechanism [61,62]; the

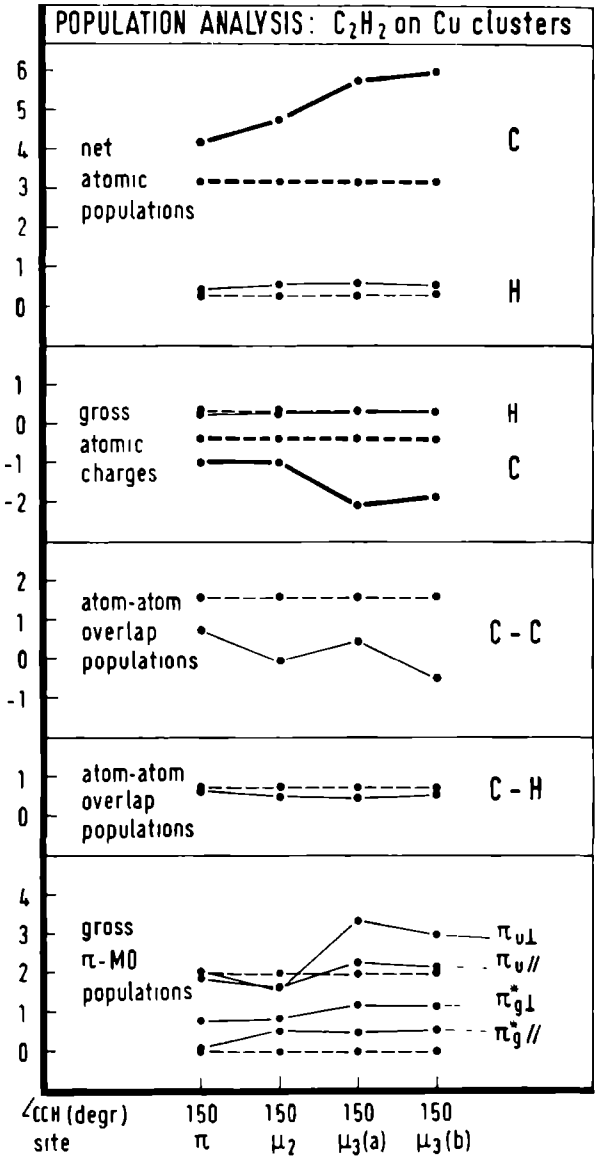

Figure 6. Population analysis data for C_2H_2 on the various Cu sites (——— and ———), compared with free C_2H_2 results [31] (– – – and - - -).

amount of back donation is larger. Both effects weaken the acetylene C-C bond. No significant differences have been found between the more dense Fe surfaces and the Ni surfaces studied earlier; Fe as a bcc metal also has more open low index surfaces, however, which we have not investigated. The bonding on Cu surfaces is different. Here, the donation effect is dominated by an interaction between the occupied acetylene valence orbitals (mainly π_u and $3\sigma_g$) and the low lying occupied copper levels; the fact that occupied Cu orbitals (with the correct symmetry to interact with the C_2H_2 orbitals) are present in this energy range must be caused by the (filled) 3d band of copper lying lower than the (partly filled) 3d bands of Ni and Fe and by the bottom of the 4s band being lower as well for Cu [66-68] (these effects are represented already by some discrete levels in our very small metal clusters). This relatively strong interaction between the occupied orbitals of nearly the same energy must cause an extra repulsion, which may well explain that the adsorption of C_2H_2 is weaker on Cu than on Ni and Fe. All these effects, donation, back donation as well as non-bonded repulsion, become more pronounced when the metal coordination of the acetylene bonding sites is higher: $\pi<di\text{-}\sigma<\mu_2<\mu_3$. The μ_3 sites are most effective when the metal atoms are packed closer: μ_3-Cu(100)$<\mu_3$-Cu(111), μ_3-Fe(110)$\lesssim\mu_3$-Ni(111).

Our cluster calculations lead to an interpretation of some typical features in the observed UPS spectra for C_2H_2 adsorbed on Fe, Ni and Cu surfaces. The bonding shift of the π_u levels (relative to the $3\sigma_g$ level) is found in all cases, but the fact that Cu is exceptional by showing two distinct π_u peaks can also be explained by the calculations. This is caused by the non-bonded interaction between the C_2H_2 valence orbitals and low lying copper orbitals (close in energy) which we have just discussed; the interaction leads to a splitting (and broadening) of the occupied levels. So, we suggest a relation between the extra peak in the UPS spectrum of C_2H_2 on Cu (observed both on the Cu(100) surface [15] and on Cu films [24]) and the weaker adsorption of C_2H_2 on Cu (as compared with Ni and Fe). Although the adsorption shifts in our calculated ionization energies are in fair agreement with the experimental UPS spectra we cannot determine from this comparison which are the preferred adsorption sites for C_2H_2 on Fe and Cu; the calculated ionization energy spectra for the different bonding sites show too small differences (also the experimental spectra are usually not very different if they have been measured on different single crystal surfaces [7,15,16,21,23] and on films [24]). We think that C_2H_2 adsorbs on Fe(110) in μ_2 or μ_3 positions and on the Fe(100)

surface in μ_2 positions (see section 3.1). The extra information which was available for C_2H_2 on the Ni(111) surface (from the ELS spectrum [17,18,30]) is still lacking for Fe and Cu surfaces.

ACKNOWLEDGEMENT

We thank Prof.Dr. P. Ros, Dr. E.J. Baerends and Dr. J.G. Snijders for making available the HFS-LCAO program.

The investigations were supported in part by the Netherlands Foundation for Chemical Research (SON) with financial aid from the Netherlands Organization for the Advancement of Pure Research (ZWO).

REFERENCES

[1] H. Conrad, G. Ertl and E.E. Latta, Surface Sci. 41 (1974) 435.

[2] K. Christmann, U. Schokev, G. Ertl and M. Neuman, J. Chem. Phys. 60 (1974) 4528.

[3] K. Christmann, G. Ertl and T. Pignet, Surface Sci. 54 (1976) 365.

[4] M. Balooch, M.J. Cardillo, D.R. Miller and R.E. Stickney, Surface Sci. 46 (1974) 358.

[5] C. Backx, B. Feuerbacher, B. Fitton and R.F. Willis, Surface Sci. 63 (1977) 193.

[6] G. Brodén, T.N. Rhodin, C. Brucker, R. Benbow and Z. Hurych, Surface Sci. 59 (1976) 593.

[7] G. Brodén, G. Gafner and H.P. Bonzel, Appl. Phys. 13 (1977) 333.

[8] S.L. Bernasek and G.A. Somorjai, J. Chem. Phys. 62 (1975) 3149.

[9] R.J. Gale, M. Salmeron and G.A. Somorjai, Phys. Rev. Letters 38 (1977) 1027.

[10] D.G. Castner, B.A. Sexton and G.A. Somorjai, Surface Sci. 71 (1978) 519.

[11] K. Yoshida and G.A. Somorjai, Surface Sci. 75 (1978) 46.

[12] D.G. Castner and G.A. Somorjai, Surface Sci. 83 (1979) 60.

[13] J.E. Demuth and D.E. Eastman, Phys. Rev. Letters 32 (1974) 1123.

[14] J.E. Demuth, Surface Sci. 69 (1977) 365.

[15] J.E. Demuth, IBM J. Res. Develop. 22 (1978) 265.

[16] J.E. Demuth, Surface Sci. 84 (1979) 315.

[17] J.E. Demuth and H. Ibach, Surface Sci. 85 (1979) 365.

[18] J.C. Bertolini, J. Massardier and G. Dalmai-Imelik, J.C.S. Faraday I 74 (1978) 1720.

[19] J.E. Demuth and H. Ibach, Surface Sci. 78 (1978) L238.

[20] S. Lehwald and H. Ibach, Surface Sci. 89 (1979) 425.

[21] J.E. Demuth, Phys. Rev. Letters 40 (1978) 409.

[22] R. Mason and M. Textor, Proc. R. Soc. Lond. A. 356 (1977) 47.

[23] C. Brucker and T. Rhodin, J. Catal. 47 (1977) 214.

[24] K.Y. Yu, W.E. Spicer, I. Lindau, P. Pianetta and S.F. Lin, Surface Sci. 57 (1976) 157.

[25] S. Lehwald, W. Erley, H. Ibach and H. Wagner, Chem. Phys. Letters 62 (1979) 360.

[26] G. Casalone, M.G. Cattania, M. Simonetta and M. Tescari, Surface Sci. 62 (1977) 321.

[27] M.G. Cattania, M. Simonetta and M. Tescari, Surface Sci. 82 (1979) L615.

[28] J.C. Hemminger, E.L. Muetterties and G.A. Somorjai, J. Am. Chem. Soc. 101 (1979) 62.

[29] C.R. Brundle, Faraday Discussions 58 (1974) 138.

[30] J.C. Bertolini and J. Rousseau, Surface Sci. 83 (1979) 531.

[31] P. Geurts and A. van der Avoird, paper I in this series, accepted for publication in Surface Sci.

[32] A.B. Anderson, J. Am. Chem. Soc. 99 (1977) 696.

[33] T.N. Rhodin, C.F. Brucker and A.B. Anderson, J. Phys. Chem. 82 (1978) 894.

[34] J.E. Demuth and D.E. Eastman, Phys. Rev. B 13 (1976) 1523.

[35] H. Itoh and A.B. Kunz, Chem. Phys. Letters 66 (1979) 531.

[36] E.J. Baerends, D.E. Ellis and P. Ros, Chem. Phys. 2 (1973) 41.

[37] E.J. Baerends and P. Ros, Chem. Phys. 2 (1973) 52.

[38] E.J. Baerends and P. Ros, Intern. J. Quantum Chem. S12 (1978) 169, and references therein.

[39] E. Clementi and C. Roetti, Atomic data and nuclear data tables, Vol. 14 (Academic Press, New York, 1974) p. 177.

[40] J.G. Snijders and E.J. Baerends, Molec. Phys. 33 (1977) 1651.

[41] R.C. Weast, ed., Handbook of chemistry and physics, 55th Ed. (CRC Press, Cleveland, 1974) p. F-200, 201.

[42] H.C. Allen, Jr. and E.K. Plyler, J. Am. Chem. Soc. 80 (1958) 2673.

[43] K. Nicholas, L.S. Bray, R.E. Davis and R. Pettit, Chem. Commun. (1971) 608.

[44] H.J. Schmitt and M.L. Ziegler, Z. Naturforsch. 28b (1973) 508.

[45] F.A. Cotton, J.D. Jamerson and B.R. Stults, J. Organometal. Chem. 94 (1975) C53.

[46] R.P. Dodge and V. Schomaker, J. Organometal. Chem. 3 (1965) 274.

[47] J.F. Blount, L.F. Dahl, C. Hoogzand and W. Hübel, J. Am. Chem. Soc. 88 (1966) 292.

[48] E. Sappa, A. Tiripicchio and M. Tiripicchio Camellini, J.C.S. Dalton (1978) 419.

[49] F.A. Cotton, J.D. Jamerson and B.R. Stults, J. Am. Chem. Soc. 98 (1976) 1774.

[50] W.G. Sly, J. Am. Chem. Soc. 81 (1959) 18; see also ref. 9 in D.A. Brown, J. Chem. Phys. 33 (1960) 1037.

[51] L.F. Dahl and D.L. Smith, J. Am. Chem. Soc. 84 (1962) 2450.

[52] R.S. Dickson and J.A. Ibers, J. Organometal. Chem. 36 (1972) 191.

[53] Y. Wang and P. Coppens, Inorg. Chem. 15 (1976) 1122.

[54] O.S. Mills and B.W. Shaw, J. Organometal. Chem. 11 (1968) 595.

[55] V.W. Day, S.S. Abdel-Meguid, S. Dabestani, M.G. Thomas, W.R. Pretzer and E.L. Muetterties, J. Am. Chem. Soc. 98 (1976) 8289.

[56] J.L. Davidson, M. Green, F.G.A. Stone and A.J. Welch, J. Am. Chem. Soc. 97 (1975) 7490.

[57] M.G. Thomas, E.L. Muetterties, R.O. Day and V.W. Day, J. Am. Chem. Soc. 98 (1976) 4645.

[58] J.C. Slater, Quantum theory of molecules and solids, Vol. 4 (McGraw-Hill, New York, 1974).

[59] R.S. Mulliken, J. Chem. Phys. 23 (1955) 1833.

[60] R.S. Mulliken, J. Chem. Phys. 23 (1955) 1841.

[61] M.J.S. Dewar, Bull. Soc. Chim. Fr. 18 (1951) C79.

[62] J. Chatt and L.A. Duncanson, J. Chem. Soc. (1953) 2939.

[63] D.W. Turner, C. Baker, A.D. Baker and C.R. Brundle, Molecular photoelectron spectroscopy (John Wiley & Sons, London, 1970).

[64] E.J. Baerends and P. Ros, Molec. Phys. 30 (1975) 1735.

[65] D.E. Ellis, E.J. Baerends, H. Adachi and F.W. Averill, Surface Sci. 64 (1977) 649.

[66] H. Ehrenreich and L.M. Schwartz, Solid State Phys. 31 (1976) 149.

[67] V.L. Moruzzi, J.F. Janak and A.R. Williams, Calculated electronic properties of metals (Pergamon Press, New York, 1978).

[68] M. Mehta and C.S. Fadley, Phys. Rev. B 20 (1979) 2280.

Hartree-Fock-Slater-LCAO studies of the acetylene-transition metal interaction. III. Binding to mono- and dinuclear Ni complexes with carbonyl and isocyanide ligands.

Petro Geurts, Hans Burgers and Ad van der Avoird
Institute of Theoretical Chemistry
University of Nijmegen
Toernooiveld, Nijmegen, The Netherlands

ABSTRACT

The bonding of C_2H_2 in the nickel complexes $[\pi\text{-}(C_2H_2)Ni(CO)_2]$, $[\pi\text{-}(C_2H_2)Ni(CNH)_2]$ and $[\mu_2\text{-}(C_2H_2)\{Ni(CNH)_2\}_2]$ has been studied by the non-empirical self-consistent Hartree-Fock-Slater-LCAO method. Calculations have been made, not only for these complexes, but also for free C_2H_2 and its substituted analogues, propyne, but-2-yne and hexafluorobut-2-yne, and for the mono- and dinuclear complex fragments, $[Ni(CNH)_2]$ and $[\{Ni(CNH)_2\}_2]$, which interact with the C_2H_2 molecule. The main difference with nickel surfaces, which have analogous π and μ_2 adsorption sites for C_2H_2 that we have studied by the same method, is the much stronger 3d, 4s, 4p hybridization induced by the CNH and CO ligands. In the bis(diisocyanide-nickel) complex these hybrids form a rather broad dsp "band". The low lying occupied levels in this "band" cause a non-bonded interaction with the filled acetylene π_u orbitals which dominates the π to metal donation effect. In the mononickel-acetylene complex this donation does occur, however, just as for acetylene adsorbed on nickel surfaces (in combination with the more prominent metal to π^* back donation which we find in all cases). A linear relation has been derived between the C≡C stretch frequencies in coordinated C_2H_2 molecules and the calculated C≡C overlap populations. Substitution of the H atoms in (free) C_2H_2 by CH_3 or CF_3 groups has almost no effect on the C≡C overlap population and force constant.

1. *INTRODUCTION*

The last two decades, many transition metal complexes containing alkyne ligands have been synthesized and characterized by different methods: infrared (IR) and Raman spectroscopy, NMR, mass spectrometry and X-ray diffraction

[1-3]. In parallel, one has investigated the reactivity of these complexes in homogeneous catalytic processes. At the same time, many workers [1,4] have experimentally explored the interaction of acetylene (the simplest alkyne) with transition metal surfaces, for a better understanding of heterogeneous catalysis. The relation between the bonding of the same compounds (alkynes) to the same transition metals either in the form of a complex (with other ligands) or in the form of a solid surface is interesting indeed. The information obtained by studying this relation will probably lead to a better view of the points that are important in catalytic reactions.

Previously, we have studied (in papers I and II of this series) the molecular adsorption of acetylene on three different transition metal surfaces, nickel [5, paper I], iron and copper [5, paper II], by means of molecular orbital calculations on model clusters. In this paper III we investigate, again by MO calculations, the binding of acetylene to some nickel complexes and we make comparisons, for the reason implied above. The second reason for this investigation is that we want to establish the relation between the measured C≡C stretch frequency ($\nu_{C\equiv C}$) in coordinated acetylene and the calculated C≡C overlap population ($q_{C\equiv C}$). This relation has been used in our previous studies (paper I) to identify the adsorption state of acetylene on the Ni(111) surface by means of our calculated results for $q_{C\equiv C}$ and the frequency $\nu_{C\equiv C}$ measured by electron energy loss spectroscopy (ELS). It can be quantitatively calibrated via the present calculations on nickel-acetylene complexes where the C≡C stretch frequencies have been measured by IR spectroscopy.

2. *MODEL SYSTEMS AND METHOD*

For our purposes outlined in the introduction we had to find nickel-acetylene (alkyne) complexes for which the structural data are available and the C≡C stretch frequencies $\nu_{C\equiv C}$ have been reported. Moreover, it would be most interesting for comparison with chemisorbed acetylene (see papers I and II) if both mono- and multinuclear transition metal complexes were known in which the acetylene ligand is coordinated to different numbers of metal atoms. Only one complex satisfies the first two conditions: π-(diphenylacetylene)bis(tert-butyl isocyanide)nickel, $[\pi\text{-}(C_6H_5C{\equiv}CC_6H_5)Ni\{CNC(CH_3)_3\}_2]$ [6,7]. However, taking this complex as a starting point, we have found four nickel-alkyne complexes that have similar ligands and for which the C≡C stretch frequencies have been measured and identified [6,8,9], see table 1. Three of these complexes are mononuclear with π bonded acetylene; one is dinuclear with μ_2 bonded acetylene bridging over the two Ni atoms, i.e. the C≡C axis is perpendicu-

Table 1. Nickel-alkyne complexes with acetylenic C≡C stretch frequencies $\nu_{C\equiv C}$

complex	$\nu_{C\equiv C}$ [cm^{-1}]
$[\pi\text{-}(C_6H_5C\equiv CC_6H_5)Ni\{CNC(CH_3)_3\}_2]$	1810[a]
$[\pi\text{-}(CF_3C\equiv CCF_3)Ni(CO)_2]$	1905[b]
$[\pi\text{-}(CF_3C\equiv CCF_3)Ni\{CNC(CH_3)_3\}_2]$	1848,1825[b]
$[\mu_2\text{-}(CF_3C\equiv CCF_3)\{Ni[CNC(CH_3)_3]_2\}_2]$	1562[a]

a) from ref. [6]

b) from ref. [8]

c) from ref. [9]

lar to the Ni-Ni axis. The structures have been based on the data known for the first complex [7]. Furthermore, we have made the following assumptions:

1. The R groups in the substituted acetylene ligands C_2R_2 ($R=C_6H_5$, CF_3) have been replaced by hydrogen atoms.
2. Also the tert-butyl groups in the isocyanide ligands have been substituted by hydrogen atoms.
3. The nickel-acetylene part of the complexes is given the same geometry as in the adsorption model clusters: Ni-C distance 1.9Å, Ni-Ni distance 2.492Å, C≡C and C-H distances varying (linearly) from the free acetylene values [10] to the ethylene values [11] for CCH bond angles of 180°, 150° and 120°, respectively. (Cf. the $\pi\text{-}C_2H_2\text{-}Ni$ cluster and the $\mu_2\text{-}C_2H_2\text{-}Ni_2$ cluster in paper I). The mononuclear complex [7] and three different dinuclear $\mu_2\text{-}C_2H_2$ complexes [12-14] are very close to this structure, which is not surprising since the adsorption model geometries have actually been based on data measured for complexes [7,12-14]. The CCR angle ranges from 149° to 140°. But, also the Ni-Ni distance in the dinuclear complexes (2.33Å to 2.62Å) [12-14] appears to be close to the metal nearest neighbour distance (2.49Å) [10]. Moreover, the geometric similarity between the adsorption clusters and the metal complexes facilitates the comparison of the calculated results.

So the complexes we have studied finally are: $[\pi\text{-}(C_2H_2)Ni(CO)_2]$, $[\pi\text{-}(C_2H_2)Ni(CNH)_2]$ and $[\mu_2\text{-}(C_2H_2)\{Ni(CNH)_2\}_2]$; all relevant structural information is given in fig. 1.

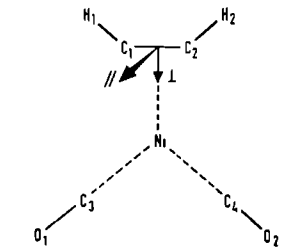

π-(acetylene) dicarbonylnickel

$\angle C_1C_2H_2 = \angle C_2C_1H_1$ 150°

C_1-C_2 1.271 Å
$C_1-H_1 = C_2-H_2$ 1.071 Å
$Ni-C_{1,2}$ 1.908 Å

$C_3-O_1 = C_4-O_2$ 1.128 Å
$Ni-C_{3,4}$ 1.820 Å
$\angle C_3NiC_4$ 106.3°

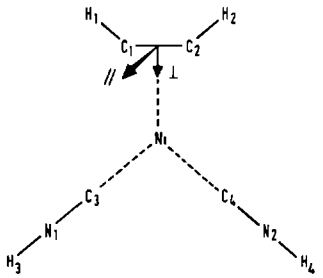

π-(acetylene) diisocyanidenickel

$\angle C_1C_2H_2 = \angle C_2C_1H_1$ 150°

C_1-C_2 1.271 Å
$C_1-H_1 = C_2-H_2$ 1.071 Å
$Ni-C_{1,2}$ 1.908 Å

$C_3-N_1 = C_4-N_2$ 1.142 Å
$N_1-H_3 = N_2-H_4$ 1.011 Å
$Ni-C_{3,4}$ 1.832 Å
$\angle C_3NiC_4$ 106.3°

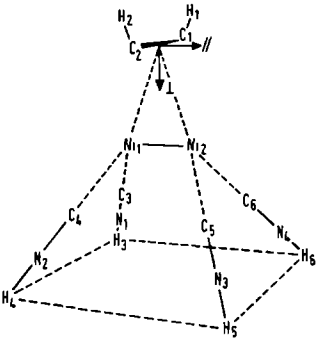

μ_2-(acetylene)-bis(diisocyanidenickel)

$\angle C_1C_2H_2 = \angle C_2C_1H_1$ 150° $\angle C_1C_2H_2 = \angle C_2C_1H_1$ 120°

C_1-C_2 1.271 Å C_1-C_2 1.337 Å
$C_1-H_1 = C_2-H_2$ 1.071 Å $C_1-H_1 = C_2-H_2$ 1.086 Å
$Ni_{1,2}-C_{1,2}$ 1.908 Å $N_{1,2}-C_{1,2}$ 1.919 Å

$C_3-N_1 = C_4-N_2 = C_5-N_3 = C_6-N_4$ 1.142 Å
$N_1-H_3 = N_2-H_4 = N_3-H_5 = N_4-H_6$ 1.011 Å
$Ni_1-C_{3,4} = Ni_2-C_{5,6}$ 1.832 Å

Figure 1. Structure of complexes based on ref. [7]. Both π complexes are planar (C_{2v}); in the μ_2 complex (also C_{2v}) the plane of bent C_2H_2 is perpendicular to the Ni_1-Ni_2 axis and each mononuclear diisocyanide half is coplanar with the C_1-C_2 axis. The Ni-C-O and Ni-C-N-H arrangements are linear. Ni-C (carbonyl) distance from nickel-carbonyl complexes [15]; C-O distance from free CO [16]; N-H distance from ref. [10]. Other parameters from refs. [5,7], see text. The symbols ⊥ and // denote the directions of the acetylene π orbitals.

Table 2. Structural parameters (distances in Å) and $\nu_{C\equiv C}$ (in cm^{-1}) of alkynes

	$-C\equiv C-$ [a]	$\equiv C-H$ [a]	$\rangle C-C\equiv$ [b]	$X\rangle C-$ [b]	CCX angle [c]	$\nu_{C\equiv C}$ [d]
$H_3CC\equiv CH$	1.204	1.056	1.460	1.115	109.47°	2142
$H_3CC\equiv CCH_3$	1.204	-	1.460	1.115	109.47°	2236
$F_3CC\equiv CCF_3$	1.204	-	1.460	1.344	109.47°	2305

a) acetylene values [10]; see text

b) from ref. [17-20]; X = H or F

c) ideal tetrahedral angle; X = H or F

d) from ref. [21]

The replacements 1. and 2. of larger groups by hydrogen atoms serve to economize on the computations. For the acetylene ligands we have tried to assess the effect of this substitution by performing a series of calculations on the following (free) ligands: propyne $H_3CC\equiv CH$, but-2-yne $H_3CC\equiv CCH_3$ and hexafluorobut-2-yne (HFB) $F_3CC\equiv CCF_3$, and comparing the results with free acetylene data [5, paper I] (section 3.1). The structures of these alkynes have been based on gas phase electron diffraction and microwave data [17-20]; the C≡C and C-H bond lengths have been kept exactly equal to the acetylene values, however, see table 2 (actually, they are very close). For but-2-yne and HFB we have imposed the staggered conformation. For the isocyanide ligands we have not studied the effect of H atom substitution since this substitution occurs rather far away from the acetylene part of the complex, which is central to us.

In order to understand the interactions between the acetylene ligands and the nickel complexes, interactions which appear to be rather different for the mononuclear and dinuclear cases (see section 3.2), we have also made calculations on the interacting fragments as such. Acetylene results were available already (from paper I), the $[Ni(CNH)_2]$ and $[\{Ni(CNH)_2\}_2]$ results are reported in section 3.2. The structures used for the latter two fragments have been taken identical to those given in fig. 1.

As in papers I and II, the computational method used is the non-empirical self-consistent Hartree-Fock-Slater (HFS)-LCAO method in its spin-restricted version with pseudopotentials for the core electrons [22-25]. The atomic

orbital (AO) basis (double zeta Slater type orbitals [26]) and density fit functions (of s-,p-,d-,f- and g-type) have been chosen as in I and II: 3d, 4s and 4p orbitals on Ni (from the $3d^8 4s^2\ ^3F$ state), 2s and 2p on C, N, O and F and 1s on H. The character of the resulting MO's is interpreted by making a Mulliken population analysis [27,28], in terms of the AO's or in terms of the MO's of the constituents (the latter populations are easily obtained from the usual AO populations by a linear transformation, using the MO coefficients of the fragments). In this analysis we denote the acetylene contributions by their free molecule symmetry labels: $2\sigma_g$, $2\sigma_u$, $3\sigma_g$, π_u and π_g^*, even though the symmetry of complexed acetylene is lower; the subscripts $\perp$ and $/\!/$ distinguish the π orbitals (see fig. 1; cf. the adsorption models in papers I and II where $\perp$ and $/\!/$ mean perpendicular and parallel to the surface, respectively).

3. *RESULTS AND DISCUSSION*

3.1. *Alkynes*

The ground state MO level schemes calculated for $HC{\equiv}CH$, $H_3CC{=}CH$, $H_3CC{\equiv}CCH_3$ and $F_3CC{\equiv}CCF_3$ are shown in fig. 2, for the occupied valence MO's. The effects of CH_3 and CF_3 substitution are very clear: the CH_3 groups raise the positions of the acetylenic levels, whereas the electronegative CF_3 groups lower these levels. Looking at the Mulliken population analysis in table 3, we observe that the CH_3 substituents are practically neutral, while the CF_3 groups have attracted a small amount of extra electronic charge. However, the main difference, which correlates with the MO level shifts, is that the substituent car-

Table 3. Population data of alkynes

	$HC^1{\equiv}C^2H$ [a]	$H_3C^3C^1{\equiv}C^2H$	$H_3C^3C^1{\equiv}C^2C^4H_3$	$F_3C^3C^1{\equiv}C^2C^4F_3$
gross atomic charges				
$-C^1{\equiv}$	-0.32	-0.06	0.02	0.10
$=C^2-$	-0.32	-0.32	0.02	0.10
$\gtrless C^3-$	-	-0.87	-0.97	0.66
$-C^4\lessgtr$	-	-	-0.97	0.66
H (in $\equiv$CH)	0.32	0.29	-	-
X (in $-CX_3$) [b]	-	0.32	0.32	-0.25
$C^1{\equiv}C^2$ overlap population ($q_{C\equiv C}$)	1.89	1.96	1.97	1.89
gross π_u population	2.00	1.99	1.97	1.94

a) from ref. [5, paper I]

b) X = H or F

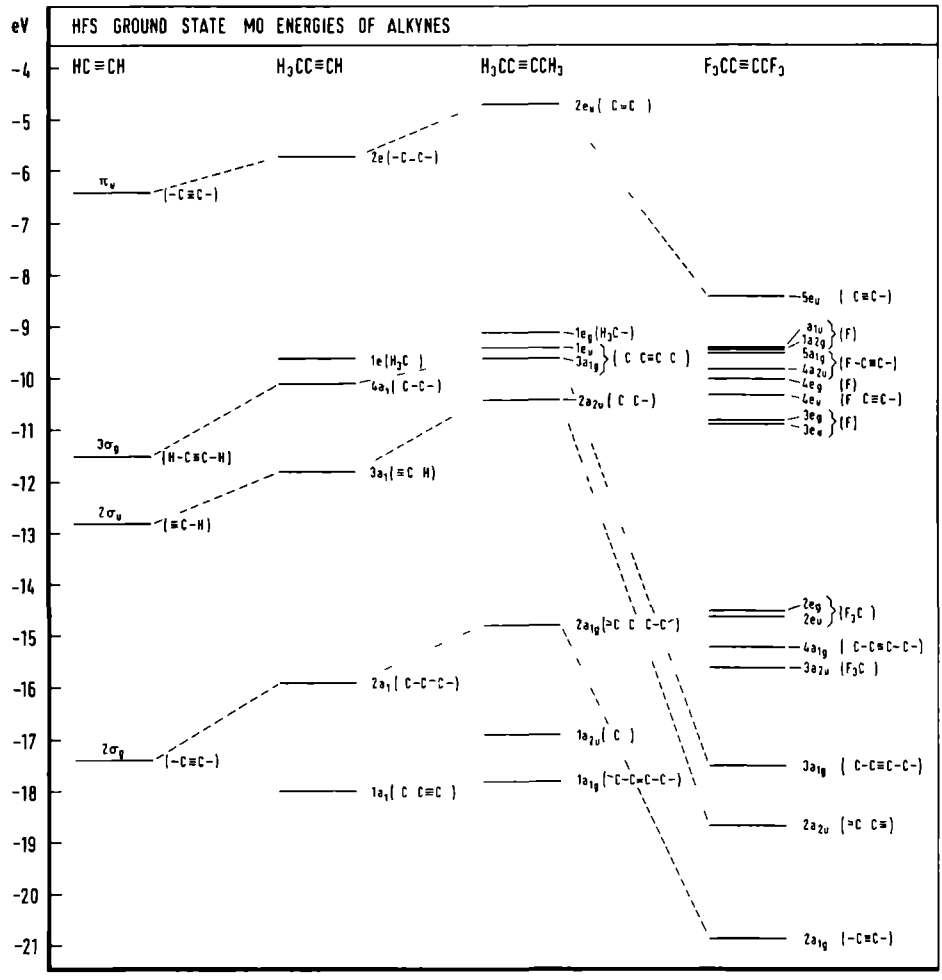

Figure 2. HFS ground state MO schemes for acetylene ($D_{\infty h}$) [5, paper I], propyne (C_{3v}), but-2-yne (D_{3d}) and hexafluorobut-2-yne (D_{3d}); for the latter the lowest orbitals ($1a_{1g}$, $1a_{2u}$, $1e_u$ and $1e_g$ lying between -34 and -30 eV with mainly CF_3 and F character) are not shown. The principal character of the levels is indicated; MO's of mainly acetylenic character are connected.

bon atoms are strongly negative in CH_3 and positive in CF_3; in the latter case the F atoms receive the electronic charge. Note that the atomic charges in the propyne molecules are practically unchanged in that part of the molecule which is opposite to the CH_3 substituent. We have calculated a dipole moment of 0.79D for this molecule; experimentally this value is 0.75D [29]. Also the C≡C overlap population $q_{C\equiv C}$ and the (gross) population of the acetylenic π_u orbitals are hardly changed by substitution. Experimentally this is reflected by the C≡C stretch frequency $\nu_{C\equiv C}$ which is almost the same for the two extreme cases of but-2-yne and HFB (see table 2). For propyne and, especially, for acetylene ($1974cm^{-1}$ [21]) $\nu_{C\equiv C}$ is lower, but, as shown by a recent empirical valence force field calculation [30], this can be explained by the coupling of the C≡C stretch mode with other vibrational modes (see also ref. [31]). The force field determination [30] yields the same force constant for the C≡C stretch in a number of alkynes, propyne, but-2-yne and several halo-propynes and but-2-ynes. Also an early ab initio Hartree-Fock-LCAO calculation has yielded the same C≡C overlap populations for acetylene and propyne [32]. So, we may safely assume in interpreting the results for coordinated acetylene ligands (section 3.2), that the mere substitutions on the acetylene do not change the C≡C overlap populations and force constants. All the calculations of the overlap populations $q_{C\equiv C}$ have been done with unsubstituted acetylene ligands, while we avoid (differences in) mode coupling effects by comparing the experimental stretch frequencies $\nu_{C\equiv C}$ always for HFB, free and coordinated.

We have also calculated the ionization energies of the alkynes which have been measured by ultraviolet photoelectron spectroscopy (UPS) [33-37]. To this end, one should make a transition state [23,38] calculation for each ionized level. For acetylene [5, paper I] and propyne we have actually done this, but for but-2-yne and HFB we have performed transition state calculations for the first ionized state (ionized from the highest occupied level) and extracted all level positions from those calculations. The latter procedure is justified if the transition state relaxation effects are uniform for all ionized levels; some additional transition state calculations have shown that this is approximately true, with the error increasing for the lower levels.

The agreement with experiment, see fig. 3, is fairly good, especially for propyne. The influence of the substituents on the calculated and experimental level positions is the same as in the ground state calculations (see above). For propyne we can assign the experimental levels individually; with regard to the order of the closely spaced 1e and $4a_1$ levels several ab initio studies

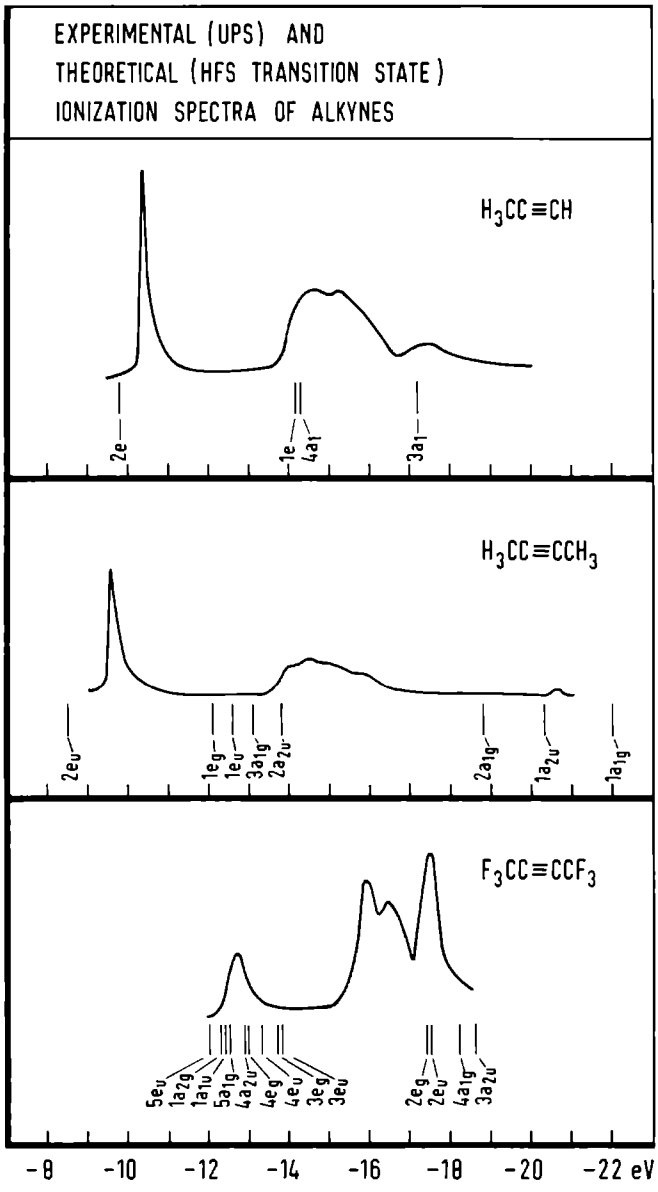

Figure 3. Calculated ionization energies (vertical bars) compared with experimental UPS spectra (propyne and but-2-yne from ref. [35], HFB from ref. [37]). The calculated results are from HFS transition state calculations in the case of propyne; for but-2-yne and HFB a transition state calculation has been performed only for the highest (e_u) orbital while the positions of the other levels have been taken from that calculation, see text.

[32,39,40] agree with our assignment, whereas several semi-empirical calculations [34,35,41] and one ab initio study [42] yield a different order. For but-2-yne and HFB we can indicate for each experimental peak which group of levels probably corresponds with this peak.

3.2. *Binding in nickel-acetylene complexes; comparison with adsorption binding*

In fig. 4 we have shown the MO schemes for the occupied (and some empty) valence orbitals of the three nickel-acetylene complexes considered (see section 2). Table 4 contains the most important Mulliken population parameters which describe the electronic charge distribution. These data for π bonded acetylene in the mononuclear nickel complexes and for μ_2 bonded C_2H_2 in the dinuclear complex are compared with the results for the analogous π and μ_2 acetylene adsorption models (from paper I). In fact, the only difference between these small (one and two nickel atom) adsorption model clusters and the nickel complexes studied here is the presence of CO or CNH ligands bonded to the nickel atoms in the latter case.

For the mononickel complexes the interaction between acetylene and the nickel atom looks rather similar to the π adsorption model. In both cases, we find π to metal donation and, more pronounced, metal to π^* back donation of electrons, in terms of the well-known Dewar-Chatt-Duncanson model for π-system transition metal interactions [43,44]. Also we observe in both cases, that for the $\pi_\perp$ orbitals, which point towards the metal atom, these effects are most prominent. The main difference is that the complexes show a much stronger 3d, 4s, 4p hybridization than the C_2H_2-Ni adsorption model. The calculations on the $[Ni(CNH)_2]$ fragment, illustrated by the MO level schemes in fig. 5 where we have also indicated the (metal) character of the MO's, demonstrate that this dsp hybridization is induced by the CNH ligands (and, similarly, by the CO ligands in the carbonyl complex). This stronger dsp hybridization on the Ni atoms in the complexes also becomes apparent by the lower populations of the 3d and 4s orbitals and the higher values for the 4p orbitals; the net charge on nickel is more positive than in the adsorption model, but the acetylene populations are very similar. There are some differences between the isocyanide and the carbonyl complexes, too. The net negative charge on CO is larger than that on CNH; this extra charge is completely donated by the nickel atom, however, the charges and overlap populations on the acetylene ligand are again practically the same. Note also (in fig. 4) that the one-electron energies of the carbonyl complex lie generally lower.

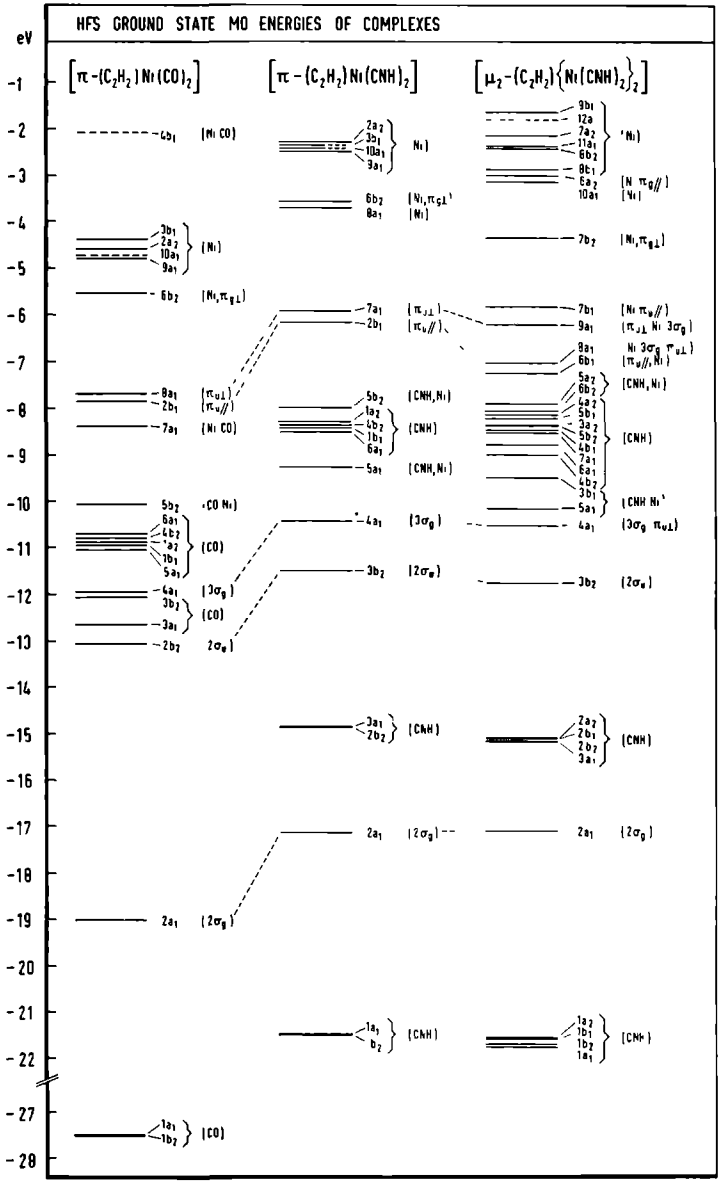

Figure 4. HFS ground state MO schemes for all doubly occupied (———), singly occupied (— --) and some empty (- - -) levels of the complexes $[\pi\text{-}(C_2H_2)Ni(CO)_2]$, $[\pi\text{-}(C_2H_2)Ni(CNH)_2]$ and $[\mu_2\text{-}(C_2H_2)\{Ni(CNH)_2\}_2]$ (for $\angle_{CCH} = 150^o$). The principal character of the levels is indicated; MO's of mainly acetylenic character are connected.

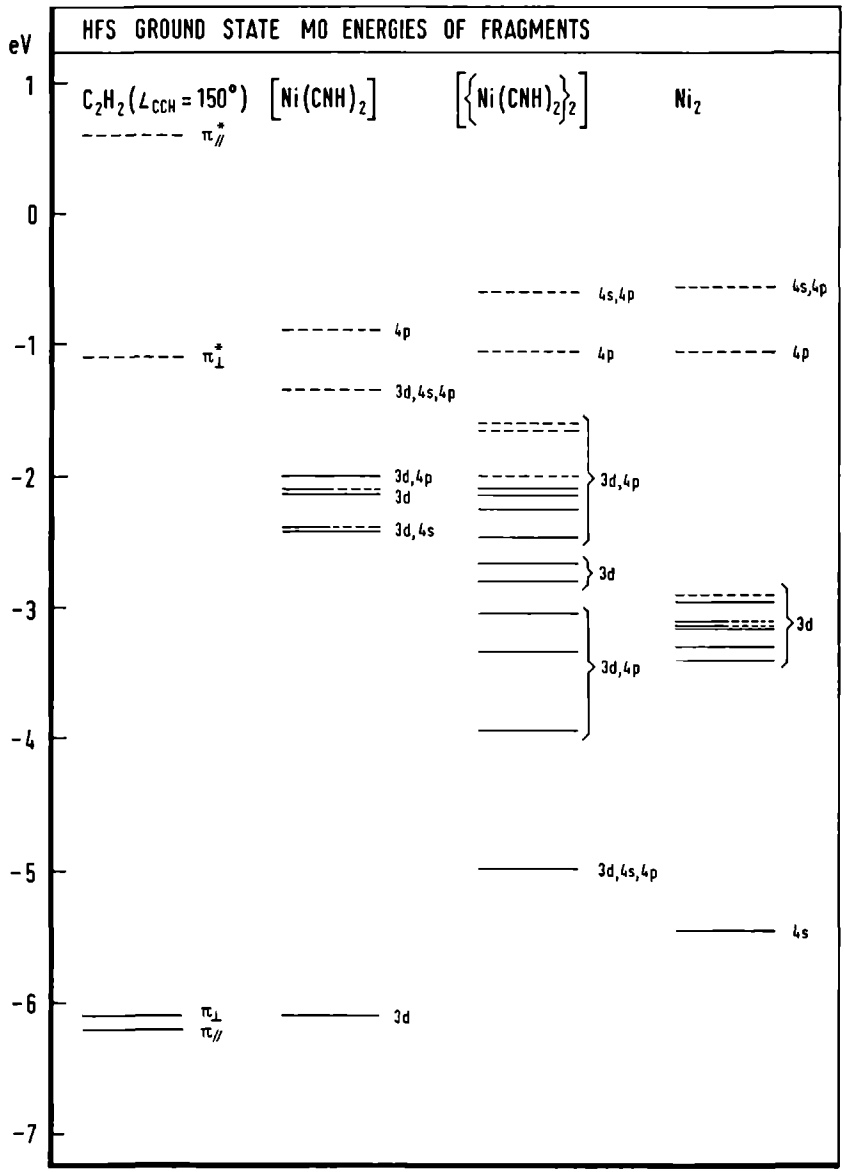

Figure 5. HFS ground state MO schemes in the energy range of −7 to +1 eV for doubly occupied (———), singly occupied (— —) and empty (- - -) levels of the fragments $[Ni(CNH)_2]$, $[\{Ni(CNH)_2\}_2]$, C_2H_2 ($\angle_{CCH}$ = 150°) [5, paper I] and Ni_2. The principal (metallic) character of the orbitals is indicated.

For the μ_2-(acetylene)-bis(diisocyanidenickel) complex the results are rather different from the corresponding μ_2 adsorption case. While the metal to π^* back donation is just what we would have expected, with both the $\pi^*_\perp$ and $\pi^*_{/\!/}$ orbitals being involved (cf. the adsorption results discussed in paper I), the π to metal donation is absent in this complex. Instead, we find acetylene π_u orbitals with populations larger than two. Moreover, the $3\sigma_g$ and π_u orbitals in the dinuclear complex (fig. 4) are extensively mixed with each other and with Ni orbitals. The same effects have been encountered in our model calculations for C_2H_2 adsorption on Cu surfaces (paper II); there they have been related to the lower (filled) 3d and 4sp levels which reflect the lower lying 3d and 4sp bands in copper, relative to nickel.

At first, we have tried to explain the occurrence or absence of the donation effects by looking at the positions of the donating acetylene π orbitals and the accepting empty orbitals of the metal fragment. These fragment MO levels are displayed in fig. 5, in the energy range where they have mainly metal character; the more specific CNH levels lie lower. No such correlation could be found, however, but the fragment results do suggest another explanation.

We have mentioned already the metal 3d,4s,4p hybridization in the mononuclear $[Ni(CNH)_2]$ fragment induced by the isocyanide ligands. The same hybridization leads to a broad 3d,4s,4p "band" in the bis(diisocyanidenickel) complex. In the Ni_2 diatom, without CNH ligands, this hybridization does practically not occur; we find a strongly bonding 4s level only (and some strongly anti-bonding 4sp levels) and a narrow 3d "band", since the 3d orbitals have much smaller interactions (see fig. 5). This picture for Ni_2, which has been found in other calculations [45-48] too, already reflects the situation in the nickel metal, despite the smallness of this cluster: a narrow 3d band, a broad 4sp band and little dsp hybridization. Thus, $[\{Ni(CNH)_2\}_2]$ distinguishes itself by the presence of 3d,4s,4p hybrid nickel orbitals, which occur in the $[Ni(CNH)_2]$ half already, but which now form a broad "band" with rather high "density of states" in the lower energy range, due to the strong interactions between the two halves. (This interaction is not present in the bare Ni_2 unit, although the Ni-Ni distance is the same,since the pure 3d orbitals have much smaller overlap than the hybrids). Apparently, these low lying filled metal levels,which are present in the copper adsorption clusters also (see paper II), lead to a strong non-bonded interaction with the filled acetylene π_u orbitals. Several of these metal orbitals have the same symmetry as the π_u orbitals and it is probably important that they do have large overlaps, as well. This

Table 4. Population data of complexes[a)]

	gross atomic charges						atom-atom overlap populations		gross π-MO populations			
		C_2H_2		CO or CNH								
	Ni	C	H	C	O/N	H	C≡C	C-H	$\pi_{u\perp}$	$\pi_{u/\!/}$	$\pi^*_{g\perp}$	$\pi^*_{g/\!/}$
$[\pi\text{-}(C_2H_2)Ni(CO)_2]$	2.34	-0.60	0.35	-0.31	-0.62	-	0.91	0.66	1.74	1.85	0.77	0.05
$[\pi\text{-}(C_2H_2)Ni(CNH)_2]$	1.38	-0.62	0.34	-0.15	-0.71	0.45	0.91	0.70	1.76	1.83	0.84	0.07
$[\mu_2\text{-}(C_2H_2)\{Ni(CNH)_2\}_2]$	1.36	-1.35	0.31	0.03	-0.62	0.43	0.36	0.58	2.24	2.06	0.88	0.57
$\pi\text{-}C_2H_2\text{-}Ni$[b)]	0.54	-0.60	0.33	-	-	-	0.69	0.66	1.78	1.91	0.83	0.09
$\mu_2\text{-}C_2H_2\text{-}Ni_2$[b)]	0.38	-0.70	0.33	-	-	-	-0.10	0.61	1.68	1.66	0.84	0.53

a) calculated for the acetylene CCH angle of 150°

b) from ref. [5, paper I]

non-bonded interaction with the filled metal orbitals can explain the splitting and the populations of the acetylene π_u orbitals (larger than two). It dominates the π to metal donation and should cause a net repulsive effect which reduces the bonding originating from the metal to π^* back donation.

Now, we discuss the relation between the calculated C≡C overlap population $q_{C\equiv C}$ and the measured C≡C stretch frequency $\nu_{C\equiv C}$ for coordinated [6,8,9] (table 1) and free (substituted) acetylene [21] (table 2). The CCR angle in the π bonded alkyne ligand in the mononickel complex [7] is 149°, close to the value of the CCH angle, 150°, used in our calculations. For μ_2 bonded alkyne in the dinickel complex we do not know the exact geometry, but we have adopted a CCH angle of 150° or 120° in the calculations, since we expect a stronger metal-alkyne interaction with possibly somewhat stronger distortion of the alkyne geometry, too. Structural data for other alkyne-transition metal complexes [8,12-14,49-58] support this expectation. We find that, indeed, the calculated C≡C overlap population is more and more reduced when we go from free C_2H_2 via the π bonded Ni complex to the μ_2 bonded Ni_2 complex, just as the experimental C≡C stretch frequency. The relation between $q_{C\equiv C}$ and $\nu_{C\equiv C}$ is almost linear, see fig. 6, as it has been found earlier for CO bonds in various carbonyl complexes [62]. Estimated error bounds due to the uncertainty about the CCH angle in the dinickel complex, are indicated in the figure. We have used this linear relation to predict the approximate value of $q_{C\equiv C}$ for C_2H_2 adsorbed on the Ni(111) surface, where we do know the frequency $\nu_{C=C}$ from ELS [59-61] but not the structure and the position of C_2H_2 relative to the surface nickel atoms and the type of bonding, π, di-σ, μ_2 or μ_3. Since the measured $\nu_{C\equiv C}$ is much lower even than the value for the dinickel complex, we must extrapolate from the complex results; this yields $q_{C=C} = -0.55\pm0.25$ for the error bounds indicated in fig. 6. This value is in agreement with q_{C-C} calculated for μ_3 bonded C_2H_2, coordinated to three nickel atoms with a Ni-C distance of 1.9Å (see paper I).

4. *CONCLUSIONS*

Summarizing the results discussed in the previous sections we can draw the following conclusions. The main difference between the nickel atoms in the carbonyl and isocyanide complexes studied here and the atoms in metal surfaces is the much stronger 3d,4s,4p hybridization in the complexes. Apparently, the CO and CNH ligands are more effective in inducing this hybridization than the neighbouring atoms in the metal. For the bis(diisocyanidenickel) complex this

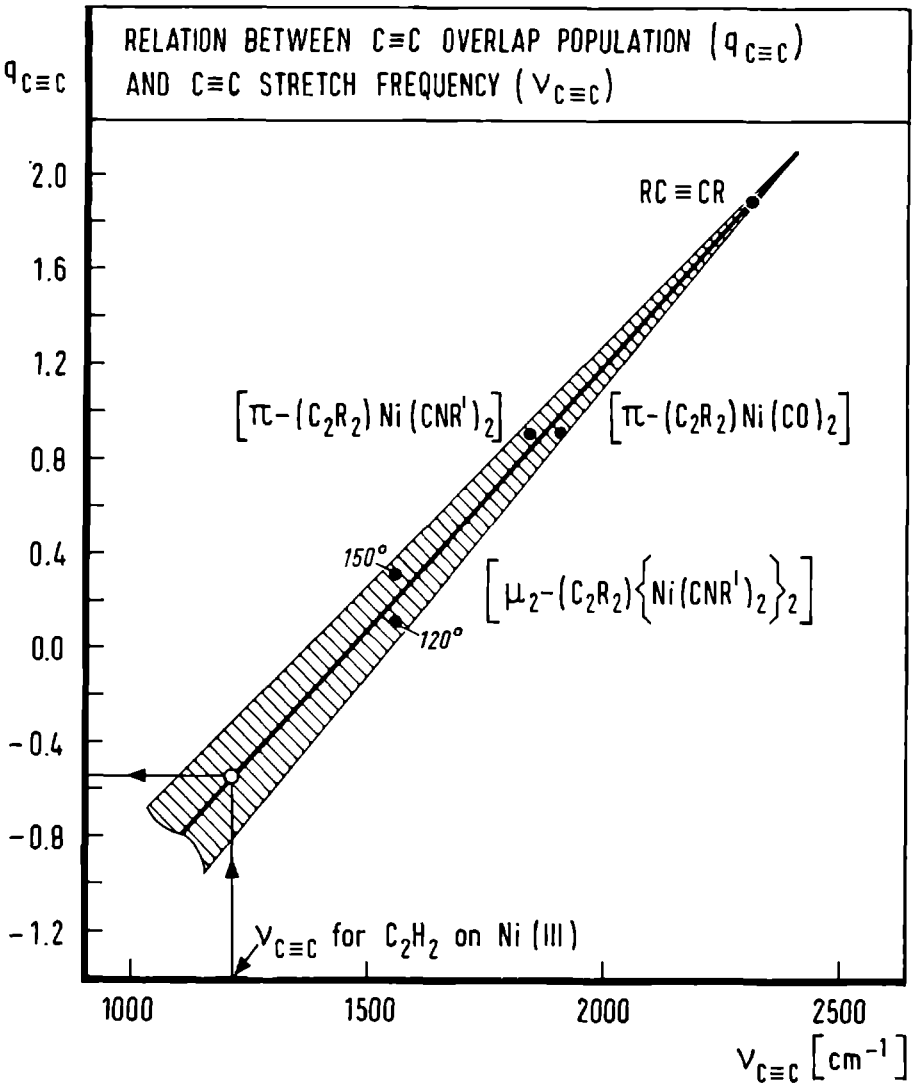

Figure 6. Calculated C≡C overlap populations $q_{C\equiv C}$ (for R = R' = H) plotted against the experimental stretch frequencies $\nu_{C\equiv C}$ (for R = CF_3, R' = $C(CH_3)_3$); $\nu_{C\equiv C}$ of complexes from refs. [8,9], $\nu_{C\equiv C}$ of HFB from ref. [21]. $\nu_{C\equiv C}$ for C_2H_2 on Ni(111) from ELS measurements [59-61]. For the dinuclear complex two $q_{C\equiv C}$ values (for $\angle_{CCH}$ = 150° and 120°) are indicated.

leads to a rather broad dsp "band" caused by the interactions between the hybrids in the two halves, which is much stronger than the interaction between the d orbitals in the metal (although the Ni-Ni distance is the same). This difference has consequences for the C_2H_2 bonding, too. In the mononickel π bonded C_2H_2 complex we find π to metal donation and, more prominent, metal to π^* back donation of electrons, just as for C_2H_2 adsorbed on nickel surfaces (paper I). In the dinickel μ_2 bonded C_2H_2 complex, however, the π to metal donation is dominated by a strong (non-bonded) interaction between the filled acetylene π_u orbitals and the low lying occupied levels in this dsp "band". The reduction in the C≡C overlap population is significantly smaller than for μ_2 adsorption. A similar effect has been found in model cluster calculations, for C_2H_2 adsorbed on Cu surfaces which have low lying filled 3d bands (paper II).

Another result from the present calculations is that we have found a (linear) relation between the measured C≡C stretch frequencies of coordinated (and free) acetylene and the calculated C≡C Mulliken overlap populations. The C≡C bond is weakened more when the acetylene molecule is coordinated to a larger number of nickel atoms. We have used this relation to obtain more quantitative information about the adsorption state of C_2H_2 on a Ni(111) surface, using the measured C≡C stretch frequency which is considerably lower than the values in the C_2H_2-nickel complexes studied here.

The calculations for propyne, but-2-yne and hexafluorobut-2-yne have shown that substituting the hydrogen atoms in C_2H_2 by CH_3 or CF_3 groups has almost no effect on the C≡C force constant and overlap population. The ionization energies calculated for these molecules (using the transition state concept) are in fairly good agreement with experimental (UPS) data. The acetylene one-electron levels are lowered by the CF_3 groups, while they are raised by the CH_3 groups. An additional check on our calculated results would be the measurement of the ionization energy spectra of the C_2H_2-nickel complexes which we could calculate by the same method.

ACKNOWLEDGEMENT

We thank Prof.Dr. P. Ros, Dr. E.J. Baerends and Dr. J.G. Snijders for making available the HFS-LCAO program.

The investigations were supported in part by the Netherlands Foundation for Chemical Research (SON) with financial aid from the Netherlands Organization for the Advancement of Pure Research (ZWO).

[1] R. Ugo, Catal. Rev.-Sci. Eng. 11 (1975) 225.

[2] S.D. Ittel and J.A. Ibers, Adv. Organometal. Chem. 14 (1976) 33.

[3] S. Otsuka and A. Nakamura, Adv. Organometal. Chem. 14 (1976) 245.

[4] T.N. Rhodin and G. Ertl, eds., The nature of the surface chemical bond (North-Holland Publishing Co., Amsterdam, 1979).

[5] P. Geurts and A. van der Avoird, papers I and II in this series, submitted for publication in Surface Sci.

[6] S. Otsuka, T. Yoshida and Y. Tatsuno, J. Am. Chem. Soc. 93 (1971) 6462.

[7] R.S. Dickson and J.A. Ibers, J. Organometal. Chem. 36 (1972) 191.

[8] J.L. Davidson, M. Green, F.G.A. Stone and A.J. Welch, J. Am. Chem. Soc. 97 (1975) 7490.

[9] N.M. Boag, M. Green, J.A.K. Howard, J.L. Spencer, R.F.D. Stansfield, F.G.A. Stone, M.D.O. Thomas, J. Vicente and P. Woodward, J.C.S. Chem. Comm. (1977) 930.

[10] R.C. Weast, ed., Handbook of chemistry and physics, 55th Ed. (CRC Press, Cleveland, 1974) p. F-200, 201, 202.

[11] H.C. Allen, Jr. and E.K. Plyler, J. Am. Chem. Soc. 80 (1958) 2673.

[12] O.S. Mills and B.W. Shaw, J. Organometal. Chem. 11 (1968) 595.

[13] Y. Wang and P. Coppens, Inorg. Chem. 15 (1976) 1122.

[14] V.W. Day, S.S. Abdel-Meguid, S. Dabestani, M.G. Thomas, W.R. Pretzer and E.L. Muetterties, J. Am. Chem. Soc. 98 (1976) 8289.

[15] P.W. Jolly and G. Wilke, The organic chemistry of nickel, Vol. 1, Organonickel complexes (Academic Press, New York, 1974).

[16] L.E. Sutton, ed., Tables of interatomic distances and configuration in molecules and ions, Special publ. no. 11 (Chem. Soc., London, 1958).

[17] C.C. Costain, J. Chem. Phys. 29 (1958) 864.

[18] J.L. Duncan, D.C. McKean, P.D. Mallinson and R.D. McCulloch, J. Molec. Spectrosc. 46 (1973) 232.

[19] M. Tanimoto, K. Kuchitsu and Y. Morino, Bull. Chem. Soc. Jpn. 42 (1969) 2519.

[20] K. Kveseth, H.M. Seip and R. Stølevik, Acta Chem. Scand. 25 (1971) 2975.

[21] F.R. Dollish, W.G. Fateley and F.F. Bentley, Characteristic Raman frequencies of organic compounds (John Wiley & Sons, New York, 1974).

[22] E.J. Baerends, D.E. Ellis and P. Ros, Chem. Phys. 2 (1973) 41.

[23] E.J. Baerends and P. Ros, Chem. Phys. 2 (1973) 52.

[24] J.G. Snijders and E.J. Baerends, Molec. Phys. 33 (1977) 1651.

[25] E.J. Baerends and P. Ros, Intern. J. Quantum Chem. S12 (1978) 169.

[26] E. Clementi and C. Roetti, Atomic data and nuclear data tables, Vol. 14 (Academic Press, New York, 1974) p. 177.

[27] R.S. Mulliken, J. Chem. Phys. 23 (1955) 1833.

[28] R.S. Mulliken, J. Chem. Phys. 23 (1955) 1841.

[29] A.L. McClellan, Tables of experimental dipole moments (W.H. Freeman and Co., San Francisco, 1963) p. 77.

[30] F. Lichene, G. Dellepiane and V. Lorenzelli, J. Chem. Phys. 70 (1979) 4786.

[31] N. Sheppard and D.M. Simpson, Quart. Rev. 6 (1952) 1.

[32] M.D. Newton and W.N. Lipscomb, J. Am. Chem. Soc. 89 (1967) 4261.

[33] D.W. Turner, C. Baker, A.D. Baker and C.R. Brundle, Molecular photoelectron spectroscopy (John Wiley & Sons, London, 1970).

[34] M.V. Andreocci, P. Bitchev, P. Carusi and A. Furlani, J. Electron Spectrosc. Relat. Phenom. 16 (1979) 25.

[35] W. Ensslin, H. Bock and G. Becker, J. Am. Chem. Soc. 96 (1974) 2757.

[36] P. Carlier, J.E. Dubois, P. Masclet and G. Mouvier, J. Electron Spectrosc. Relat. Phenom. 7 (1975) 55.

[37] J.P. Delwiche, M-Th. Praet, G. Caprace, M-J. Hubin-Franskin, P. Natalis and J.E. Collin, J. Electron Spectrosc. Relat. Phenom. 12 (1977) 395.

[38] J.C. Slater, Quantum theory of molecules and solids, Vol. 4 (McGraw-Hill, New York, 1974).

[39] S.D. Peyerimhoff and R.J. Buenker, Theoret. Chim. Acta (Berl.) 14 (1969) 305.

[40] B.V. Cheney, Chem. Phys. Letters 18 (1973) 31.

[41] H. Bock and B.G. Ramsey, Angew. Chem. 85 (1973) 773.

[42] D.C. Frost, F.G. Herring, C.A. McDowell and I.A. Stenhouse, Chem. Phys. Letters 4 (1970) 533.

[43] M.J.S. Dewar, Bull. Soc. Chim. Fr. 18 (1951) C79.

[44] J. Chatt and L.A. Duncanson, J. Chem. Soc. (1953) 2939.

[45] N. Rösch and D. Menzel, Chem. Phys. 13 (1976) 243.

[46] C.F. Melius, Chem. Phys. Letters 39 (1976) 287.

[47] C.F. Melius, J.W. Moskowitz, A.P. Mortola, M.B. Baillie and M.A. Ratner, Surface Sci. 59 (1976) 279.

[48] R.P. Messmer, D.R. Salahub, K.H. Johnson and C.Y. Yang, Chem. Phys. Letters 51 (1977) 84.

[49] M.G. Thomas, E.L. Muetterties, R.O. Day and V.W. Day, J. Am. Chem. Soc. 98 (1976) 4645.

[50] K. Nicholas, L.S. Bray, R.E. Davis and R. Pettit, Chem. Commun. (1971) 608.

[51] H.J. Schmitt and M.L. Ziegler, Z. Naturforsch. 28b (1973) 508.

[52] F.A. Cotton, J.D. Jamerson and B.R. Stults, J. Organometal. Chem. 94 (1975) C53.

[53] R.P. Dodge and V. Schomaker, J. Organometal. Chem. 3 (1965) 274.

[54] J.F. Blount, L.F. Dahl, C. Hoogzand and W. Hübel, J. Am. Chem. Soc. 88 (1966) 292.

[55] E. Sappa, A. Tiripicchio and M. Tiripicchio Camellini, J.C.S. Dalton (1978) 419.

[56] F.A. Cotton, J.D. Jamerson and B.R. Stults, J. Am. Chem. Soc. 98 (1976) 1774.

[57] W.G. Sly, J. Am. Chem. Soc. 81 (1959) 18; see also ref. 9 in D.A. Brown, J. Chem. Phys. 33 (1960) 1037.

[58] L.F. Dahl and D.L. Smith, J. Am. Chem. Soc. 84 (1962) 2450.

[59] J.C. Bertolini, J. Massardier and G. Dalmai-Imelik, J.C.S. Faraday I 74 (1978) 1720.

[60] J.C. Bertolini and J. Rousseau, Surface Sci. 83 (1979) 531.

[61] J.E. Demuth and H. Ibach, Surface Sci. 85 (1979) 365.

[62] E.J. Baerends and P. Ros, Molec. Phys. 30 (1975) 1735.

Hartree-Fock-Slater-LCAO studies of the acetylene-transition metal interaction. IV. Dissociation fragments on Ni surfaces; cluster models.

Petro Geurts, Walter Ravenek and Ad van der Avoird
Institute of Theoretical Chemistry
University of Nijmegen
Toernooiveld, Nijmegen, The Netherlands

ABSTRACT

Using the Hartree-Fock-Slater-LCAO method we have calculated the ionization energies for the acetylene fragments CH, CH_2 and C_2H adsorbed on small Ni clusters and we have compared these with the UPS spectrum measured for dissociatively adsorbed C_2H_2 on the Ni(111) surface. For none of these fragments the calculated spectrum is in one-to-one correspondence with the experimental one. Although one should perform further, more extensive, calculations in order to be conclusive, we suggest as a possible explanation of this discrepancy that other (low intensity or strongly broadened) peaks might be hidden in the experimental spectrum. If such peaks would be found, our results can be used to identify the adsorbed fragments since the spectra calculated for the different species are rather different. On the other hand, we conclude that these spectra do not depend sensitively on the adsorption site or on the position of the adsorbed fragments.

1. INTRODUCTION

In the previous papers I and II [1,2] in this series we have studied the molecular adsorption of acetylene on Ni, Fe and Cu surfaces. This was done by means of Hartree-Fock-Slater (HFS)-LCAO calculations on C_2H_2 interacting with small metal clusters which model different adsorption sites on the transition metal low index planes and comparison of the calculated properties with experimental (spectroscopic) data. A comparison has been made also (in paper III [3]) with C_2H_2 binding to mono- and dinuclear nickel complexes with carbonyl and isocyanide ligands. In catalytic processes involving hydrocarbons bond breaking by the (transition metal) catalyst is an important step. For C_2H_2 adsorbed on the low index planes of Fe [4-7] and Ni [8-10] such bond breaking has been found experimentally at somewhat higher temperatures and coverages (compared with the molecularly adsorbed state). In order to study the various possible reaction pathways one must identify the dissociation fragments, but this identification is not so easy. Much work has been done, for instance, on the dissociative adsorption of C_2H_2 on the Pt(111) surface but three different structures have been suggested, CH_3-CH [11,12], CH_3-C [13,14] and CH_2=C [12,14, 15], for what is probably the same species. From ultraviolet photoelectron spectroscopy (UPS), temperature programmed desorption (TPD) and low energy electron diffraction (LEED) [8] and from electron energy loss spectroscopy (ELS) [9,10] it has been concluded that on Ni(111) C_2H_2 dissociates into CH species, at T ≃ 300 to 400K; in paper I we have found indications for a considerable C-C bond weakening, by the interaction with the Ni surface, which must precede this dissociation. At still higher temperatures $T \gtrsim 450K$, CH_2 fragments seem to occur [9]. Also on Fe(100) and Fe(111) surfaces CH, CH_2 and other species have been suggested [4-7].

In the present paper we study three possible dissociation products of acetylene, CH, CH_2 and C_2H, adsorbed on nickel surfaces at different sites, represented by small clusters of Ni atoms (1,2 or 3 atoms). The non-empirical MO method used is the same as in our previous work [1-3], i.e. the HFS-LCAO method. We try to characterize the adsorbed fragments by comparing the calculated ionization energies for the different species at different sites with the UPS spectrum measured for dissociated C_2H_2 on Ni(111) at T ≃ 300 to 400K [8]. Other theoretical studies which have been performed on models for adsorbed hydrocarbon fragments are semi-empirical extended Hückel calculations of these fragments interacting with Fe, Ni and Pt clusters [16-20] and ab initio Hartree-Fock-LCAO (and GVB and CI) calculations of the fragments binding to a

single metal atom, Mn [21], Ni [22-24] or Li [15].

2. METHOD AND CALCULATIONS

As in paper I, we have used the self-consistent spin-restricted HFS-LCAO method in its core pseudopotential version [25-28]. Also the atomic orbital basis (double zeta Slater type orbitals [29]) and electron density fit functions (s-,p-,d-,f- and g-type) have been chosen as in I: 3d,4s and 4p orbitals on Ni (from the $3d^8 4s^2\ ^3F$ state), 2s and 2p on C and 1s on H.

The metal-CH clusters studied are NiCH (linear, $C_{\infty v}$), Ni_2CH (with CH perpendicular to the Ni-Ni axis, C_{2v}) and Ni_3CH (CH perpendicular to the Ni_3 plane, C_{3v}). For CH_2 adsorption we have considered $NiCH_2$ (planar, C_{2v}) and Ni_2CH_2 (the CH_2 plane perpendicular to the Ni-Ni axis, C_{2v}). These clusters model different adsorption sites (on top, bridged, threefold) occurring on the Ni(111) surface (and some of them on other surfaces too). The CH and CH_2 fragments are placed with the carbon end to the "surface" with all Ni-C distances equal to 1.90Å (the same as the Ni-C distance in the nickel-C_2H_2 clusters in paper I); for Ni_3CH we have also performed a calculation with shorter Ni-C distance: 1.69Å. The C-H distance in the Ni_nCH clusters equals 1.06Å (the acetylenic value [30]); in the Ni_nCH_2 clusters it is 1.09Å, while the HCH angle is 120° (these values are averages from the experimental singlet and triplet CH_2 structures [31-34]). The structure of the Ni_3C_2H cluster (C_s symmetry) is taken from the similar inorganic complexes $[\pi\text{-}(C_5H_5)Fe_3(CO)_7C_2C_6H_5]$ [35] and $[Ru_3(CO)_9H\{C_2C(CH_3)_3\}]$ [36]. The plane of the bent C_2H fragment, CCH angle 135° with the H atom pointing away from the Ni_3 plane, is perpendicular to this Ni_3 plane and contains one Ni atom (Ni_γ), while it bisects the Ni-Ni axis of the other two metal atoms (Ni_α-Ni_β). The C-C axis makes an angle of 10.5° with the Ni_3 plane (the C atom closest to the "surface" is denoted as C_α; the other one, which bears the H atom, is labelled C_β). The following distances have been chosen: Ni_γ-C_α: 1.83Å, Ni_γ-C_β: 2.98Å, $Ni_{\alpha,\beta}$-$C_{\alpha,\beta}$: 2.04Å, C_α-C_β: 1.30Å, C_β-H: 1.06Å. This model corresponds with threefold bonding of the C_2H species to the surface: the C_α atom forms a single σ-type bond with Ni_γ, the (acetylenic) π-orbitals in C_2H are involved in μ_2 type bonding with the Ni_α and Ni_β atoms (cf. paper I). In all clusters (with more than one Ni atom) the Ni-Ni distances are taken equal to the metal nearest neighbour value: 2.49Å [30].

The ionization energies, which are compared with the experimental UPS spectrum, have been calculated by the HFS method, mostly in the transition state formalism [26,37]. Since the relaxation shifts for the valence levels of

the adsorbed fragments appear to be almost uniform (see section 3, cf. papers I and II also) ground state calculations of the level splittings give practically the same picture.

3. *RESULTS*

The measured UPS spectrum of dissociated C_2H_2 species (at T ≃ 300 to 400K) on the Ni(111) surface shows peaks at -15.2 and -7.3 to -8 eV, relative to the work function [8]. It is possible that the -7.3 to -8 eV peak corresponds with (at least) two ionization levels which are not well resolved. Since it is hard to predict accurately the absolute ionization energies and the work function for metal-adsorbate systems (although the HFS-LCAO results on small cluster models with C_2H_2 are reasonably good, cf. paper I), we look at the level splittings. (It would be even better to look at the changes in these splittings caused by adsorption, as we have done for molecular C_2H_2, but the UPS spectra for the acetylene fragments are not known experimentally). So the experimental data to be explained by the calculations are a gap of about 7.5 eV between two ionized levels and possibly a small splitting of the highest level of about 0.7 eV.

3.1. *Nickel-CH*

The free CH radical possesses three (partially) occupied orbitals: two of σ type, 1σ which is mainly C(2s) and 2σ which is C-H bonding, and one (doubly degenerate) π orbital. In table 1 we have summarized the relative positions of the levels of mainly CH character in the nickel-CH clusters. In the Ni_2CH cluster the doubly degenerate π orbital is split (by ~ 1 eV); we have indicated the average position of the two π levels. From this table we observe that the ground state (GS) and transition state (TS) calculations give essentially the same results (indicating a uniform relaxation shift). It is striking that the picture is not very different for the different adsorption sites (one, two or three atom clusters). The same insensitivity of the ionization spectrum with respect to the metal site has been found for molecularly adsorbed C_2H_2, cf. papers I and II. Moreover, it has been concluded there, too, that extension of the small metal clusters by one or two extra atoms did hardly affect the calculated ionization energies; so we expect that the positions of the levels would not be significantly changed if we would enlarge the metal clusters. The calculated results do not seem to agree with the experimental data, however. We never find a gap nearly as wide as 7.5 eV between two peaks. Also a

significant decrease of the Ni-C distance (from 1.90 to 1.69Å) does not provoke this result. If we would assume that the 2σ peak has small intensity and is not well visible in the experimental UPS spectrum, the agreement between the experimental (7.5 eV) and the calculated (≃ 8.5 eV) splitting is reasonably good.

3.2. *Nickel-CH_2*

Free CH_2 (methylene) has four (partially) occupied orbitals: $1a_1$, $1b_2$, $2a_1$ and $1b_1$. In table 2 we present the relative positions of the levels in the nickel-CH_2 clusters which have mainly the character of these CH_2 orbitals. Just as for CH the GS and TS results are essentially the same. Moreover, we observe also here that the two nickel sites (on top or twofold) yield almost the same ionization spectrum. Again we do not find agreement with the experimental spectrum; it would be harder to reconcile the results here by using the argument of low intensity peaks since we have calculated more levels which are all localized on the CH_2 fragment and which have no counterpart in the experimental spectrum.

3.3. *Nickel-C_2H*

The occupied orbitals of C_2H resemble those of acetylene in their character: 3σ corresponds with $2\sigma_g$, 4σ with $2\sigma_u$, 5σ with $3\sigma_g$, 1π with $1\pi_u$. In our adsorption cluster, Ni_3C_2H with C_s symmetry, the following (valence) orbitals are essentially composed of these orbitals of the C_2H fragment: $3\sigma \rightarrow 1a'$, $4\sigma \rightarrow 2a'$, $5\sigma \rightarrow 3a'$, $1\pi_\perp \rightarrow 4a'$, $1\pi_{/\!/} \rightarrow 1a''$ (the labels $\perp$ and $/\!/$ denote π orbitals perpendicular and parallel to the "surface", respectively). Table 3 shows the relative positions of these levels. It also contains the positions of the acetylenic levels in the cluster μ_3-C_2H_2-Ni_3, which models the molecular adsorption of C_2H_2 on a threefold nickel(111) site. We observe some resemblance between the calculated spectra of the adsorbed C_2H fragment and molecularly adsorbed C_2H_2, but also there is a marked difference, viz. the higher energy of the 3a' (the acetylenic $3\sigma_g$) orbital. Again, we do not find the experimentally observed two peak structure with a gap of 7.5 eV. The 2a' level divides the gap between the lower 1a' peak and the higher (broadened) peak which might be assumed to contain the 3a', 4a' and 1a'' levels. This 2a' level (corresponding with the acetylenic $2\sigma_u$ orbital) is mainly localized on the C-H bond, just as the 2σ level which divides the gap for the adsorbed CH fragment. The agreement with experiment is worse than for CH adsorption, however, even if we would as-

Table 1[a]. *Level splittings (Δ in eV) for nickel-CH clusters*

Ni-C(Å)	NiCH 1.90		Ni_2CH 1.90		Ni_3CH 1.90		1.69
	GS	TS	GS	TS	GS	TS	GS
$\Delta_{2\sigma-1\sigma}$	5.4	5.8	5.2	5.6	4.7	4.9	5.3
$\Delta_{\pi-1\sigma}$	8.8	9.8	8.5	9.2	8.0	8.7	8.1

a) GS stands for ground state, TS for transition state results

Table 2[a]. *Level splittings (Δ in eV) for nickel-CH_2 clusters*

	$NiCH_2$		Ni_2CH_2	
	GS	TS	GS	TS
$\Delta_{1b_2-1a_1}$	5.1	4.9	4.9	4.8
$\Delta_{2a_1-1a_1}$	7.5	7.5	6.2	6.6
$\Delta_{1b_1-1a_1}$	9.5	10.3	8.5	9.2

a) GS stands for ground state, TS for transition state results

Table 3[a]. *Level splittings (Δ in eV) for Ni_3C_2H and μ_3-C_2H_2-Ni_3*[b]

	Ni_3C_2H GS		μ_3-C_2H_2-Ni_3[b] $\angle_{CCH}=150°$, GS
$\Delta_{2a'-1a'}$	5.9	$\Delta_{2\sigma_u-2\sigma_g}$	5.8
$\Delta_{3a'-1a'}$	9.3	$\Delta_{3\sigma_g-2\sigma_g}$	6.9
$\Delta_{4a'-1a'}$	9.7	$\Delta_{\pi_{u\perp}-2\sigma_g}$	9.7
$\Delta_{1a''-1a'}$	10.1	$\Delta_{\pi_{u/\!/}-2\sigma_g}$	10.5

a) GS stands for ground state results

b) from paper I [1]

sume the 2a' peak to have low intensity, since the gap between the remaining two peaks would be too large (≃ 9.7 eV).

4. CONCLUSIONS

Our calculations have yielded rather different ionization spectra for different acetylene fragments CH, CH_2 and C_2H adsorbed on nickel surface models, but none of these spectra is in one-to-one correspondence with the UPS spectrum measured for dissociated C_2H_2 on the Ni(111) surface. If we assume that this discrepancy is not caused by inaccuracies in the level positions calculated by the HFS method (the errors in these level positions are larger than the errors in the level shifts caused by adsorption, cf. paper I), the following explanations can be suggested. Our models, of course, could have the wrong geometry or they could be too small, but we have found that the calculated level positions are rather insensitive to the size and geometry of the cluster models. Also one might conclude that the occurring fragments are of different chemical composition, but we think it very unlikely that larger species such as CH_3-CH, CH_3-C or CH_2=C, which have been suggested to occur on Pt(111) surfaces, would yield the UPS spectrum observed for Ni(111). Such species have various chemical bonds with more or less localized molecular orbitals which we expect to yield ionization energies over the same energy range as the smaller species that we have studied with even smaller gaps. (And certainly not just the two peaks with a wide gap of 7.5 eV found in the experimental spectrum.) The most probable conjecture, to our opinion, is that one (or more) of the calculated ionization levels corresponds with a peak of lower intensity or one which is strongly broadened by coupling to the metal bands, so that it is not well visible in the experimental UPS spectrum. If we assume this to be the case, our results are not in conflict with the CH structure proposed for the dissociation fragments of C_2H_2 on Ni(111) [8-10]. In view of this discussion we recommend to look in the experimental UPS spectrum for weak bands (in the 7.5 eV gap?); or better, to make angularly resolved UPS measurements (as have been reported for CO on Ni(100) [38]) which would facilitate the assignment of the peaks by considering the different directional character of the orbitals in the adsorbed species. From the theoretical side, it would be very useful to calculate the intensities of the different ionization peaks, as it has been done for CO and N_2 [39] and for adsorbed O [40-42] and S [41].

ACKNOWLEDGEMENT

We thank Prof.Dr. P. Ros, Dr. E.J. Baerends and Dr. J.G. Snijders for making available the HFS-LCAO program.

The investigations were supported in part by the Netherlands Foundation for Chemical Research (SON) with financial aid from the Netherlands Organization for the Advancement of Pure Research (ZWO).

REFERENCES

[1] P. Geurts and A. van der Avoird, paper I in this series, accepted for publication in Surface Sci.

[2] P. Geurts and A. van der Avoird, paper II in this series, submitted for publication in Surface Sci.

[3] P. Geurts, H. Burgers and A. van der Avoird, paper III in this series, submitted for publication in Chem. Phys.

[4] C. Brucker and T. Rhodin, J. Catal. 47 (1977) 214.

[5] T.N. Rhodin, C.F. Brucker and A.B. Anderson, J. Phys. Chem. 82 (1978) 894.

[6] R. Mason and M. Textor, Proc. R. Soc. Lond. A.356 (1977) 47.

[7] K. Yoshida and G.A. Somorjai, Surface Sci. 75 (1978) 46.

[8] J.E. Demuth, Surface Sci. 69 (1977) 365.

[9] J.E. Demuth and H. Ibach, Surface Sci. 78 (1978) L238.

[10] S. Lehwald and H. Ibach, Surface Sci. 89 (1979) 425.

[11] H. Ibach, H. Hopster and B. Sexton, Appl. Surface Sci. 1 (1977) 1.

[12] H. Ibach and S. Lehwald, J. Vacuum Sci. Technol. 15 (1978) 407.

[13] L.L. Kesmodel, L.H. Dubois and G.A. Somorjai, Chem. Phys. Letters 56 (1978) 267.

[14] L.L. Kesmodel, L.H. Dubois and G.A. Somorjai, J. Chem. Phys. 70 (1979) 2180.

[15] J.E. Demuth, Surface Sci. 80 (1979) 367.

[16] A.B. Anderson, J. Chem. Phys. 65 (1976) 1729.

[17] A.B. Anderson, J. Am. Chem. Soc. 99 (1977) 696.

[18] A.B. Anderson, J. Am. Chem. Soc. 100 (1978) 1153.

[19] A. Gavezzotti and M. Simonetta, Chem. Phys. Letters 61 (1979) 435.

[20] R.C. Baetzold, Chem. Phys. 38 (1979) 313.

[21] B.R. Brooks and H.F. Schaefer III, Molec. Phys. 34 (1977) 193.

[22] H. Johansen and B. Roos, Intern. J. Quantum Chem. S8 (1974) 137.

[23] A.K. Rappé and W.A. Goddard III, J. Am. Chem. Soc. 99 (1977) 3966.

[24] U. Wahlgren, Chem. Phys. 32 (1978) 215.

[25] E.J. Baerends, D.E. Ellis and P. Ros, Chem. Phys. 2 (1973) 41.

[26] E.J. Baerends and P. Ros, Chem. Phys. 2 (1973) 52.

[27] J.G. Snijders and E.J. Baerends, Molec. Phys. 33 (1977) 1651.

[28] E.J. Baerends and P. Ros, Intern. J. Quantum Chem. S12 (1978) 169.

[29] E. Clementi and C. Roetti, Atomic data and nuclear data tables, Vol. 14 (Academic Press, New York, 1974) p. 177.

[30] R.C. Weast, ed., Handbook of chemistry and physics, 55th Ed. (CRC Press, Cleveland, 1974) p. F-200, 201.

[31] G. Herzberg and J.W.C. Johns, Proc. R. Soc. Lond. A.295 (1966) 107.

[32] G. Herzberg and J.W.C. Johns, J. Chem. Phys. 54 (1971) 2276.

[33] E. Wasserman, V.J. Kuck, R.S. Hutton, E.D. Anderson and W.A. Yager, J. Chem. Phys. 54 (1971) 4120.

[34] R.A. Bernheim, T. Adl, H.W. Bernard, A. Songco, P.S. Wang, R. Wang, L.S. Wood and P.S. Skell, J. Chem. Phys. 64 (1976) 2747.

[35] K. Yasufuku, K. Aoki and H. Yamazaki, Bull. Chem. Soc. Japan 48 (1975) 1616.

[36] G. Gervasio and G. Ferraris, Cryst. Struct. Commun. 2 (1973) 447.

[37] J.C. Slater, Quantum theory of molecules and solids, Vol. 4 (McGraw-Hill, New York, 1974).

[38] K. Horn, A.M. Bradshaw and K. Jacobi, Surface Sci. 72 (1978) 719.

[39] J.W. Davenport, Phys. Rev. Letters 36 (1976) 945.

[40] M. Scheffler, K. Kambe and F. Forstmann, Solid State Commun. 23 (1977) 789.

[41] S.Y. Tong, C.H. Li and A.R. Lubinsky, Phys. Rev. Letters 39 (1977) 498.

[42] R.P. Messmer, D.R. Salahub and J.W. Davenport, Chem. Phys. Letters 57 (1978) 29.

This thesis describes a theoretical study of the chemisorption of acetylene (and a few possible dissociation fragments) on the low index single crystal surfaces of the transition metals iron, nickel and copper. The adsorption sites on these surfaces are modelled by clusters of one to four metal atoms. Information about the interaction of acetylene with transition metal surfaces and complexes is important for obtaining more insight in catalytic processes involving hydrocarbons. Moreover, the thesis contains an investigation of the electronic structure and properties of several inorganic complexes of the same transition metals. The quantum theoretical method used is the Hartree-Fock-Slater (HFS)-LCAO method developed by Ros and Baerends; the results are compared with experimental (mostly spectroscopic) data as far as these are available.

In chapter II the HFS method is applied to the rather large $[Fe_4S_4(SH)_4]^{n-}$ cubane complex in different oxidation states (n=0,2,3); this complex (with alkyl or aryl groups instead of H atoms) is a synthetic analogue of the biologically active sites in the redox catalysts high potential iron protein and ferredoxin. Methodologically it is important that replacement of the core electrons in the complex by a pseudopotential does not significantly influence the results of the calculations. In chapter III it is shown that the HFS method is capable of calculating rather accurately the magnetic coupling parameters and the optical excitation energies of the paramagnetic complex Cu(II) bis(dithiocarbamate). The spin-unrestricted version of the method yields practically the same results as a spin-restricted calculation, except for those properties which depend directly on the (unpaired) spin density. In the following chapters (IV to VII) the spin-restricted HFS method with a pseudopotential for the core electrons is used throughout.

In chapters IV and V the interaction of acetylene with Fe, Ni and Cu surfaces at different sites (π,di-σ,μ_2,μ_3) is evaluated in terms of π to metal donation and metal to π^* back donation mechanisms. For adsorption on Cu, the donation effect is dominated by a non-bonded interaction between the π_u (and $3\sigma_g$) electrons of C_2H_2 and the filled metal levels in the same energy range (due to the low lying 3d and 4s bands in Cu). This makes it plausible that the C_2H_2 bonding on Cu is weaker than on Fe and Ni and it also explains the different ionization spectrum. The calculated adsorption shifts in the ionization energies of acetylene agree fairly well with the experimental spectra (from UPS); they are not very site dependent.

From the study of the complexes $[\pi\text{-}(C_2H_2)Ni(CO)_2]$, $[\pi\text{-}(C_2H_2)Ni(CNH)_2]$ and $[\mu_2\text{-}(C_2H_2)\{Ni(CNH)_2\}_2]$ in chapter VI, a relation between the acetylenic C-C overlap populations and the measured infrared stretch frequencies is obtained. Using this relation, the calculated C-C overlap populations and the measured stretch frequency (from ELS) for C_2H_2 on nickel (chapter IV), it is concluded that μ_3 bonding of C_2H_2 with a Ni-C distance of about 1.9Å and a distorted CCH angle of around 150^o is most probable on Ni(111) surfaces; μ_2 type of bonding cannot be completely ruled out, however, and it occurs probably on other surfaces.

The bonding in the mononickel π complexes (chapter VI) resembles that in the nickel π adsorption cluster. Due to the broad, low lying, dsp "band" of hybrid Ni orbitals (induced by the CNH ligands) in the dinickel μ_2 complex, the bonding of C_2H_2 is in this case more similar to the adsorption bonding on Cu: the π donation effect is dominated by non-bonded interactions.

Finally, in chapter VII, the ionization spectra of three acetylene fragments, viz. CH, CH_2 and C_2H, on Ni clusters are calculated. None of these spectra shows a one-to-one correspondence with the experimental UPS spectrum of C_2H_2 dissociatively adsorbed on Ni(111). Possible explanations for this discrepancy are discussed; one must also consider the possibility that the experimental spectrum contains weak or strongly broadened peaks which have not been identified.

Dit proefschrift beschrijft een theoretische studie van de chemisorptie van acetyleen (en enkele dissociatie fragmenten) op één-kristal oppervlakken van de overgangsmetalen ijzer, nikkel en koper. De adsorptieplaatsen op deze oppervlakken zijn voorgesteld door "clusters" van een tot vier metaal atomen. Informatie over de interactie van acetyleen met overgangsmetaal oppervlakken en complexen is van belang voor het inzicht in katalytische processen waarbij koolwaterstoffen betrokken zijn. Daarnaast bevat het proefschrift een onderzoek naar de electronen structuur en eigenschappen van enkele anorganische complexen van de genoemde overgangsmetalen. De quantumtheoretische methode die gebruikt is, is de Hartree-Fock-Slater (HFS)-LCAO methode ontwikkeld door Ros en Baerends; de verkregen resultaten zijn zoveel mogelijk vergeleken met experimentele (meestal spectroscopische) gegevens.

In hoofdstuk II is de HFS methode toegepast op het vrij grote $[Fe_4S_4(SH)_4]^{n-}$ cubaan complex in verschillende oxidatietoestanden (n=0,2,3); dit complex (met alkyl of aryl groepen in plaats van H atomen) is een synthetisch analogon van de biologisch actieve centra in de redox katalysatoren "high potential" ijzer proteïne en ferredoxine. Methodologisch is het van belang dat de vervanging van de "core" electronen in het complex door een pseudopotentiaal geen significante invloed heeft op de resultaten van de berekeningen. In hoofdstuk III is aangetoond dat de HFS methode in staat is om vrij nauwkeurig magnetische koppelingsparameters en optische excitatie energieën uit te rekenen in het paramagnetische complex Cu(II) bis(dithiocarbamaat). De spin-"unrestricted" versie van de methode geeft resultaten die weinig afwijken van een spin-"restricted" berekening, behalve voor die eigenschappen die direct bepaald worden door de (ongepaarde) spindichtheid. In de volgende hoofdstukken (IV tot VII) is altijd de spin-"restricted" HFS methode met een pseudopotentiaal voor de "core" electronen gebruikt.

In de hoofdstukken IV en V is de interactie van acetyleen met Fe, Ni en Cu oppervlakken op verschillende adsorptieplaatsen (π,di-σ,μ_2,μ_3) uitgerekend in termen van π naar metaal donatie en metaal naar π^* "back" donatie mechanismen. Bij adsorptie op Cu wordt het donatie effect overheerst door een "non-bonded" interactie tussen de π_u (en $3\sigma_g$) electronen van C_2H_2 en de gevulde metaal niveau's in hetzelfde energiegebied (als gevolg van de laag liggende 3d en 4s banden in Cu). Dit maakt het aannemelijk dat de C_2H_2 binding op Cu zwakker is dan op Fe en Ni en het verklaart tevens het afwijkende ionisatie spectrum. De

berekende adsorptie verschuivingen in de ionisatie energieën van acetyleen zijn in goede overeenstemming met de experimentele spectra (gemeten met behulp van UPS) en zijn niet erg afhankelijk van de adsorptieplaats.

Uit de studie van de complexen $[\pi\text{-}(C_2H_2)Ni(CO)_2]$, $[\pi\text{-}(C_2H_2)Ni(CNH)_2]$ en $[\mu_2\text{-}(C_2H_2)\{Ni(CNH)_2\}_2]$ in hoofdstuk VI, is een relatie tussen de acetyleenachtige C-C overlap populaties en de gemeten infrarood rek frequenties verkregen. Met behulp van deze relatie, de berekende C-C overlap populaties en de rek frequentie (gemeten met ELS) van C_2H_2 op nikkel (hoofdstuk IV), blijkt μ_3 binding van C_2H_2 met een Ni-C afstand van ongeveer 1.9Å en een CCH buigingshoek van rond de 150^o het meest waarschijnlijk op Ni(111) oppervlakken; binding van het μ_2 type kan echter niet geheel worden uitgesloten en komt waarschijnlijk voor op andere oppervlakken.

De binding in de mononikkel π complexen (hoofdstuk VI) lijkt op die in de nikkel π adsorptie "cluster". Als gevolg van de brede, laag liggende, dsp "band" van hybride Ni orbitals (ontstaan door de binding met de CNH liganden) in het dinikkel μ_2 complex, lijkt de binding van C_2H_2 in dit geval meer op de adsorptie binding op Cu: het π donatie effect wordt overheerst door "non-bonded" interacties.

Tenslotte zijn in hoofdstuk VII de ionisatie spectra van een drietal acetyleen fragmenten, CH, CH_2 en C_2H op Ni "clusters" berekend. Geen enkel spectrum is in overeenstemming met het experimentele UPS spectrum van gedissocieerd C_2H_2 op Ni(111). Mogelijke verklaringen voor dit verschil zijn besproken; men moet ook rekening houden met de mogelijkheid dat het experimentele spectrum zwakke of sterk verbrede pieken bevat die niet zijn geïdentificeerd.

CURRICULUM VITAE

Petro Geurts,

geboren op 21 augustus 1950 te Kerkrade.

juni 1968	Eindexamen HBS-b, St. Antonius Doctor, Kerkrade.
september 1968 - juli 1975	Studie scheikunde, Katholieke Universiteit, Nijmegen.
. mei 1971	Kandidaatsexamen.
. juni 1975	Doctoraalexamen. Hoofdvak : Theoretische Chemie. Bijvakken: Anorganische Chemie, Molecuulspectroscopie.
juli 1975 - juli 1979	Wetenschappelijk medewerker, Instituut voor Theoretische Chemie, Katholieke Universiteit, Nijmegen (in dienstverband met ZWO/SON).
oktober 1979 - april 1980	Wetenschappelijk medewerker, Instituut voor Theoretische Chemie, Katholieke Universiteit, Nijmegen.

STELLINGEN

1

Het verdient aanbeveling de continuïteit van samenwerkingsverbanden op het gebied van de automatisering in de gezondheidszorg beter te waarborgen.

2

Nog veel kwalitatieve beschouwingen over resonantiestructuren aan de hand van het "valence bond" model missen de juiste quantumtheoretische fundering. In een studie van benzeen waar deze fundering wel aanwezig is, blijken die beschouwingen onjuist te zijn.

- J.M. Norbeck and G.A. Gallup, J. Am. Chem. Soc. 95 (1973) 4460.
- J.M. Norbeck and G.A. Gallup, J. Am. Chem. Soc. 96 (1974) 3386.

3

In een ab initio studie van overgangsmetaal tetrahydrides leggen Hood, Pitzer en Schaefer tussen orbital energieën en metaal-waterstof bindingssterkten een verband dat in tegenspraak is met de resultaten van hun berekeningen.

- D.M. Hood, R.M. Pitzer and H.F. Schaefer III,
  J. Chem. Phys. 71 (1979) 705.

4

Het is wenselijk dat huisdieren geen anderen dan hun bezitters overlast aandoen.

De grote discrepantie tussen ab initio waarden voor hogere dispersie interactie coëfficiënten (zoals C_8 en C_{10}) en resultaten berekend volgens een model ontwikkeld door Amos en Yoffe is te wijten aan het niet in rekening brengen in dit model van translaties van een globale moleculaire oorsprong naar lokale bindingsoorsprongen in het molecuul.

- A.T. Amos and J.A. Yoffe,
  Theoret. Chim. Acta (Berl.) 42 (1976) 247.
- J.A. Yoffe, Theoret. Chim. Acta (Berl.) 51 (1979) 107.
- J.A. Yoffe, Chem. Phys. Letters 61 (1979) 593.

6

Abraham en Stölevik propageren het gebruik van een Morse potentiaal in plaats van een exp-6 potentiaal voor "non-bonded" interacties. Op basis van theoretische overwegingen is dit verwerpelijk.

- R.J. Abraham and R. Stölevik, Chem. Phys. Letters 58 (1978) 622.

7

Er dient beter gewaakt te worden voor de originaliteit van een stelling.

- J. van Dongen Torman, Thesis, Nijmegen (mei 1978).
- J. Rijnsdorp, Thesis, Groningen (september 1978).
- R. Meij, Thesis, Amsterdam (november 1978).

De manier waarop Kasai, McLeod en Watanabe de electronen structuur van in matrices geïsoleerde acetyleen en ethyleen complexen van koper en zilver analyseren is dubieus.

- P.H. Kasai and D. McLeod, Jr., J. Am. Chem. Soc. 100 (1978) 625.
- P.H. Kasai, D. McLeod, Jr. and T. Watanabe, J. Am. Chem. Soc. 102 (1980) 179.

9

Anderson is zo inconsequent in de beoordeling van door hem berekende roosterconstanten aan "clusters" van ijzer, nikkel en koper, dat aan de waarde van zijn conclusies ernstig moet worden getwijfeld.

- A.B. Anderson, Chem. Phys. Letters 61 (1979) 388.

10

De prijs/prestatie verhouding van de meeste stellingen is onredelijk groot.

Nijmegen, 25 september 1980 Petro Geurts